

WOODS HOLE OCEANOGRAPHIC INSTITUTION
Woods Hole, Massachusetts

REFERENCE NO. 72-6

ON THE CALCULATION OF WIND STRESS CURL OVER OPEN
OCEAN AREAS FROM SYNOPTIC METEOROLOGICAL DATA
WITH APPLICATION TO TIME DEPENDENT OCEAN CIRCULATION.

by

Christopher S. Welch

February 1972

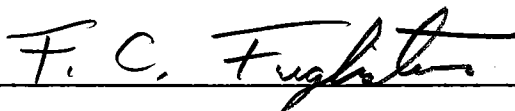
TECHNICAL REPORT

*Supported by the Office of Naval Research
under Contract N00014-66-C0241; NR 083-004,
and the U. S. Coast Guard contract DOT-CG-
10618-A.*

*Reproduction in whole or in part is permitted
for any purpose of the United States Government.
In citing this manuscript in a bibliography, the
reference should be followed by the phrase:
UNPUBLISHED MANUSCRIPT.*

Approved for public release, distribution unlimited.

Approved for Distribution



F. C. Fuglister, Acting Chairman
Department of Physical Oceanography



ON THE CALCULATION OF WIND STRESS CURL OVER OPEN
OCEAN AREAS FROM SYNOPTIC METEOROLOGICAL DATA
WITH APPLICATION TO TIME DEPENDENT OCEAN CIRCULATION

by

CHRISTOPHER SLOCOMBE WELCH

B.S., Stanford University
(1966)

SUBMITTED IN PARTIAL FULFILLMENT OF THE
REQUIREMENTS FOR THE DEGREE OF
DOCTOR OF PHILOSOPHY

at the

MASSACHUSETTS INSTITUTE OF TECHNOLOGY

and the

WOODS HOLE OCEANOGRAPHIC INSTITUTION

January, 1972

Signature of Author... *Christopher S. Welch*
Joint Program in Oceanography, Massachu-
setts Institute of Technology - Woods Hole
Oceanographic Institution, and Department
of Meteorology, Massachusetts Institute of
Technology, January 1972

Certified by.....
Thesis Supervisor

.....
Thesis Supervisor

Accepted by.....
Chairman, Joint Oceanography Committee in
the Earth Sciences, Massachusetts Institute
of Technology - Woods Hole Oceanographic
Institution

ON THE CALCULATION OF WIND STRESS CURL OVER OPEN
OCEAN AREAS FROM SYNOPTIC METEOROLOGICAL DATA
WITH APPLICATION TO TIME DEPENDENT OCEAN CIRCULATION

Christopher Slocombe Welch

Submitted to the Massachusetts Institute of Technology -
Woods Hole Oceanographic Institution Joint program in Ocean-
ography on January 23, 1972 in partial fulfillment of the
requirements for the degree of Doctor of Philosophy.

ABSTRACT

The method used by N. P. Fofonoff for estimating wind stress curl from surface atmospheric pressure maps is developed for use with the National Meteorological Center analysis grid. A formula is developed relating the wind stress curl directly to geometrically apparent features of the surface pressure analyses. The sensitivity of the formula to small deviations in the basic pressure field is estimated.

Some statistical properties of the resulting formula as applied to actual pressure analyses are investigated. In particular, the geostrophic wind estimated for two finite difference grids is compared to observed winds from an independent anemometer located at W.H.O.I. site "D". The statistical distribution of wind stress curl estimates is found to be non-Gaussian. The difficulty in estimating a mean value from such distributions is discussed. The root mean square values of wind stress curl are found to be approximately 10 times the mean values. Means are estimated and found to be inadequate to drive the mean transports in the Gulf Stream and Kuroshio.

The formula is applied at Bermuda and the results compared to the record from the tide gauge located there. A significant relation between wind stress curl and sea level is found after tidal and inverted barometer effects are suppressed.

The formula is applied to time dependent motions of the Labrador Current as evidenced by iceberg drifts for the 1959 ice season. Agreement is found between calculated and observed iceberg motions on the eastern slope of the Grand Banks using static Sverdrup dynamics.

Thesis Supervisors:

W.H.O.I.: Dr. Nicholas P. Fofonoff
Title: Senior Scientist

M.I.T.: Professor Carl I. Wunsch
Title: Associate Professor
 Department of Earth and Planetary Sciences

To my lovely wife Betty

First and foremost, the author is grateful to his wife, Betty Welch, for unflagging support and help in the completion of this project. In addition to unfailing moral support, she helped key-punch the programs, draft the figures, and proofread the manuscript.

Sincere thanks are also due to Dr. Nicholas Fofonoff and Professor Carl Wunsch. Both of these gentlemen have given freely of their time, data, and financial support to a student who has no doubt seemed ungrateful and recalcitrant. Dr. Fofonoff has offered both sure guidance and low key and patient criticism. He has also been most generous with his resources during the final period of preparation. Professor Wunsch has been unswerving in his standards of scientific excellence while maintaining, at the same time, an open ear and mind.

The effort of Professor Henry Stommel as agent is also appreciated. It is he who first arranged the author's introduction to the wind stress curl problem.

Audrey Williams prepared the final form and kept unerring track of its progress. The author is grateful for these efforts.

Mention must also be made of the excellent technical support the author received from members of the buoy group at the Woods Hole Oceanographic Institution. In particular, John Maltais wrote several excellent machine language

programs for reading packed binary computer tapes, thereby solving in one stroke one of the most time-consuming and frustrating potential problems associated with data analysis by computer. Robert Millard also was generous with his knowledge of anemometer data. Susan Tarbell, Dolores Chausse, and Caroline Harlow patiently and efficiently mediated between the author and the W.H.O.I. computer in processing data of various kinds.

Acknowledgement must be given to the enthusiastic support of my parents. Without that support, moral, technical, and financial, the project would have likely never been started, let alone completed.

I must also thank Mrs. Joyce Chen, who started as an employer and became a friend. Her many kindnesses have helped to support this endeavor in more ways than can be mentioned here.

Finally, the financial support of many taxpayers is happily acknowledged. The agencies of this support have been the National Science Foundation, through contract GA 13880, the International Ice Patrol Office of the United States Coast Guard, which supplied the iceberg data as well as financial support through contract DOT-CG-10618-A, and the Office of Naval Research through contract N00014-66-C0241; NR083-004.

TABLE OF CONTENTS

	Page	
Chapter I	INTRODUCTION	12
Chapter II	FORMULA DEVELOPMENT	39
Chapter III	STATISTICAL STUDY	79
Chapter IV	BERMUDA SEA LEVEL STUDY	109
Chapter V	THE MEAN TRANSPORT PROBLEM	117
Chapter VI	ICEBERG EXPERIMENT	131
Appendix I	STEREOGRAPHIC PROJECTION FORMULAS	147
Appendix II	FORMULA VALIDITY CHECK	153
Appendix III	ICEBERG DATA	159
Bibliography		186
Biographical Sketch		189

List of Figure Captions

Figure 1.1a. July monthly mean surface atmospheric pressure in mb over the North Atlantic Ocean according to Montgomery (1936a).

Figure 1.1b. July monthly mean convergence of the surface water in cm/day over the North Atlantic Ocean according to Montgomery (1936a).

Figure 1.2a. July monthly mean surface atmospheric pressure in mb over the North Atlantic Ocean after Fofonoff and Dobson (1963a).

Figure 1.2b. July monthly mean convergence of the surface water in cm/day over the North Atlantic Ocean after Fofonoff and Dobson (1963a).

Figure 1.3. Calculated integrated transport for various averaging and sampling frequencies over the Greenland Sea during February, 1965 according to Aagaard (1970). The contour interval is 10 Sverdrups.

Figure 1.4. The response of the calculations shown in figure 1.3 to the frequency at which the pressure data are averaged and sampled before the wind stress curl is computed. The relative response of each gyre is defined as the ratio of the largest integrated transport in that gyre for a sampling frequency of 4 times/day to the largest transport for the sampling frequency in question. These ratios, represented by circles for the northern gyre and triangles for the southern gyre, are plotted as a function of the sampling rate on a log scale. The dashed line is an imaginary response function which might be approximated by the data.

Figure 2.1a. The relationship among the quantities defined in the text and used for transforming physical coordinates to computer coordinates.

Figure 2.1b. The relationship between the NMC 51x47 computer addressable grid and a polar stereographic projection of the northern hemisphere.

Figure 2.2. The steps, using the surface wind as an intermediate result, between a 1000 mb height field varying only sinusoidally in latitude and the corresponding wind stress curl. The height field is a member of the set used to test the wind stress curl approximation in appendix 2 with $k=1$. Vertical scales are approximate.

Figure 2.3. Normalized curves of 1000 mb height and wind stress curl for the example of a Gaussian pressure pattern as discussed in the text.

Figure 3.1. Zonally averaged estimates of monthly averaged geostrophic wind speed for January and July, 1968. The areas covered are the North Atlantic Ocean and the North Pacific Ocean north of 20°N

Figure 3.2. Histograms of ratio of observed surface wind speed to calculated geostrophic wind speed for W.H.O.I. wind record 2801. In the upper figure, the geostrophic wind is estimated using the diamond grid used by the Canadian Fisheries Research Board. In the lower figure, the NMC grid used in the present study is used. The vertical line at .7 marks the value of R_s used in the present study.

Figure 3.3. Histogram of veering angle between calculated geostrophic wind and observed surface wind for W.H.O.I. record 2801. The vertical line at 15° marks the value of λ used in the present study.

Figure 3.4. Progressive vector representation of computed and observed surface wind at W.H.O.I. site D for record 2801.

Figure 3.5. Magnitude of the error vector between estimated and observed surface wind for W.H.O.I. wind record 2801 at site D.

Figure 3.6. Unaveraged power spectra for observed and estimated fluctuating surface wind at site D for W.H.O.I. record 2801.

Figure 3.7. Coherency between observed and estimated fluctuating surface wind at site D for W.H.O.I. record 2801.

Figure 3.8. Histograms of estimated geostrophic wind speeds during January and July 1968 over a 10° wide zonal band of the North Atlantic Ocean. The histograms are compared to the best fit Rayleigh distribution.

Figure 3.9. Typical histogram and associated cumulative probability curve of wind stress curl over a 10° wide zonal band of the North Atlantic Ocean during a single month. This figure illustrates the non-Gaussian character of the wind stress curl distribution as discussed in the text.

3.10a. Histograms of the estimated wind stress curl over the North Atlantic Ocean between 30°N and 40°N during January, 1968. The solid line shows the best fit Cauchy distribution as discussed in the text.

Figure Captions (cont.)

Figure 3.10b. Same as figure 3.10a for July 1968.

Figure 3.11. The right hand panel shows a typical winter 1000 mb height analysis over the Atlantic Ocean. The units are meters with a 100 meter contour interval. This particular analysis is for March 3, 1968 1200Z. The left hand panel shows the corresponding wind stress curl analysis with units of 10^{-8} dyne-cm $^{-3}$. An interpretation of these figures is given in the text.

Figure 3.12a. Meridional Sverdrup transport over the North Pacific Ocean calculated from 1000 mb height analyses every 12 hours and averaged over January 1968. Contour interval is 10^{-2} Sverdrups/km.

Figure 3.12b. Meridional Sverdrup transport over the North Pacific Ocean calculated from average monthly 1000 mb height analysis for January 1968.

Figure 4.1. Western boundary transport in the North Atlantic and North Pacific Oceans as observed and estimated in several different studies from estimated wind stress.

Figure 4.2. Western boundary transport for the North Pacific Ocean calculated several different ways as discussed in the text.

Figure 5.1. Power spectra of variables used in the Bermuda sea level experiment.

Figure 5.2. Linear regression coefficients of sea level on wind stress curl and 1000 mb height for the Bermuda sea level experiment.

Figure 5.3. Multiple coherence of the linear regression model for the Bermuda sea level experiment.

Figure 5.4. Partial coherence coefficients of 1000 mb height and wind stress curl with sea level for the Bermuda sea level experiment.

Figure Captions (cont.)

Figure 6.1. The geography relevant to the iceberg study. A schematic iceberg track is presented including the various paths an iceberg can take in the vicinity of the Grand Banks (region 19 on the chart). Regions 14-17 are $2\frac{1}{2}^\circ$ wide zonal sections over which the average value of wind stress curl was calculated. The dots give the location of NMC gridpoints in this region.

Figure 6.2. Labrador current transport calculated at 12 hour intervals across section 14 as discussed in text during the iceberg season of 1959.

Figure 6.3. The same as figure 6.2 averaged over successive three day intervals.

Figure 6.4a. Time section for Labrador current transport during the iceberg season of 1959 calculated according to the text. The iceberg motions deduced from the data are represented by the superimposed arrows and line segments. The periods over which the deductions are made is shown at each latitude by the extent of the horizontal segment. The vertical arrows indicate the direction of deduced motion, an upward pointing arrow denoting a northward drift and a downward pointing arrow denoting a southward drift. A broken vertical line indicates that a single iceberg has moved to a new section.

Figure 6.4b. Time sections for the horizontal divergence of the Labrador Current calculated according to the text and compared to deduced iceberg motions. The deduced motions are indicated as in figure 6.4a with upward pointing arrows denoting divergence and downward pointing arrows denoting convergence.

Figure 6.5. Time sections of monthly averaged calculated Labrador Current transports for January through August 1959. Units are 10^{-1} Sverdrups with a contour interval of 10 Sverdrups.

CHAPTER I

The steady state theory of wind driven ocean circulation is a product of the present century. One of the results of this development has been an increasing awareness of the importance of the curl of the wind stress as a driving term for general wind driven ocean circulation. This thesis is concerned with a technique for the calculation of this field over open ocean areas.

The first major contribution to the modern theory of wind driven ocean circulation was a classic paper by V. W. Ekman (1905) in which he showed that surface stress in the ocean was absorbed in a thin layer near the surface. In this paper, he noted that the total transport due to the surface stress is at right angles to the stress. This transport, requiring only that the stress be constant and the depth of the water be deeper than the frictional layer depth, is called Ekman transport and can be expressed with the equation

$$\underline{U}_E = -\hat{k} \times \left(\frac{\underline{\tau}}{f} \right). \quad 1.1)$$

Here \underline{U}_E is the horizontal mass transport per unit distance, f is the Coriolis parameter, and $\underline{\tau}$ the stress vector. We take $f = 2\Omega \sin \phi$ with Ω being the angular velocity of the

earth's rotation and ϕ being the latitude. \hat{k} is a unit vector normal to the surface and pointing "up".

An important feature of this transport was stated later by Ekman (1923) for the case of a non-uniform stress field. He related the horizontal divergence of the surface frictional transport to the curl of the wind stress. It is by this mechanism, now called Ekman pumping or Ekman suction, that the effect of stress is carried to the interior circulation of a rotating fluid from a boundary not parallel with the rotation vector. In a boundary layer context, the vertical velocity due to a steady non-uniform stress at the surface can be expressed with the equation

$$w(-\infty) = \hat{k} \cdot \nabla \times \left(\frac{\tau}{f} \right) \quad 1.2)$$

Here $w(-\infty)$ refers to the velocity in the frictionless part of the fluid below the Ekman layer produced by the wind stress acting on the surface through the agency of the Ekman layer.

The two next major steps in wind driven ocean circulation theory occurred nearly simultaneously and apparently independently. They both involved an appreciation of the importance of the change of Coriolis parameter with latitude. The first step was taken by H. U. Sverdrup (1947).

Sverdrup defined transport integrals by integrating vertically from the surface to a depth d , "where d is equal to or greater than the depth at which the horizontal pressure gradient becomes zero". He then related the north component of the total transport V_T to the wind stress curl in what is now called the Sverdrup relation. It can be written

$$\beta V_T = \hat{k} \cdot \text{curl } \underline{\tau} \quad 1.3)$$

where $\beta = \frac{1}{R} \frac{\partial f}{\partial \phi}$, R being the radius of the earth. The next year, Stommel (1948) showed that the change of Coriolis parameter with latitude was responsible for the crowding of oceanic streamlines near the western sides of oceans.

With these two results in hand, Munk (1950) wrote a comprehensive paper on wind driven ocean circulation. He presented the concept of gyres in this paper as areas bounded north and south by the line of zero wind stress curl. He also presented the first estimate of longitudinally averaged wind stress curl over the North Atlantic and North Pacific from 60°N to 20°S . This study established a scale for mean wind stress curl as 1×10^{-8} dyne-cm⁻³.

These papers brought mean wind driven ocean circulation theory over the interior ocean areas to its present state. They have developed successively an awareness of

the curl of the wind stress as an important driving term. In conjunction with this development, several studies of the field of wind stress and its curl have been made.

In his 1905 paper, Ekman referred to a study of wind stress by A. Colding in the Baltic Sea. In this study, an empirical relation between wind stress and wind speed was developed. The relation can be expressed using the equation

$$\tau = \rho_a C_D |\underline{U}_S| \underline{U}_S. \quad 1.4)$$

Here \underline{U}_S is the velocity of the wind at the surface, ρ_a is the density of air, and C_D is a non-dimensional drag coefficient. The value of C_D found by Ekman was 2.6×10^{-3} if ρ_a is given as $1.3 \times 10^{-3} \text{ gm-cm}^{-3}$.

In 1935, C.-G. Rossby and R. B. Montgomery published two complementary studies of oceanic wind stress. The first part of the study was an attempt to determine the factors that are important in determining wind stress and to produce a formula relating wind stress to external and hopefully measurable quantities. To quote from Rossby (1935),

"Our immediate object must be to indicate the general character of the relationships connecting the mean motion

and hence the eddy-viscosity with the controlling external parameters and to serve as a guide in the organization of the proper measurements and in their interpretation".

The proper measurements referred to by Rossby form a large part of the modern field of air-sea interaction. A comprehensive account of this field is given in Roll, (1965).

The results of Rossby's study are consistent with formula 1.4) if \underline{U}_s is considered to be measured at a specific height (usually given as 15 meters) and C_D is a function of this height. A relation between gradient wind above the surface frictional layer and \underline{U}_s were also obtained by Rossby and Montgomery.

Montgomery (1935) used the results of the first part of the study to calculate estimates of wind stress over the North Atlantic Ocean from the field of surface atmospheric pressure. The approach he used is first to compute the gradient wind \underline{U}_g from the atmospheric pressure field. He then relates the surface wind \underline{U}_s to the gradient wind by a linear transformation of the components which has the effect of reducing the magnitude in going from the gradient wind to the surface wind and also in veering the surface wind somewhat towards low pressures from the gradient wind. There are two parameters which can describe this transformation, R_s , the shrinking constant and λ , the veering angle.

R_s is the ratio of the surface to the gradient wind while λ is the angle at which the surface wind veers towards low pressures. Both the angle and the ratio were obtained by Montgomery from the first part of the study. The data used by Montgomery were climatological averages from an atlas compiled by Defant. From these, he calculated surface winds as mentioned above. His values for λ ranged from 22° in the northern latitudes to 16.5° in the tropics. For an anemometer height of 15 meters, his value for R_s was $2 \sin \lambda$ and came to about .64. The drag coefficient was also evaluated from the theoretical work and came to about 2.4×10^{-3} . The stress law Montgomery used is of the form of equation 1.4). In his study, Montgomery was aware of many of the perils and pitfalls in his approach. Indeed, his words can hardly be improved upon.

"In carrying through this computation it has been necessary to make use of assumptions which may have introduced considerable error. The basic assumption is that the mean of the instantaneous transports is the same as the transport computed from the mean pressure-distribution. The correctness of this assumption becomes doubtful when we remember that the deviations from the mean (pressure-gradient, for instance) are greater than the mean itself, which may be seen by the fact that the synoptic map often shows no resemblance to the mean map. Since the gradient-

wind and the pressure-gradient become quickly adjusted, and since there is a linear relation between the two, there is no reason to doubt that the mean air-movement at the gradient wind-level is given approximately by the mean pressure-distribution. But between the gradient-wind and the surface-stress there is not a linear relation. It would be possible to use as the mean surface-stress the mean computed from synoptic maps for a given period, but this lengthy computation has not yet been attempted. Further, the adjustment between surface-stress and transport of water is far from instantaneous, and, whether the time-mean of the relation between the two for the unsteady state is exactly the same as the relation for the steady state, is subject to doubt".

From the stress, Montgomery used equation 1.1) to compute components of Ekman transport. He then calculated the total Ekman transport across the 4 sides of each 5° by 5° square to give the convergence or divergence in each square. The pressure distribution and convergence calculated by Montgomery are given in figure 1.1a,b. In the convergence chart a large upwelling area near the African coast was noted by Montgomery but not contoured. The peak value in this area was 34 cm/day. A slight change in Montgomery's contours has been made to include a positive value of convergence calculated in the northern half of the Bay of Biscay on the positive side.

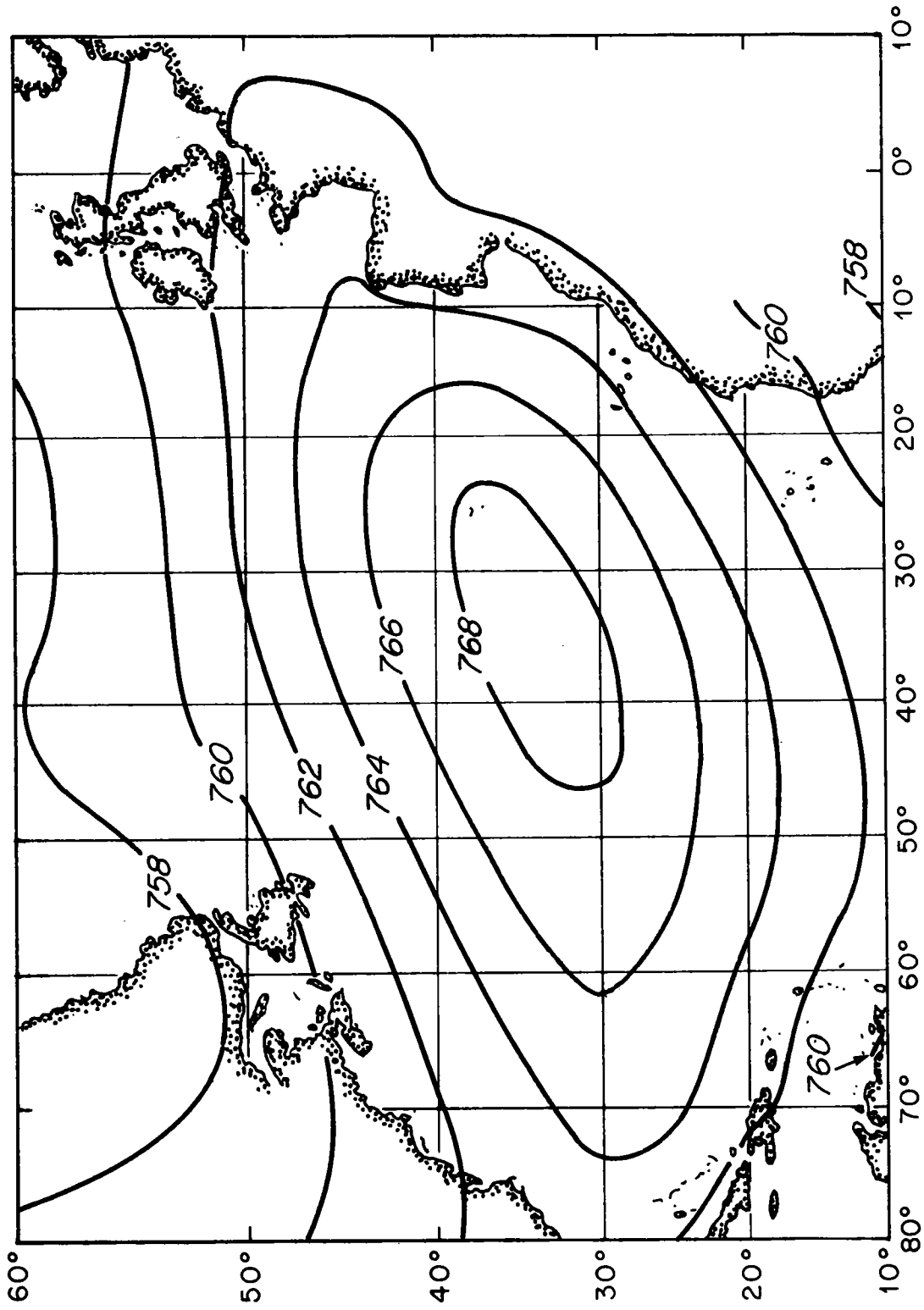


Figure 1.1a. July monthly mean surface atmospheric pressure in mb over the North Atlantic Ocean according to Montgomery (1936a).

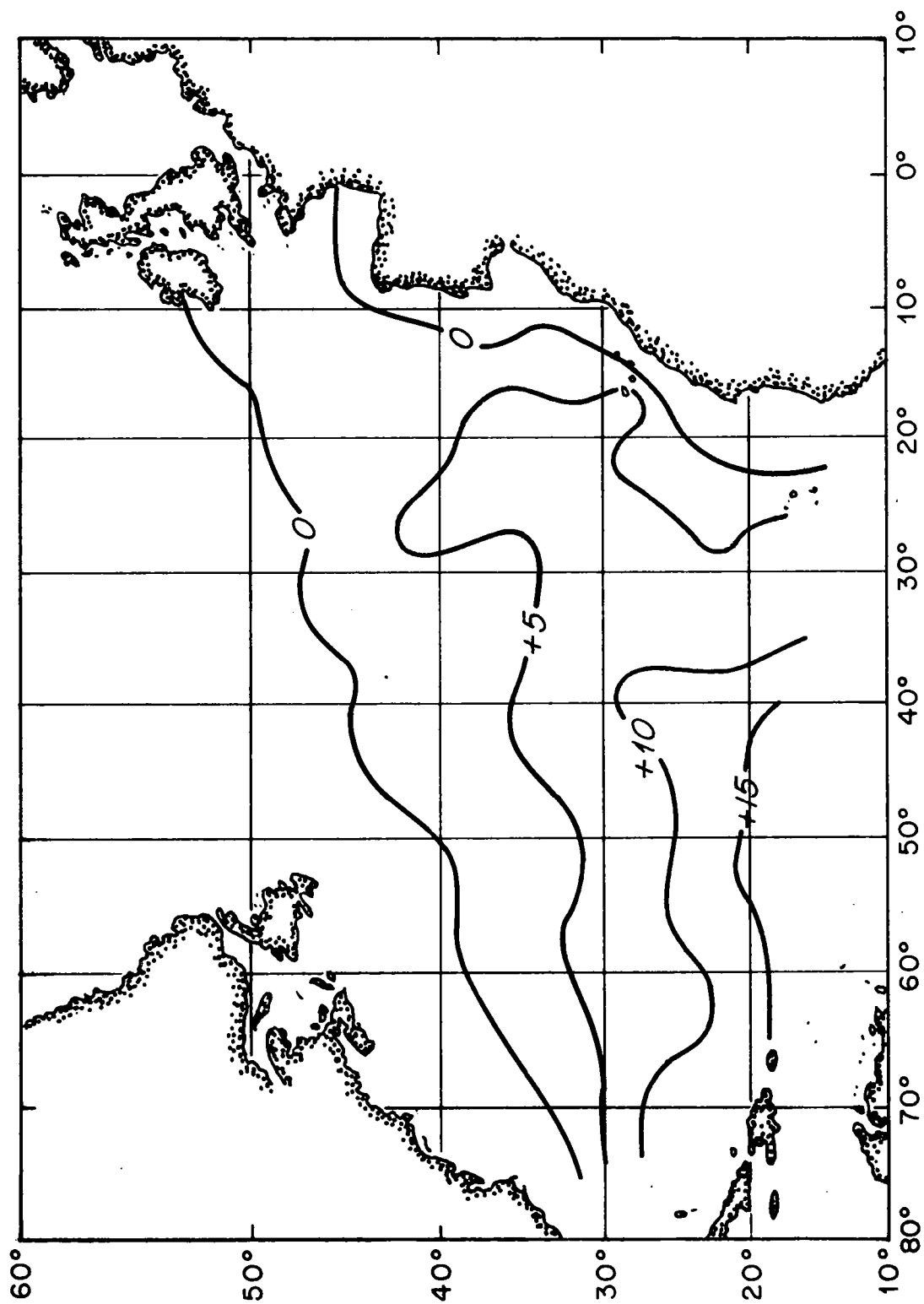


Figure 1.1b. July monthly mean convergence of the surface water in cm/day over the North Atlantic Ocean according to Montgomery (1936a).

of the zero contour. The most interesting part of the study, from Montgomery's point of view, was the displacement to the southwest of the region of maximum convergence from the center of the pressure cell.

In order to facilitate comparisons with other studies, the areal density of analysis points is given as 1 point per 5° square or 1 point per $R^2 \sin \phi (5 \times \frac{\pi}{180})^2$. This comes to $3.2 \times 10^{-6} \text{ sec } \phi$ points per square kilometer. The time sample is essentially infinite, the Defant Atlas being compiled from 30 years of data.

The next major determination of the field of wind stress was done by a group at the Scripps Institution of Oceanography. This study was done over the northern and equatorial Pacific Ocean in response to the development of Sverdrup's theory. The approach was different from that used by Montgomery as climatological winds were used as primary data rather than climatological pressures. These winds were obtained on 5° squares from wind roses on the pilot charts of the U. S. Hydrographic Office. The method of computation is given in Reid (1948). An attempt was made in this study to take into account the variability of the winds going into the non-linear formula. To the north of 30°N , the variability was obtained from the Atlas of Climatic Charts of the Ocean, (1938). To the south of 30°N ,

the distribution of speeds was assumed to be Gaussian with a standard deviation of 1/2 Beaufort number. The Scripps study was extended to the world ocean by Hidaka (1958) for seasonal and annual climatological values. The extension does not include any attempt to account for variability. The Scripps study and the Hidaka extension form one of the basic source documents available today for the climatology of the oceans. The sampling density is the same as that of the Montgomery study, or 3.2×10^{-6} sec ϕ analysis points per square kilometer. The parameters R_s and λ do not occur in a study based on wind observations. The value of C_D was taken to be 2.6×10^{-3} at speeds above 6.6 m/sec and 0.8×10^{-3} at lower speeds, in accordance with a paper by Munk (1947).

By the early 1960's, the theory of wind driven ocean circulation had been further advanced through the efforts of Stommel and Munk in particular. At this time, another project was undertaken by N. P. Fofonoff (1962) to compute wind stress, wind stress curl, and associated oceanic circulations under the sponsorship of the Canadian Fisheries Research Board. This study has been continued by the CFRB until the present.

The computation method is similar to the one used by Montgomery in that the basic data are pressure data.

The data are produced by the extended forecast branch of the U. S. Weather Bureau as monthly average pressures on a diamond grid. This grid contains points at the intersection of latitudes and longitudes both ending in a 5° or a 0° . For example 20°N , 40°E or 35°N , 15°E would be points in the grid. The areal density of this grid is exactly half that of the ones used in the previous studies being given by 1.6×10^{-6} sec ϕ analysis points per square kilometer. For the first time, a time sampling density can be defined of 1 sample per month. A particular kind of sampling is meant in this case. Synoptic analyses of pressure prepared at 6 hour (or 12 hour) intervals are averaged over the period of the sample to produce the "sampled" analysis. In this project, the values of R_s , C_D , and λ used are 0.7, 2.6×10^{-3} , and 15° respectively.

Following Montgomery's analysis, Fofonoff first calculated for each month values of both components of Ekman transports. Next, using a 7 point finite difference grid, he calculated estimates of the curl of the wind stress from estimates of the 2 first and 3 second partial derivatives of the pressure field. These were used in a two step process to calculate the curl of the wind stress. This was converted to total meridional transport using the Sverdrup relation (equation 1.3) Using Stommel's result that boundary currents occurred.

primarily on the western side of the ocean, he computed the net meridional total transport or stream function.

$$\psi(\phi, \theta_1) = \int_{\theta_1}^{\theta_0} V_T R \cos \phi d\theta \quad 1.5)$$

Here ψ is the stream function, θ_0 is the longitude of the eastern boundary at latitude ϕ , and θ_1 is the longitude at which the stream function is computed. Next, assuming that the currents were all in geostrophic equilibrium with the exception of the Ekman transport, he calculated the geostrophic stream function

$$\psi_g(\phi, \theta_1) = \int_{\theta_1}^{\theta_0} (V_T - V_E) R \cos \phi d\theta. \quad 1.6)$$

In both these cases contours connecting values of equal ψ are stream lines of the flow. The meridional geostrophic transport is thus

$$V_g = V_T - V_E. \quad 1.7)$$

The vertical velocity beneath the Ekman layer is assumed to be equal to the convergence of the geostrophic transport. This can be expressed as

$$w(-\infty) = \frac{\beta}{f} V_g \quad 1.8)$$

This final formula was used to estimate the vertical velocity beneath the Ekman layer for some calculations. The values of these transports over the North Pacific Ocean are compiled every year in a manuscript report of the Canadian Fisheries Research Board.

From the monthly values calculated during the 10 years 1950-1959, Fofonoff compiled an atlas of 10 year climatological values for each month in the year. He also computed the standard deviations of values from the same data. One interesting result of this study is that the standard deviations of all but the integrated quantities are generally as large as the mean values themselves.

The 10 year monthly values are roughly comparable to the 25 year climatological values from Defant which were used by Montgomery. Accordingly values of 10 year mean atmospheric pressure and vertical velocity were computed from Fofonoff's July values and plotted on a chart so as to be directly comparable to Montgomery's previous values. These charts are presented as figure 1.2a,b and may be compared directly to figure 1.1a,b. Perhaps the most striking conclusion from the comparison is the similarity of many of the features both the mean pressure cell and the computed vertical velocity. In particular, the important line of zero curl across the Atlantic from south of Cape Hatteras to Ireland is virtually coincident in the two studies.

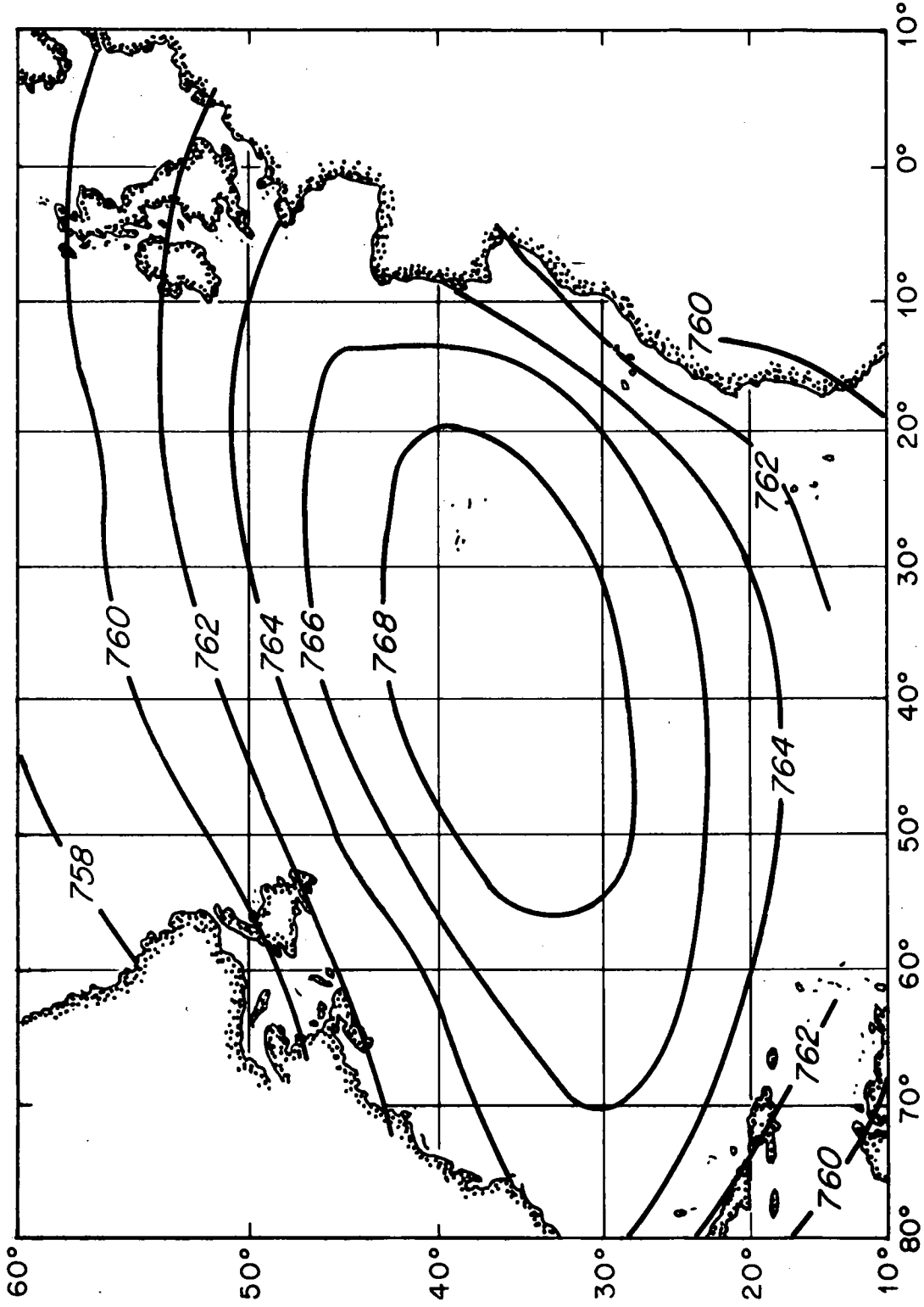


Figure 1.2a. July monthly mean surface atmospheric pressure in mb over North Atlantic Ocean after Fofonoff and Dobson (1963a).

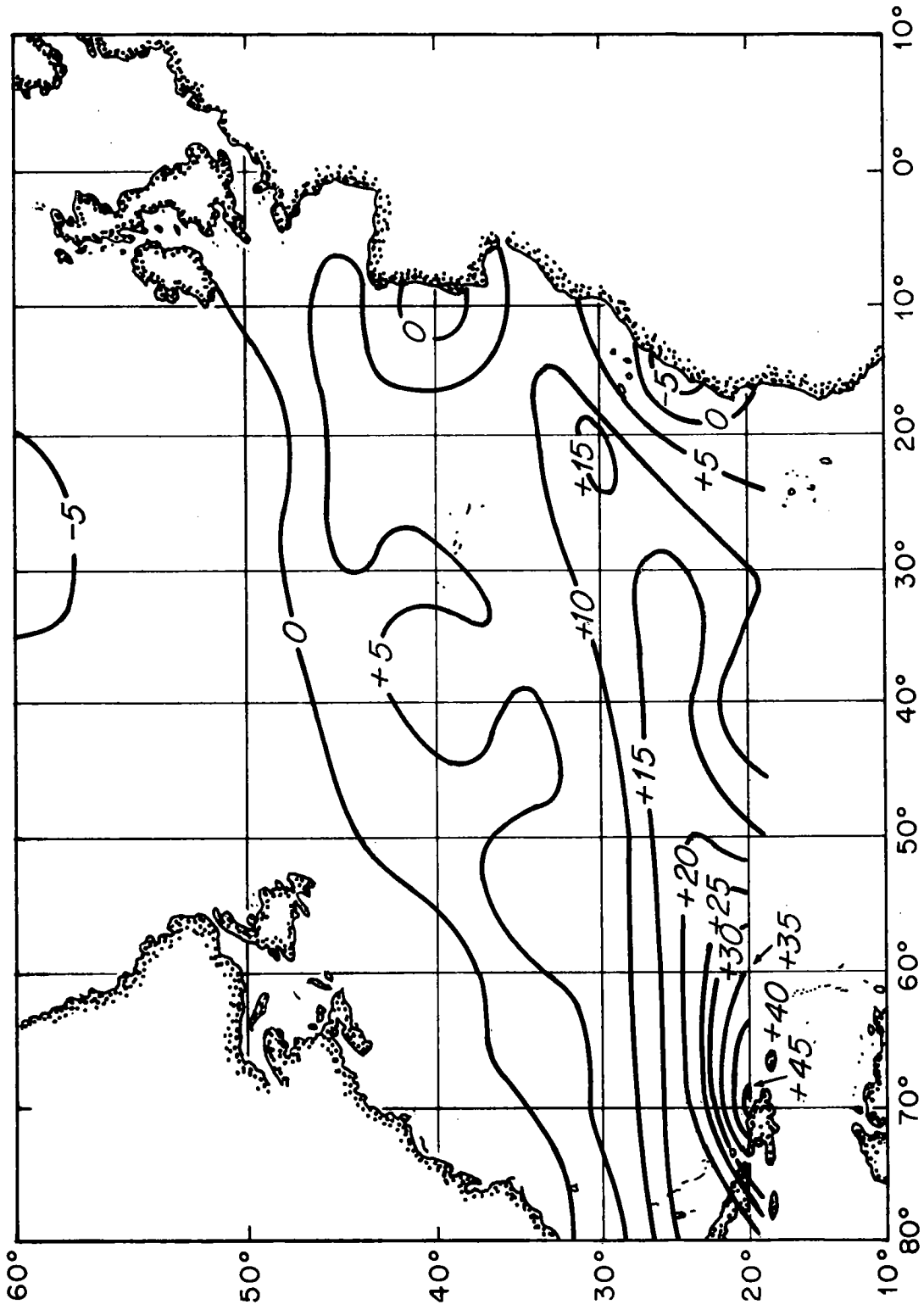


Figure 1.2b. July monthly mean convergence of the surface water in cm/day over the North Atlantic Ocean after Fofonoff and Dobson (1963a).

There are two interesting points of difference between the two studies. The first is the upwelling area along the African coast. In Montgomery's study, it was easy to take the coastal barrier into account while computing transports across sides of the square. In Fofonoff's study, no allowance for a coastal barrier is made. The difference is an "image" transport \tilde{U}_I required to bring Ekman transport to zero normal to the coast.

$$\tilde{U}_I \equiv (-U_E \cdot \hat{n})\hat{n} \quad 1.8)$$

Here \hat{n} is a unit vector normal to the coast pointing towards land. From 1.1), we can write

$$\tilde{U}_I = [\hat{k} \times \left(\frac{\tau}{f}\right) \cdot \hat{n}]\hat{n} = [\hat{n} \times \hat{k} \cdot \frac{\tau}{f}]\hat{n} = [-\hat{s} \cdot \frac{\tau}{f}]\hat{n} \quad 1.9)$$

Here \hat{s} is a unit vector tangential to the coast where $\hat{s} = \hat{k} \times \hat{n}$ is oriented so that it points north at the African coast. It is assumed that the circulation from this image current is confined to a narrow upwelling region near the eastern boundary. The interesting point is that the Fofonoff calculation estimates a slight upwelling area off the African coast without taking the image transport into account. The other interesting point of difference is in the high vertical

velocity in the southeast corner of the chart. This mean velocity is three times as large in the Fofonoff study as in the Montgomery study. It arises from a systematically larger estimation of the wind stress curl in the Fofonoff study than the equivalent quantity estimated in the Montgomery study.

A closer inspection of the convergence charts shows that Fofonoff's convergences are generally larger than Montgomery's, particularly in the maximum gradient region of the pressure cell south of the center of the cell. This difference when considered in conjunction with the large standard deviations in the Fofonoff study, points to the importance of the variable part of the wind to the mean value of the transports. The rectification of time varying pressure gradients by the non-linear stress formula accounts for a significant part of the mean transports.

During the last half of the 1960's, studies of oceanic wind stress were made by S. Hellerman (1965, 1967). These were done using the method of the Scripps study using data from the U. S. Navy Marine Climatic Atlas of the World (1955, 1958). These data were superior to those available to Scripps and Hidaka in that frequencies of wind speeds were presented for each wind rose as a function of direction. As part of this study (1965), the effect of various

estimates of C_D on western boundary current transports was investigated. These results will be repeated as part of chapter 3 of this study. In Hellerman's second study (1967), the work of Hidaka was repeated using the new Navy data. In addition, the net zonal stress was estimated and compared with both the Hidaka study and with studies estimating global zonal momentum transport from independent meteorological data. The agreement with the Hidaka study is excellent with a maximum difference of 0.3 dynes/cm². The agreement with the independent studies in the Northern hemisphere is almost as good (0.4 dynes/cm² maximum difference) under the assumption that mean zonal oceanic stresses at a given latitude are equal to mean continental zonal stresses at the same latitude. The value of C_D used in this balance was a function of wind speed introduced by Deacon, Sheppard, and Webb which is nearly a smoothing of the step function used by Scripps and Hidaka.

The rectification of time varying pressure gradients was further studied by Aagaard (1970) in a study of transports in the Greenland Sea using essentially the Fofonoff method. For comparisons with other studies, Aagaard used values of 1 for R_s , 1.1×10^{-3} for C_D and 17° for λ . He used six hourly weather charts of the Weather Bureau at Bergen reanalyzing them "whenever it was felt the original analyst had deviated unduly from

linear interpolation between pressure observations". The analysis points were on a square grid at $1\frac{2}{3}^\circ$ intervals in latitude and 5° intervals of longitude south of 72°N and 10° intervals north of 72°N . This comes to about 10×10^{-6} sec ϕ points per square kilometer south of 72°N and 5×10^{-6} sec ϕ points per square kilometer between 72°N and the northern extent of the study at 80°N . The abrupt change in scale is necessitated by the rapid change of sec ϕ in northern latitudes going from 2.4 at 65°N to 3.2 at 72°N and 5.8 at 80°N .

As a particular part of his study, Aagaard presented a series of charts of streamfunction over the Greenland and Norwegian seas. These charts, all for the month of February, 1965, differ only in that the sampling and averaging time used to compute the pressure field from which the wind stress curl is calculated was varied from 1 sample per month to 4 samples per day. These charts are reproduced as figure 1.3. Perhaps the most interesting feature of these charts is that the general shape of the streamlines is not dramatically affected by the sampling time, consisting in this case of two gyres. The strength of the gyres, in contrast, is a strong function of the sampling time. Because the shape of the flow seems not to change, the entire effect can be approximately described by a scalar response function.

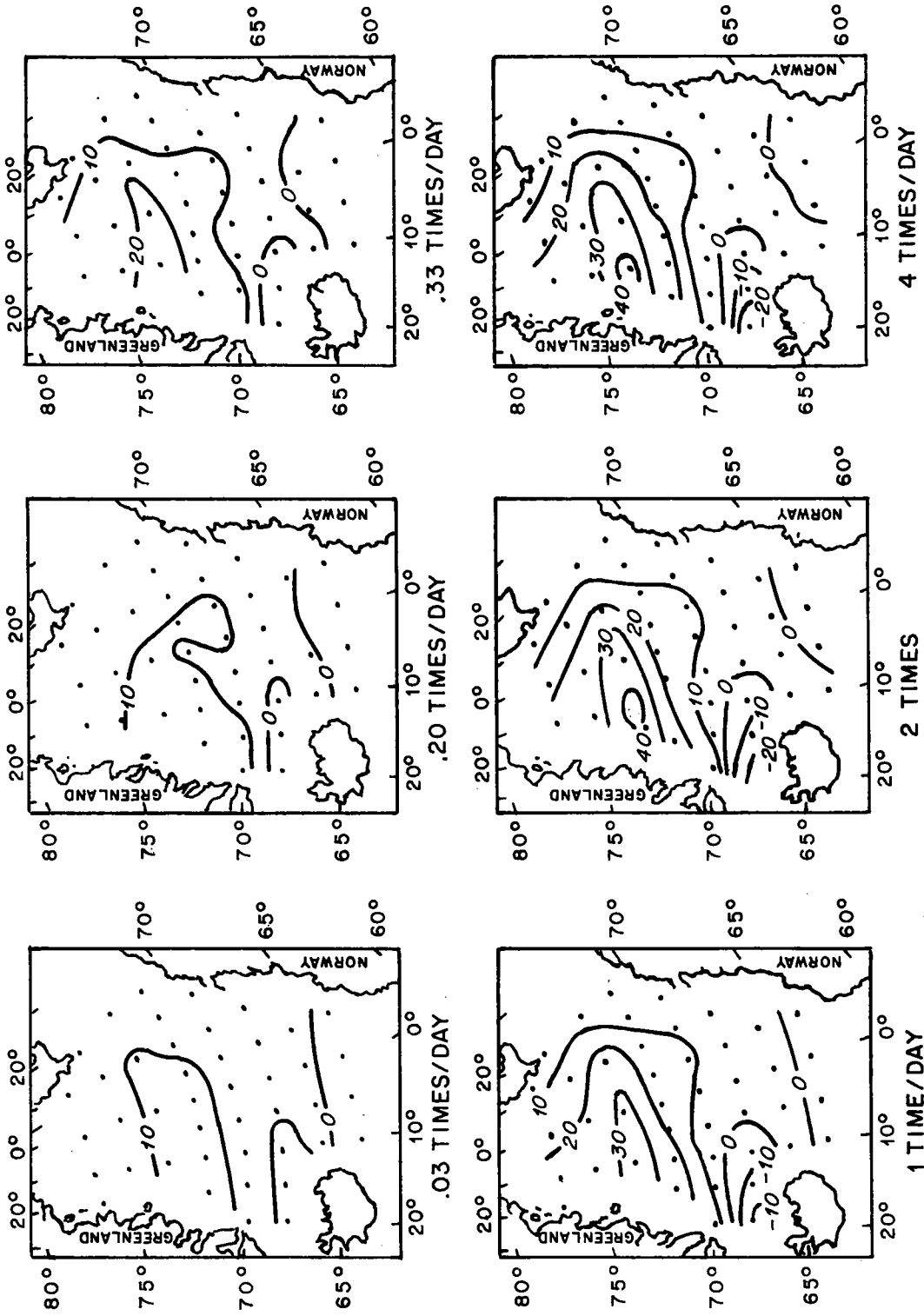


Figure 1.3. Calculated integrated transport for various averaging and sampling frequencies over the Greenland Sea during February, 1965 according to Aagaard (1970). The contour interval is 10 Sverdrups.

Such a function is shown as figure 1.4. In this figure, relative response is defined as the largest transport in each gyre as a fraction of the largest transport in that gyre at the highest sampling rate (4 samples per day). The conclusion drawn from this response curve is that frequent analyses are necessary to compute all the total transport using the Fofonoff method. The response curve seems to level off at 2 samples per day indicating that that frequency of sampling is sufficient to estimate 90% of the total mean transport. Conditions over the Greenland Sea in February are likely to be more variable than general oceanographic conditions. So Aagaard's study indicates that 2 samples per day are sufficient to calculate mean ocean transports from pressure analyses.

The various studies done to compute wind stress curl over the oceans are summarized in Table 1.1. Included in Table 1.1 are the comparable quantities used in the study which forms much of the rest of this work.

Before proceeding with another set of calculations of wind stress curl, the problem of verification should be mentioned. There are relatively few oceanic transports which have been established well enough to serve as a test or calibration of these calculations. If transports are integrated across entire oceans, they can be compared with the transports in western boundary currents, an idea first suggested by Munk (1950). Such comparisons

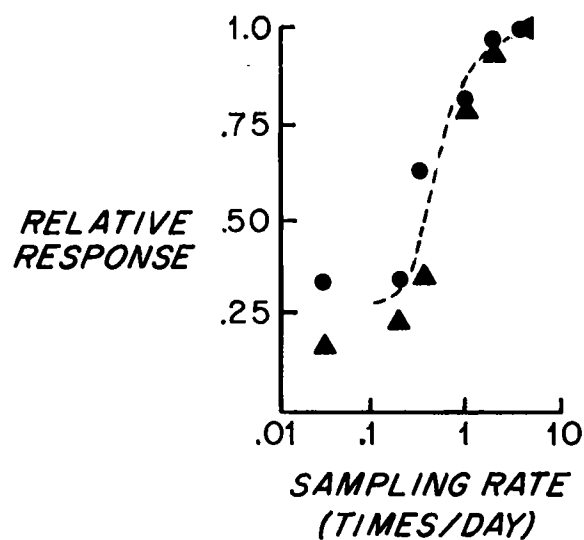


Figure 1.4. The response of the calculations shown in figure 1.3 to the frequency at which the pressure data are averaged and sampled before the wind stress curl is computed. The relative response of each gyre is defined as the ratio of the largest integrated transport in that gyre for a sampling frequency of 4 times/day to the largest transport for the sampling frequency in question. These ratios, represented by circles for the northern gyre and triangles for the southern gyre, are plotted as a function of the sampling rate on a log scale. The dashed line is an imaginary response function which might be approximated by the data.

Table 1.1

AUTHOR	YEAR	SOURCE DATA	R_s	λ	C_D	SAMPLE TIME	AREA DENSITY	GEOGRAPHICAL EXTENT	TEMPORAL EXTENT
Montgomery	1936	Pressure (Defant Atlas)	$2 \sin \lambda$	16.5° to 22°	2.4×10^{-3}	Climo.	3.2×10^{-6} sec ϕ	N. Atlantic	Climo.
Scripps	1948	Wind Pilot Charts	N.A.	N.A.	2.6×10^{-3} for $ u_g > 6.6 \text{ m/s}$ 0.8×10^{-3} for $ u_g < 6.6 \text{ m/s}$	Climo.	3.2×10^{-6} sec ϕ	N. Pacific	Climo.
Hidaka	1958	Wind Pilot Chart	N.A.	N.A.	Same as Scripps	Climo.	3.2×10^{-6} sec ϕ	World Ocean	Climo.
Fofonoff	1962	Pressure Monthly Means from U.S. W.B.	.7	15°	2.6×10^{-3}	1 mo.	1.6×10^{-6} sec ϕ	N. Atlantic N. Pacific $20^\circ \text{N} - 60^\circ \text{N}$	1950-60 N. Pacific study continued to present
Hellerman	1965 1967	Wind Navy Atlas Pilot Charts Polar Atlas	N.A.	N.A.	Various	Climo.	1.6×10^{-6} sec ϕ	World Ocean	Climo.
Aagaard	1970	Pressure 6-hr. analysis from Bergen W.B.	1	17°	1.1×10^{-3}	6 hrs. to 1 mo.	10×10^{-6} sec ϕ of 72°N 5×10^{-6} sec ϕ N of 72°N	Greenland and Norwegian Seas	1965
Welch	1971	Pressure 12-hr. ave. from U.S.W.B.	.7	15°	2.6×10^{-3}	12 hrs.	$\frac{24 \times 10^{-6}}{(1 + \sin \phi)^2}$	Parts of Oceans north of 20°N	1968-69 1959

agree moderately well with the shapes of western boundary transport vs. latitude curves, but the numbers are not good enough to be more than a general indicator. Another possible verification procedure is to try to calculate time dependent wind driven circulations. A calculation of this type was done by Fofonoff (1962). Such a verification is not so dependent on absolute scales as mean value comparisons, but the incomplete state of time dependent circulation theory as well as the lack of time series of oceanic variables makes such verifications difficult. Some kind of verification is necessary if the wind stress calculations are to be improved, and some attempts at this are made in later sections.

The rest of this study is arranged in several sections. The next chapter is concerned with development of a formula and a corresponding numerical calculation scheme which can be used to estimate wind stress curl directly from synoptic analyses of sea level pressure. The formula is first developed in a coordinate free notation and then a finite difference scheme is fitted to it. The sensitivity of the formula to various parameters and input noise is then estimated in certain easily recognizable pressure patterns. Several examples are then constructed and the formula evaluated for each of them.

Chapter 3 consists of the calculation of several statistical properties of wind driven ocean circulation as estimated using the formula with actual analyses. Included in this chapter are estimates of transport in the major gyres of the North Pacific Ocean. In addition histograms are calculated for various zonal bands over the North Atlantic and North Pacific Oceans. The non-Gaussian nature of the wind stress curl is noted and some difficulties associated with a particular distribution resembling the experimental distribution are noted.

In chapter 4, several calculations are performed to investigate the validity of the calculation technique. Geostrophic winds are calculated from the pressure analyses and compared to climatological values and also to a particular anemometer record which is independent of the analyses. Next a brief study is made to determine the effect of a possible spatial sampling rectification effect analagous to the time sampling effect studied by Aagaard. Finally, a specific comparison is made with the Canadian Fisheries Research Board calculations for 1968 in the Pacific Ocean.

The last two chapters consist of two time dependent experiments. The first is a time series analysis of computed wind stress curl and pressure at Bermuda compared with the recorded sea level during portions of the years

1968 and 1969. Finally, a comparison is made between instantaneous transports computed during 1959 in the Labrador Current from pressure data and the behavior of icebergs observed in the Labrador Current by the International Ice Patrol.

CHAPTER II

In the introductory chapter, the importance of the field of wind stress curl in ocean circulation theory is emphasized. Next, we shall derive a single equation incorporating the elements of the Fofonoff method into a single equation relating surface atmospheric pressure to wind stress curl. For this calculation, the stress is assumed to satisfy equation 1.4, the square law stress formula. The shrinking constant, R_s , and veering angle, λ , are considered as constants. The surface wind can then be analyzed into a geostrophic component and an ageostrophic component.

$$\underline{U}_s = \frac{R_s}{\rho_a f} [\hat{k} \times \nabla p \cos \lambda - \nabla p \sin \lambda] \quad (2.1)$$

The magnitude of \underline{U}_s is then

$$|\underline{U}_s| = \frac{R_s}{\rho_a f} |\nabla p| \quad (2.2)$$

and the stress becomes

$$\underline{\tau} = \frac{R_s^2 C_D}{\rho_a f^2} |\nabla p| (\hat{k} \times \nabla p \cos \lambda - \nabla p \sin \lambda) \quad (2.3)$$

Taking the vertical component of the curl of this expression

is straightforward but complicated, partly because f is a function of latitude. The result is

$$\hat{k} \cdot \nabla \times \underline{\tau} = \frac{R_s C_D}{\rho_a f^2} \{ \cos \lambda (\nabla - \frac{2}{f} \nabla f) \cdot |\nabla p| \nabla p - \sin \lambda \hat{k} \cdot (\nabla - \frac{2}{f} \nabla f) \times |\nabla p| \nabla p \}. \quad (2.4)$$

An interesting point is that the stress and its curl both depend on pressure only through the vector square gradient $|\nabla p| \nabla p$ mimicking the stress law (1.4). The formula for the curl (2.4) is particularly simple consisting of a single operator $(\nabla - \frac{2}{f} \nabla f)$ dotted and crossed with the vector square pressure gradient.

In order to evaluate this formula and presumably others which might describe oceanic driving terms, it is necessary to develop a facility for estimating synoptic values of meteorological variables and their partial derivatives. The scheme for doing this is based partly on the availability of synoptic data on computer tapes.

Data for surface atmospheric pressure (or equivalently 1000 mb height) were obtained from NCAR. These data were accepted fairly uncritically as a reasonable basis from which to attempt computation of wind stress curl terms for the following reasons: These data are the same as those used for running the NOAA numerical weather forecasts. The success of these forecasts depends crucially on the accuracy and adequacy of the 1000 mb height field. One of

the required constraints on the data is that they have high enough resolution to make them suitable for a reasonable specification of the weather fields. The data received over the North Atlantic Ocean with its well travelled shipping lanes are probably the best oceanic data from this standpoint. As a measure of the general accuracy of the objective analyses, NOAA calculates the analyzed wind velocity at selected observation sites and forms the vector differences. (U. S. Department of Commerce, 1971). For February, 1971 at the 850 mb pressure level, the RMS vector error was about 3.2 meters per second. The 850 mb pressure surface is about at a height of 1.5 km from the surface.

The general strategy followed was first to derive a formula analytically relating the wind stress curl to the sea level atmospheric pressure (or 1000 mb height), then to transform the coordinate system to one for which the axes were those of the analysis grid (computer coordinates) rather than physical coordinates, and finally to express various finite difference formulas in the computer coordinates directly. Details of this approach follow.

The projection used in the NOAA analysis is a stereographic projection overlaid with a rectangular grid. This particular stereographic projection is aligned so that the plane of projection is perpendicular to the axis of the

earth (figure 2.1a). The rays of the projection all originate at the South Pole (S). The plane of projection is passed perpendicular to the axis of the earth through the 60°N latitude circle as a matter of definiteness. The position of the plane turns out not to matter as long as it remains perpendicular to the axis. The coordinates of the projection are an intermediate set of coordinates (x,y) which are still dimensional.

From the figure we have a point P on the earth with north latitude ϕ and east longitude θ projected onto the plane at P' whose coordinates are (x',y'). If the distance from the South Pole to the projection plane is called R', then the point P' is a distance $R' \tan \alpha$ from the axis. Let this distance be called r. Now, letting the x axis be coplanar with the 10°E longitude arc, we can write

$$x' = r \cos(\theta - 10^\circ)$$

$$y' = r \sin(\theta - 10^\circ)$$

The angle α is determined by noting that as line segments SC and CP are earth radii, they are equal so that CPS is an isosceles triangle and angle α equals angle γ . But $\alpha + \gamma + \phi + 90^\circ = 180^\circ$ as the sum of the angles of CPS. So we have

$$\alpha = \frac{90^\circ - \phi}{2}$$

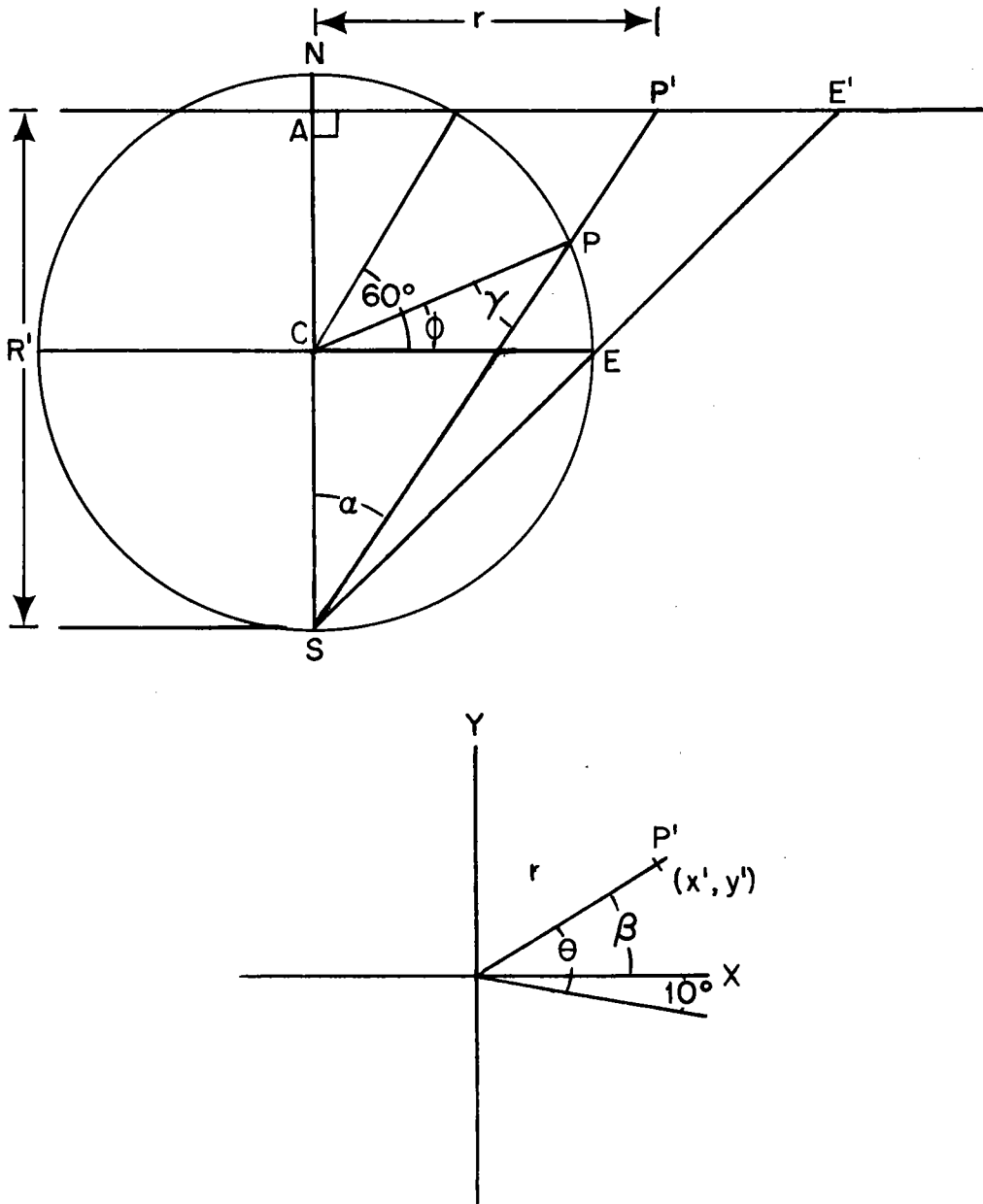


Figure 2.1a. The relationship among the quantities defined in the text and used for transforming physical coordinates to computer coordinates.

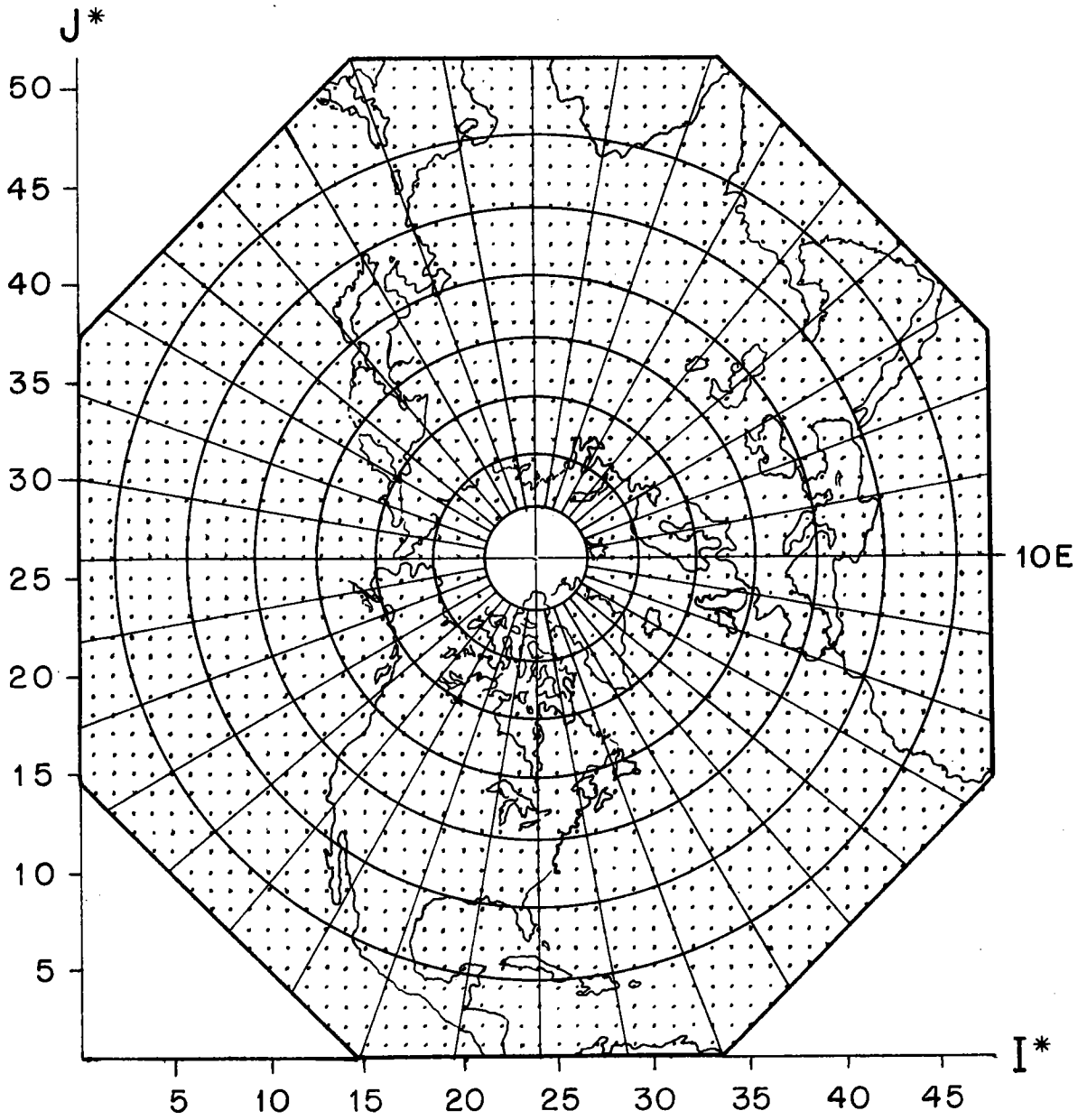


Figure 2.1b. The relationship between the NMC 51x47 computer addressable grid and a polar stereographic projection of the northern hemisphere.

and hence we can write

$$x' = R' \tan \left[\frac{90^\circ - \phi}{2} \right] \cos (\theta - 10^\circ) \quad 2.5a)$$

$$y' = R' \tan \left[\frac{90^\circ - \phi}{2} \right] \sin (\theta - 10^\circ) \quad 2.5b)$$

relating the projected coordinates to the spherical ones. To complete the transformation, we note that if $\phi = 0$, then $AE' = R'$ because triangle SCE' and hence SAE' is a right isosceles triangle. This allows us to non-dimensionalize the new coordinates. The non-dimensionalization and scaling is chosen such that the new scales are incremented by a unit when the projected distance is one grid length. Because on the NCAR projection there are 31 gridlengths between the projected pole and the projected equator, we choose

$$I = \frac{31x'}{R'}$$

$$J = \frac{31y'}{R'}$$

substituting this scale in equation 2.5 gives

$$I = 31 \tan \left[\frac{90^\circ - \phi}{2} \right] \cos (\theta - 10^\circ) \quad 2.6a)$$

$$J = 31 \tan \left[\frac{90^\circ - \phi}{2} \right] \sin (\theta - 10^\circ) \quad 2.6b)$$

with the inverse transformations

$$\phi = 90^\circ - 2 \tan^{-1} \left[\frac{(I^2 + J^2)^{\frac{1}{2}}}{3I} \right] \quad 2.7a)$$

$$\theta = 10^\circ + \tan^{-1} \left[\frac{J}{I} \right] \quad 2.7b)$$

The inverse tangent in the last equation is defined in the four quadrant sense considering the signs of both numerator and denominator (Appendix I). Finally if two coordinates are defined by the translation $I^* = I+24, J^* = J+26$, we note that the gridpoints can be addressed directly from an array (shown in figure 2.1b) stored in a computer using the FORTRAN language.

The scale lengths of the I and J coordinates are both the same given by

$$h_I = h_J = \frac{62R}{I^2+J^2+961} = \frac{R}{3I} (1+\sin \phi) \quad 2.8)$$

Thus the mapping from the earth's surface to the computer coordinates is a conformal one. As such, it preserves angles, an important consideration when representing vectors for example. The distance between gridpoints decreases by a factor of two between the pole and the equator, and the area of a grid square therefore decreases by a factor of four. The equatorial grid spacing is 205 km. Further information about the transformation is given in appendix I.

With the coordinate transformation formulas in hand, the physical equations can now be set over into computer coordinates directly and partial derivatives with respect to computer coordinates. The next step will be to obtain finite difference formulas for the partial derivatives in terms of the values at the computer coordinate intersections. An important result of this transformation is that the final finite difference formulas are independent of position on the grid. To illustrate the technique, the geostrophic wind formula is set over into computer coordinates below.

The geostrophic wind velocity is

$$\vec{U}_g = \frac{g}{2\Omega \sin \phi} \hat{k} \times \nabla h \quad (2.9)$$

To transform to computer coordinates, we note from appendix I that

$$\sin \phi = \frac{961 - r_I^2}{961 + r_I^2} \text{ where } r_I^2 = I^2 + J^2 \quad (I-7)$$

and

$$\nabla h = \frac{961 + r_I^2}{62R} \nabla_I h \quad (I-16)$$

Inserting these relations into equation 2.9 gives the transformed equation

$$\vec{U}_g = \frac{g}{124\Omega R} \frac{(961 + r_I^2)^2}{961 - r_I^2} \hat{k} \times \nabla_I h. \quad (2.10)$$

The magnitude of the geostrophic wind is

$$|\underline{U}_g| = \frac{g}{124\Omega R} \frac{(961 + r_I^2)^2}{961 - r_I^2} |\nabla_I h| \quad (2.11)$$

In these formulas, the singularity at $r_I^2 = 961$ corresponds to the singularity in the geostrophic wind at the equator.

The important formula to be transformed is the one for the curl of the wind stress, which is rewritten here in terms of the 1000 mb height.

$$\hat{k} \cdot \nabla \times \underline{\tau} = \frac{R_s^2 \rho_a C_D g^2}{4\Omega^2 \sin^2 \phi} \left\{ \cos \lambda (\nabla - \frac{2}{f} \nabla f) \cdot \hat{k} \cdot \sin \lambda (\nabla - \frac{2}{f} \nabla f) \times \right\} \otimes |\nabla h| \nabla h \quad (2.12)$$

This formula can be directly transformed to computer coordinates yielding the following complicated expression:

$$\begin{aligned} \hat{k} \cdot \nabla \times \underline{\tau} = & \frac{R_s^2 \rho_a C_D g^2}{124\Omega^2 R^3} \frac{(961+r_I^2)^4}{(961-r_I^2)^2} \cdot |\nabla_I h|. \\ & \left\{ \left[\frac{(961+r_I^2)}{8.31^2} \right] \left[\frac{1}{|\nabla_I h|^2} \left\{ \cos \lambda \left\{ \left[\frac{\partial h}{\partial I} \right]^2 \frac{\partial^2 h}{\partial I^2} + 2 \frac{\partial h}{\partial I} \frac{\partial h}{\partial J} \frac{\partial^2 h}{\partial I \partial J} + \left[\frac{\partial h}{\partial J} \right]^2 \frac{\partial^2 h}{\partial J^2} \right\} \right. \right. \right. \\ & \left. \left. - \sin \lambda \left\{ \frac{\partial h}{\partial I} \frac{\partial h}{\partial J} \left[\frac{\partial^2 h}{\partial I^2} - \frac{\partial^2 h}{\partial J^2} \right] + \frac{\partial^2 h}{\partial I \partial J} \left[\left(\frac{\partial h}{\partial J} \right)^2 - \left(\frac{\partial h}{\partial I} \right)^2 \right] \right\} \right] \right. \\ & \left. + \left(\frac{\partial^2 h}{\partial I^2} + \frac{\partial^2 h}{\partial J^2} \right) \cos \lambda \right\} \\ & + \frac{1}{(961-r_I^2)} \left[\cos \lambda \left(I \frac{\partial h}{\partial I} + J \frac{\partial h}{\partial J} \right) - \sin \lambda \left(I \frac{\partial h}{\partial J} - J \frac{\partial h}{\partial I} \right) \right] \end{aligned} \quad (2.13)$$

The physical significance of the various terms in this complicated expression can be seen if we consider a special case in which $\frac{\partial h}{\partial J} > 0$ and $\frac{\partial h}{\partial I} = 0$. Keeping the same parentheses, we get a "principal axis" representation:

$$\hat{k} \cdot \nabla \times \underline{\tau} = \frac{R^2 \rho_a C_D g^2}{124 \Omega^2 R^3} \frac{(961 + r_I^2)^4}{(961 - r_I^2)^2} |\nabla_I h|.$$

$$\left\{ \left[\frac{961 + r_I^2}{8.31^2} \right] \left[\cos \lambda \frac{\partial^2 h}{\partial J^2} - \sin \lambda \frac{\partial^2 h}{\partial I \partial J} \right] \right. \quad (a)$$

$$\left. + \cos \lambda \left[\frac{\partial^2 h}{\partial I^2} + \frac{\partial^2 h}{\partial J^2} \right] \right\} \quad (b)$$

$$+ \frac{1}{(961 - r_I^2)} \left[\cos \lambda J \frac{\partial h}{\partial J} - \sin \lambda I \frac{\partial h}{\partial J} \right] \quad (c)$$

2.14)

With this special form, the terms grouped as (a) are identified with the shear of the surface wind. The terms grouped as (b) are identified with the curvature of the surface wind. Finally, the terms grouped as (c) are identified with the β effect. That is, if a constant pressure gradient is maintained over a range of latitudes, the geostrophic winds will be stronger at the southern part of the range than at the northern part. This will result in an additional shear term in the wind stress curl.

Finally, the curl formula can be written in a form where the physical terms get mixed together, but the effect

of the various terms mathematically can be assessed.

First, we define a slope parameter S and an angle α by

$$S = |\nabla_I h|$$

$$\cos \alpha = \frac{\frac{\partial h}{\partial I}}{S} \quad 2.15)$$

$$\sin \alpha = \frac{\frac{\partial h}{\partial J}}{S}$$

This definition is convenient because in the curl formula, all the first derivative factors which multiply second derivative terms in h occur in just such combinations. Geometrically, α is the angle which the height gradient makes with the positive I axis. If we use again the angle $\beta = \theta - 10^\circ$, and a little trigonometry, the curl formula can be expressed as

$$\hat{k} \cdot \nabla \times \underline{I} = \frac{R_S^2 \rho_a C_D g^2}{124 \Omega^2 R^3} \frac{(961 + r_I^2)^4}{(961 - r_I^2)} \cdot S \cdot$$

$$\left\{ \frac{961 + r_I^2}{16.31^2} \left[\cos(2\alpha + \lambda) \left(\frac{\partial^2 h}{\partial I^2} - \frac{\partial^2 h}{\partial J^2} \right) + 2 \sin(2\alpha + \lambda) \frac{\partial^2 h}{\partial I \partial J} + 3 \cos \lambda \left(\frac{\partial^2 h}{\partial I^2} + \frac{\partial^2 h}{\partial J^2} \right) \right] \right.$$

$$\left. + \frac{S r_I}{961 - r_I^2} \cos(\alpha + \lambda - \beta) \right\} \cdot \quad 2.16)$$

This formula can be simplified still more by interpreting the combinations of second derivatives geometrically. Let

us return, for the moment, to the Taylor series expansion of the h field in two dimensions.

$$h = h_0 + \frac{\partial h}{\partial I} \Delta I + \frac{\partial h}{\partial J} \Delta J + \frac{1}{2} \left[\frac{\partial^2 h}{\partial I^2} (\Delta I)^2 + 2 \frac{\partial^2 h}{\partial I \partial J} \Delta I \Delta J + \frac{\partial^2 h}{\partial J^2} (\Delta J)^2 \right] + O(\Delta I^3, \Delta J^3) \quad (2.17)$$

We can rewrite this expansion in terms of a mean value h_0 , a slope and its associated angle S and α , a bulginess parameter B related to the Laplacian

$$B = \frac{1}{2} \left(\frac{\partial^2 h}{\partial I^2} + \frac{\partial^2 h}{\partial J^2} \right) \quad (2.18)$$

and whatever else is left over. This results in

$$h = h_0 + S(\Delta I \cos \alpha + \Delta J \sin \alpha) + \frac{1}{2} B(\Delta I^2 + \Delta J^2) + \frac{1}{4} \left(\frac{\partial^2 h}{\partial I^2} - \frac{\partial^2 h}{\partial J^2} \right) (\Delta I^2 - \Delta J^2) + \frac{\partial^2 h}{\partial I \partial J} (\Delta I \Delta J) + O(\Delta I^3, \Delta J^3). \quad (2.19)$$

The second order left-over terms can be represented by an amplitude C and an angle δ as follows:

$$C = \left\{ \left[\frac{1}{2} \left(\frac{\partial^2 h}{\partial I^2} - \frac{\partial^2 h}{\partial J^2} \right) \right]^2 + \left[\frac{\partial^2 h}{\partial I \partial J} \right]^2 \right\}^{\frac{1}{2}} \quad (2.20)$$

$$\cos 2\delta = \frac{1}{2C} \left[\frac{\partial^2 h}{\partial I^2} - \frac{\partial^2 h}{\partial J^2} \right] \quad 2.21a)$$

$$\sin 2\delta = \frac{1}{C} \frac{\partial^2 h}{\partial I \partial J} \quad 2.21b)$$

The interpretation of C is similar to B . At a point, B represents the amount which the two dimensional field bulges in or out. Similarly, C represents the amount which the two dimensional field resembles a saddle or a col. Accordingly, in the absence of a comprehensive geometrical dictionary, I have called it "colity". The angle δ is the angle which the principal axis of the saddle makes with the positive I axis. Thus, we can rewrite the second order expansion of a two dimensional scalar field about a point in the form

$$h = h_0 + S(\Delta I \cos \alpha + \Delta J \sin \alpha) + \frac{1}{2}B(\Delta I^2 + \Delta J^2) + \frac{1}{2}C[(\Delta I^2 - \Delta J^2) \cos 2\delta + 2\Delta I \Delta J \sin 2\delta] + \dots \quad 2.22)$$

This form, in terms of four amplitudes and two angles has the advantage that the amplitudes are invariant under coordinate rotation. Now, we apply this expansion to the formula for the curl of the wind stress and get

$$\hat{k} \cdot \nabla \times \underline{\tau} = \frac{R_s^2 \rho_a C_D g^2}{124 \Omega^2 R^3} \frac{(961 + r_1^2)^4}{(961 - r_1^2)^2} \cdot S.$$

$$\left\{ \frac{961+r_I^2}{8.31} [C(\cos(2\alpha+\lambda)\cos 2\delta + \sin(2\alpha+\lambda)\sin 2\delta) + 3B\cos\lambda] \right. \\ \left. + \frac{r_I}{961-r_I^2} \cos(\alpha-\beta+\lambda)S \right\} \quad 2.23)$$

The trigonometrical factors of C are now clearly in the form of the formula for the difference of two angles and we get

$$\hat{k} \cdot \nabla \times \underline{v} = \frac{R_S^2 \rho_a C_D g^2}{124 \Omega^2 R^3} \frac{(961+r_I^2)^4}{(961-r_I^2)^2} \cdot S.$$

$$\left\{ \frac{961+r_I^2}{8.31^2} [C \cos[2(\alpha-\delta)+\lambda] + 3B\cos\lambda] + \frac{r_I}{961-r_I^2} S \cos(\alpha-\beta+\lambda) \right\}. 2.24)$$

In this form, it is apparent that the curl formula is independent of the coordinate system depending only on the latitude, the angle at which the surface wind crosses latitude lines ($\alpha-\beta$), the angle between the principal axes of the slope and the colity of the height field ($\alpha-\delta$) and the magnitude of the three shape amplitudes, slope S, bulginess B, and colity C.

The next step in developing a numerical formula is to choose a finite difference scheme with which to approximate the first and second derivative terms in the curl formula. One way to develop such a finite difference scheme is to expand the height field around a given point in a Taylor series keeping terms up to second order only.

The resulting quadratic formula is then chosen to obtain a least-squares fit to a set of gridpoints near the point in question. This approach was used for this study with a few modifications. When this was done, the curl equation still looked like equation 2.13 as equation 2.24 had not been developed. It would not surprise me if an approach based on this form were to yield a more elegant set of finite difference formulas.

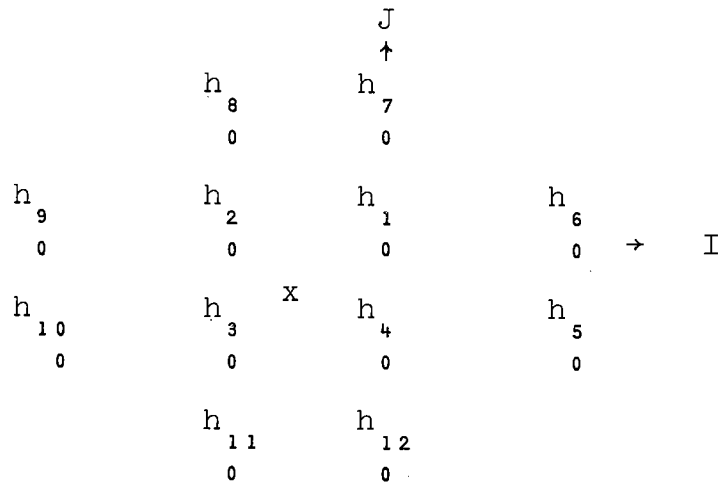
The only constraint on the local grid used to apply the least squares approach is that there be more points than there are constants to be determined arranged so that the equations are not underspecified. In this case, the minimum grid size permissible is 6 points with at least 1 three-point line in each of two primary directions and at least 1 point off those lines. With this constraint, many possible finite difference schemes are still allowable. To reduce this number still further, an arbitrary constraint was added. The grid was required to be symmetrical under reflections about the two major axes and the two primary diagonal axes. Several grids were discovered meeting these requirements and still having relatively few points. These and the tests performed to choose between them are discussed in appendix II.

The final scheme chosen is one in which the 12 point least squares formulas are used to estimate the second

derivatives while only the four center points are used to estimate the first derivatives. Although the scheme seems to behave the best of several tried, there is no proof that is optimal. It can in all likelihood be improved upon.

The final grid used in calculations and its finite difference formulas are given on the following page.

FINITE DIFFERENCE GRID



FINITE DIFFERENCE FORMULAS

$$\frac{\partial h}{\partial I} = (h_1 - h_2 - h_3 + h_4) / 2 \quad (2.25a)$$

$$\frac{\partial h}{\partial J} = (h_1 + h_2 - h_3 - h_4) / 2 \quad (2.25b)$$

$$\frac{\partial^2 h}{\partial I^2} = (-h_1 - h_2 - h_3 - h_4 + h_5 + h_6 + h_9 + h_{10}) / 4 \quad (2.25c)$$

$$\frac{\partial^2 h}{\partial I \partial J} = (h_1 - h_2 + h_3 - h_4 + 3(-h_5 + h_6 + h_7 - h_8 - h_9 + h_{10} + h_{11} - h_{12})) / 19 \quad (2.25d)$$

$$\frac{\partial^2 h}{\partial J^2} = (-h_1 - h_2 - h_3 - h_4 + h_7 + h_8 + h_{11} + h_{12}) / 4 \quad (2.25e)$$

Equation 2.24 is in a form convenient for analysis of sensitivity to various parameters in the problem and noise in the input pressure field. For added convenience, the equation will be rewritten as

$$\hat{k} \cdot \nabla \times \underline{I} = \frac{R_s^2 \rho_a C_D g^2}{32 \cdot 31^2 \Omega^2 R^3} \frac{(961 + r_I^2)^5}{(961 - r_I^2)} \cdot S \cdot \left\{ C \cos[2(\alpha - \delta) + \lambda] \right. \\ \left. + 3B \cos \lambda + MS \cos(\alpha - \beta + \lambda) \right\} \quad (2.26)$$

Here M gives the ratio between the shear and curvature contributions and the β -plane contribution.

$$M = \frac{r_I}{961 - r_I^2} \cdot \frac{8 \cdot 31^2}{961 + r_I^2} = \frac{8 \cdot 31^2 r_I}{(961^2 - r_I^4)} \quad (2.27)$$

Now let ϵ be the fractional equatorial radius of a given point in computer coordinates.

$$\epsilon = \frac{r_I}{31} = \tan\left(\frac{90^\circ - \phi}{2}\right)$$

Then we have

$$M = \frac{8 \cdot 31^2 \cdot 31 \epsilon}{31^4 (1 - \epsilon^4)} = \frac{8}{31} \frac{\epsilon}{(1 - \epsilon^4)} \quad (2.28)$$

This function varies quite rapidly from ∞ at the equator to .4 at $10^\circ N$, .1 at $45^\circ N$ and 0 at the pole.

The form of equation 2.26) in terms of dependence is

$$\hat{k} \cdot \nabla \times \underline{\tau} = F_1 \times F_2 \times S \times (F_3 + MF_4). \quad (2.29)$$

Here F_1 , is a function only of various physical parameters and constants, F_2 and M depend only on the radius of the position (r_I), S depends only on the input field, and F_3 and F_4 depend only on the input field and the veering angle. The dependence of the wind stress curl on R_s and C_D then is entirely through term F_1

$$F_1 = \frac{R_s^2 \rho_a C_D g^2}{124 \Omega^2 R^3} \quad (2.30)$$

F_1 is linear in C_D and quadratic in R_s . So if C_D has a small percentage error, the wind stress curl will have the same percentage error, if R_s has a small percentage error, the wind stress curl will have twice that percentage error.

The sensitivity of the curl formula to small changes in veering angle is slightly more complicated. To discuss this, let $F_3 + MF_4$ be denoted by E , which contains all the λ dependence in the curl formula. The relative sensitivity of E on λ would ordinarily be given by

$$\left\langle \frac{\frac{\partial E}{\partial \lambda}}{E} \right\rangle$$

but that is not really appropriate for the following reason. In a case where the divergence of \underline{v} is large compared to the curl of \underline{v} , such as can occur in a narrow neck between a high and low pressure area, a small change in λ can serve to change the relative size of curl \underline{v} greatly, even reversing its sign. If the above expression is evaluated, these situations will dominate the calculations. But in any actual calculation using the curl formula, these situations are not important for the reason that the curl is small. A more comprehensive measure of the sensitivity of the formula is given by

$$\left| \frac{\left\langle \frac{\partial E}{\partial \lambda} \right\rangle}{\left\langle E \right\rangle} \right| \quad 2.31)$$

where the brackets denote an ensemble average over a large number of weather maps. This expression is given by

$$\left| \frac{\left\langle \frac{\partial E}{\partial \lambda} \right\rangle}{\left\langle E \right\rangle} \right| = \frac{\left| \left\langle -C \sin[2(\alpha - \delta) + \lambda] - 3B \sin \lambda - M S \sin(\alpha - \beta + \lambda) \right\rangle \right|}{\left| \left\langle C \cos[2(\alpha - \delta) + \lambda] + 3B \cos \lambda + M S \cos(\alpha - \beta + \lambda) \right\rangle \right|} \quad 2.32)$$

Now if we assume that the angles between the slope and the colity and between the slope and the parallels of latitude

are distributed uniformly from 0 - 360°, an assumption which I imagine is well borne out in the middle and high latitudes, the expected value of the trigonometric functions of those angles is 0. This gives

$$\left| \frac{\langle \frac{\partial E}{\partial \lambda} \rangle}{\langle E \rangle} \right| = \tan \lambda \quad 2.33)$$

Now λ is usually a small angle, so we can use $\tan \lambda \approx \lambda$.

If we take $\lambda = 15^\circ = .26$ radians and $\Delta\lambda = 10^\circ = .17$ radians, this measure of sensitivity gives about a 5% change in the curl for a 10° change in the veering angle. This result agrees essentially with an analysis of the λ dependence by Fofonoff (1962). Fofonoff shows that $\langle E(\lambda) \rangle = \langle E(0) \rangle \cos \lambda$ to a moderately good approximation. Thus

$$\frac{\partial \langle E \rangle}{\partial \lambda} = - \langle E(0) \rangle \sin \lambda$$

and

$$\left| \frac{1}{\langle E \rangle} \left\langle \frac{\partial E}{\partial \lambda} \right\rangle \right| = \left| \frac{-\langle E(0) \rangle \sin \lambda}{\langle E(0) \rangle \cos \lambda} \right| = \tan \lambda \quad 2.34)$$

The final sensitivity analysis for the curl formula will be to estimate the effect on a single estimate of wind stress curl of a random error in each of the pressure analyses. If the random error in the 1000 mb height field is Gaussian and independent at each point with a variance

of σ_h^2 , we can write

$$\sigma_{\hat{k} \cdot \text{curl} \underline{\tau}}^2 = \sigma_h^2 \sum_{j=1}^N \left[\frac{\partial}{\partial h_j} (\hat{k} \cdot \text{curl} \underline{\tau}) \right]^2 \quad 2.35)$$

Now, from equation 2.29, we have the part of the formula which depends on 1000 mb height estimates as

$$G = S [F_3 + MF_4] \quad 2.36)$$

To simplify the calculation somewhat, the finite difference formula for the cross derivation has been altered somewhat in the calculation of colity. We have, from 2.20)

$$C = \left\{ \left[\frac{1}{2} \left(\frac{\partial^2 h}{\partial I^2} - \frac{\partial^2 h}{\partial J^2} \right) \right]^2 + \left[\frac{\partial^2 h}{\partial I \partial J} \right]^2 \right\}^{\frac{1}{2}}$$

Using the finite difference formulas, the combination $\frac{\partial^2 h}{\partial I^2} - \frac{\partial^2 h}{\partial J^2}$ is given in terms of the outer h's only ($h_5 - h_{12}$).

It is certainly more convenient and may even be more consistent to express the cross derivative in terms also of the outer h's. If this is done and the resulting formula is required to represent a quadratic field exactly, the cross derivative becomes

$$\frac{\partial^2 h}{\partial I \partial J} = \frac{1}{6} (-h_5 + h_6 + h_7 - h_8 - h_9 + h_{10} + h_{11} - h_{12}) \quad 2.37)$$

It is seen that the weights of the inner h's (h_1-h_4) have gone from 1 to 0 and that the weights given the outer h's increase only from $\frac{3}{19}$ to $\frac{3}{18}$ to compensate. With this modification, the colity C and its angle δ are functions only of the outer h's. The slope S and its angle α are functions of only the inner h's. Finally, the "bulginess" B which appears in a simple manner is a function of all the h's.

Now these 5 parameters are related to the partial derivatives in equation 2.15, 2.18, 2.20, and 2.21. The partial derivatives are related to the height analysis points in equations 2.25 and 2.37. Finally, the curl formula is related to the 5 parameters in equation 2.26, the essential part of which is called G. This allows us to write equations for $\frac{\partial G}{\partial h_i}$, and $\frac{\partial G}{\partial h_o}$ in terms of the amplitudes and some simple functions of the analysis point positions (1-12). In particular

$$G = S(h_i)[C(h_o)\cos[2\alpha(h_i)-2\delta(h_o)+\lambda]+3B(h_i,h_o)\cos\lambda + MS(h_i)\cos[\alpha(h_i)-\beta+\lambda]] \quad 2.38)$$

$$\begin{aligned} \text{so } \frac{\partial G}{\partial h_i} &= \frac{\partial S}{\partial h_i}[C\cos(2\alpha-2\delta+\lambda)+3B\cos\lambda+MS\cos(\alpha-\beta+\lambda)] \\ &+ S[-C\sin(2\alpha-2\delta+\lambda) \cdot 2\frac{\partial\alpha}{\partial h_i} + 3\frac{\partial B}{\partial h_i}\cos\lambda - MS\sin(\alpha-\beta+\lambda)\frac{\partial\alpha}{\partial h_i} \\ &+ M\frac{\partial S}{\partial h_i}\cos(\alpha-\beta+\lambda)]. \quad 2.39) \end{aligned}$$

The required partial derivatives can be obtained in a straightforward manner. They are given in the following table:

	$\frac{\partial}{\partial h_0}$	$\frac{\partial}{\partial h_i}$
S	0	$\frac{1}{\sqrt{2}} S_1 (\xi, i)$
B	$\frac{1}{8}$	$-\frac{1}{4}$
C	$\frac{1}{4} \cos \delta S_2 (o) + \frac{1}{3} \sin \delta S_3 (o)$	0
α	0	$\frac{1}{\sqrt{2}} S_4 (\xi, i)$
δ	$\frac{1}{C} [\frac{1}{6} \cos \delta S_2 (o) - \frac{1}{8} \sin \delta S_3 (o)]$	0

2.41)

where $\xi = \alpha + 45^\circ$ and the S_n 's are given by the following table

Point Number	S_1	S_2	S_3	S_4
1	$\sin \xi$			$-\cos \xi$
2	$\cos \xi$			$\sin \xi$
3	$-\sin \xi$			$\cos \xi$
4	$-\cos \xi$			$-\sin \xi$
5		+1	-1	
6		+1	-1	
7		-1	+1	
8		-1	+1	
9		+1	-1	
10		+1	-1	
11		-1	+1	
12		-1	+1	

When forming $\sum_{i=1}^4 \left(\frac{\partial G}{\partial h_i}\right)^2$ and $\sum_{0=5}^{12} \left(\frac{\partial G}{\partial h_0}\right)^2$ the cross terms

among the S's all sum to zero, resulting in a great simplification. We are left with cross-terms between various angles such as

$$\cos(2\alpha-2\delta+\lambda)\cos(\alpha-\beta+\lambda)$$

Because angle δ is not necessarily related to the angle β , the expected value of these cross-products is zero. The worst case value is 1. Setting them equal to 1 along with setting $\cos \lambda = 1$ leads to the formula:

$$\sum_{j=1}^{12} \left(\frac{\partial G}{\partial h_j}\right)^2 \leq 8C^2 + 18B^2 + \left(\frac{361}{48} + 8M^2\right)S^2 \quad 2.43)$$

In order to apply this formula to a calculation of the expected error in the wind stress curl, values for σ_h^2 , $\langle C^2 \rangle$, $\langle B^2 \rangle$ and $\langle S^2 \rangle$ must be obtained. The only work done to date is connected with the distribution of S, which is related to the geostrophic wind. This work can be used to get only a crude idea of the uncertainty in the wind stress curl at present, but the result is so important that the approximation will be done. The largest values of wind stress curl are calculated in areas

where the slope is usually great, so we will evaluate the standard deviation due to the slope term. The geostrophic wind can be written as

$$|\tilde{U}_g| = \frac{g}{124\Omega R} \frac{(961+r_I^2)^2}{(961-r_I^2)} S \quad 2.44$$

and so

$$S^2 = \frac{(124)^2 \Omega^2 R^2}{g^2} \frac{(961-r_I^2)^2}{(961+r_I^2)^4} |\tilde{U}_g|^2 \quad 2.45$$

or

$$\sigma_G^2 \approx (7.52+8M^2) \frac{(124)^2 \Omega^2 R^2}{g^2} \frac{(961-r_I^2)^2}{(961+r_I^2)^4} |\tilde{U}_g|^2 \sigma_h^2 \quad 2.46$$

If we consider the latitude of site D or about 40°N and severe conditions (in January, $|\tilde{U}_g|$ of 20 m/sec is exceeded only about 7% of the time) with the standard deviation of the random error in 1000 mb height to be about 5 m, we have

$$\begin{aligned} M &= .125 & R &= 6.37 \times 10^8 \text{ cm} \\ r_I^2 &= 209 & |\tilde{U}_g| &= 2 \times 10^3 \text{ cm-sec}^{-1} \\ \Omega &= 7.29 \times 10^{-5} \text{ sec}^{-1} & \sigma_h &= 5 \times 10^2 \text{ cm} \\ g &= 980 \text{ cm/sec}^2 \end{aligned}$$

$$\sigma_G^2 = 76.4 \times 10^{12} \text{ CGS} \quad \sigma_G = 8.75 \times 10^6 \text{ CGS}$$

or

$$\sigma_{\hat{k} \cdot \text{curl} \tilde{\tau}} = 8.75 \times 10^6 \times 4.42 \times 10^{-15} = 347 \times 10^{-10} \text{ CGS}$$

from the S part of the formula. If S, B and C are all the same size, the figure will be increased by a ratio of $\sqrt{\frac{34}{8}}$ giving a standard deviation of 72×10^{-9} CGS. The magnitude of wind stress curl in the Atlantic Ocean in January between 40°N and 50°N is greater than 150×10^{-9} CGS about 7% of the time, corresponding to the same severity of the weather. Thus, a random error of 5 m in the height analysis will, under these conditions, result in an error of about 50% in the wind stress curl.

The greatest utility of equation 2.43 is not so much to perform calculations such as this one as to point out that the accuracy of an estimate depends on the local shape of the height field. To obtain a qualitative idea of the influence of a local pressure field, we return to the equation for G

$$G = S[C \cos(2\alpha - 2\delta + \lambda) + 3B \cos \lambda + MS \cos(\alpha - \beta + \lambda)] \quad 2.47)$$

The angle $\alpha - \delta$ is the angle between the principle axes of the colity and the slope. Now near the center of a low pressure area in mid latitudes, for instance, we have essentially

$$G = 3SB \cos \lambda \quad 2.48)$$

In such a place, the angles of things are not very important, but the magnitude of the slope varies considerably over a distance comparable to a gridlength. The bulginess, on the other hand is not so sensitive to position. If one were to use the wind stress curl formula to follow a North Atlantic low for a period of several days, this effect would be likely to introduce considerable jitter in the strength of the storm. In such a case, heavy smoothing of the estimates in time, following the storm in its path, would be justified.

As another important example, in a region near the "skirt" of a high or between a high and low with a steep 1000 mb height gradient, we have approximately

$$G \approx S[C\cos(2\alpha-2\delta+\lambda)+3B\cos\lambda] \quad 2.49)$$

In such an area, the three shape amplitudes are likely to be fairly well specified, but the influence of the angle $2(\alpha-\delta)$ is quite important. In the next chapter, a typical synoptic map of 1000 mb height and its associated wind stress curl pattern is presented. In the eastern part of the Atlantic Ocean, there are three dipole patterns of wind stress curl associated with the skirts of a large high pressure area.

In the case of the low pressure area, filtering of the resulting jitter in time was justified because of the

idea that a given storm changes its intensity as a smooth function of time. No such justification exists for smoothing out these dipole wind stress curls in space, and it is a moot point whether they are numerical artifacts or good estimates of the actual situation.

The curl formula as developed is subject to several errors. The most severe systematic ones come from two basic sources. The first is the assumption of constant R_s and λ . In chapter 3, a graph showing the values of R_s and λ for a measured surface wind and a computed geostrophic wind is shown. The second is the simple stress law. In all likelihood, R_s , λ , and C_D all vary to some extent depending on present and past conditions. The major source of random error is in the position sensitivity at the present sampling interval. The specification of the wind stress curl to a given percentage accuracy requires a denser grid of pressure readings than a similarly accurate specification of the pressure field.

From the second of these considerations, it might seem advisable to go to finer spatial and temporal scales of analysis. Perhaps a factor of two in each is justified. More to the point, the structure of the wind and pressure fields at small scales is not well known. A more fruitful approach than increasing the number of calculations eight-fold would be, in my opinion, to run an experiment consisting of a close packed array of barometers and anemometers in an open ocean area both to investigate the physics

of the momentum transfer process and to determine a minimum scale for which the assumptions going into the calculations are valid. With this information, a suitable time step and grid spacing could be estimated.

Perhaps a more comprehensive feeling for the wind stress curl formula can be obtained by examining some examples. The first example is that of a sinusoidal distribution of pressure in latitude with pressure constant in longitude. Such a distribution is given by the equation for 1000 mb height

$$h = -h_1 \cos(4k\phi) \quad 2.50)$$

This pressure is illustrated in 2.2a with $k = 1$. The geostrophic wind is entirely zonal from such a height distribution. The zonal part of the surface wind is $U_g \cos \lambda$ (figure 2.2b) while the meridional component, $U_g \sin \lambda$, is similar and independent of latitude. The zonal part of the wind stress from equation 1.4 is given schematically in 2.2c. The most important effect of the square law is to make the first order zeroes of 2.2b into second order (flattened) zero crossings. The major part of the wind stress curl is $-\frac{1}{R} \frac{\partial \tau}{\partial \phi}$ while there is no contribution from the zonally constant component. This results in a curve for wind stress curl which looks like

2.2d. This curve has much more structure than the pressure curve from which it is derived. One new feature is the cusp at 45°N . Cusps are common in calculations of wind stress curl fields from smooth pressure patterns. They are not resolved in synoptic studies using finite difference grids. The value of wind stress curl at a cusp must be zero because they always occur where $S = 0$. Thus their omission is not an important error source in calculations of wind stress curls. The equation for this particular calculation is

$$\hat{k} \cdot \nabla \times \underline{\tau} = \frac{\rho_a C_D}{R^3} \left[\frac{2kh R_s g}{\Omega} \right]^2 \cos \lambda \operatorname{sgn}(\sin(4k\phi)) \frac{\sin 4k\phi}{\sin \phi} \cdot$$

$$\left[\frac{8k \sin \phi \cos 4k\phi - 2 \cos \phi \sin 4k\phi}{\sin^2 \phi} - \frac{\sin 4k\phi}{\cos \phi} \right] \quad 2.51)$$

where the function $\operatorname{sgn}(x) = \frac{|x|}{x}$. Figure 2.2 corresponds to the case $k = 1$.

For a second case, consider an "isolated pressure cell" with a 1000 mb height of

$$h = h_1 \ell - \frac{x^2 + y^2}{a^2} = h_1 \ell - \frac{r^2}{a^2} \quad 2.52)$$

on an f plane ($M=0$). In this case, we have $\alpha - \delta = \pi$ so $\cos[2(\alpha - \delta) + \lambda] = \cos \lambda$. This allows us to write

$$G = \cos \lambda S[C + 3B] \quad 2.53)$$

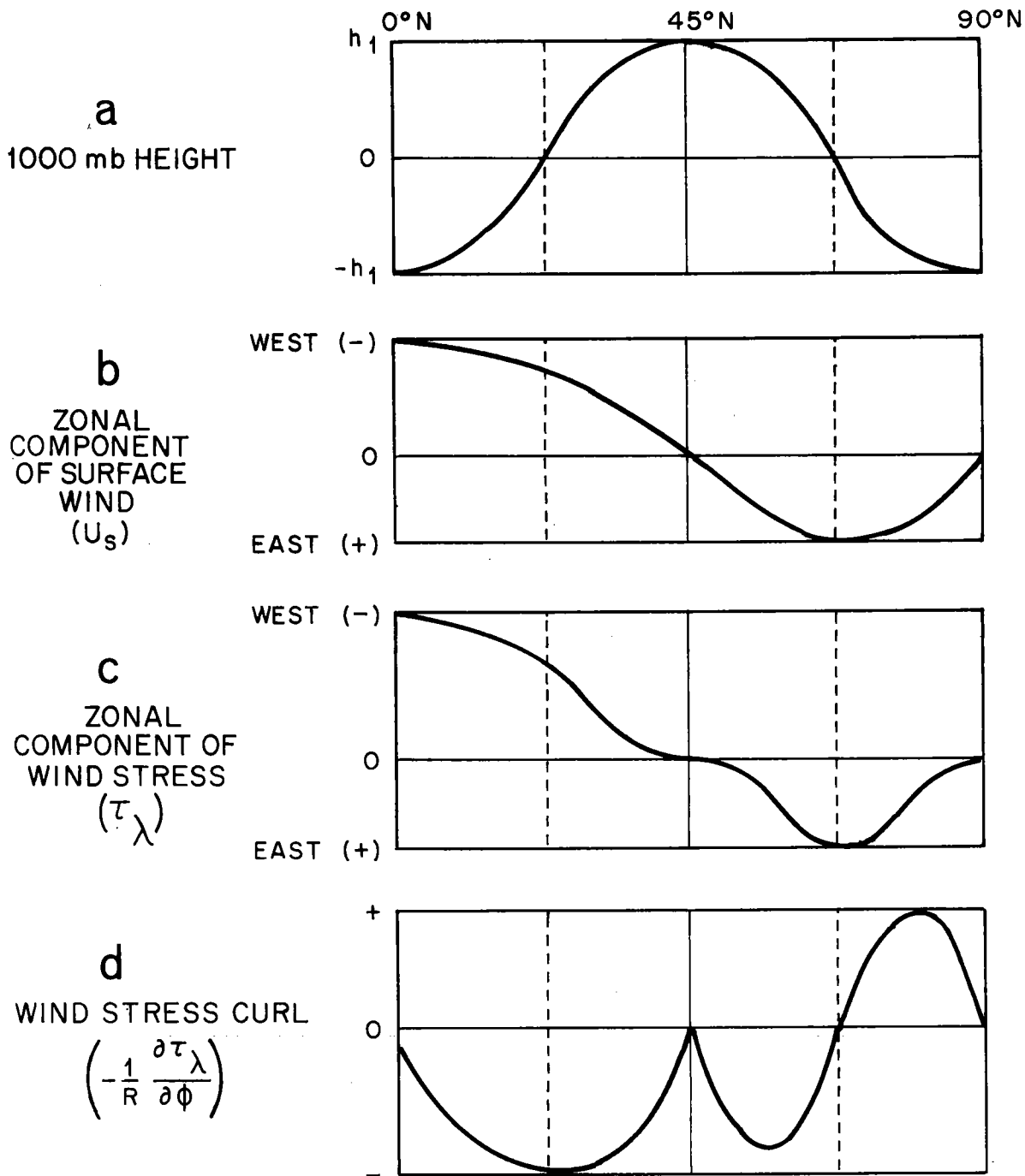


Figure 2.2. The steps, using the surface wind as an intermediate result, between a 1000 mb height field varying only sinusoidally in latitude and the corresponding wind stress curl. The height field is a member of the set used to test the wind stress curl approximation in appendix 2 with $k=1$. Vertical scales are approximate.

Evaluating C, B, and S in terms of the height field given by equation 2.52 gives

$$G = \frac{4}{a^3} \cos \lambda [4\left(\frac{r}{a}\right)^3 - 3\frac{r}{a}] \ell^{-2\left(\frac{r}{a}\right)^2} \quad 2.54)$$

If we let $\rho = \frac{r}{a}$ be a scaled variable, we have

$$G = \frac{4}{a^3} \cos \lambda H(\rho) \quad 2.55)$$

In this case, the amplitude of the wind stress curl is seen to go as the inverse cube of the diameter of the storm. This strongly emphasizes the effect of small storms on local values of wind stress curl. A plot of $H(\rho)$ and $h(\rho) = \ell^{-\rho^2}$ is given in figure 2.3. Again, the cusp is found in the radial dependence with a central "hole" of $.4a$ in radius. While the cusp can never be resolved, the central hole can be resolved using a finite difference grid with 2-1/2 times the linear density as one required to resolve the corresponding pressure feature.

The occurrence of curl patterns with a central core of one sign surrounded by a ring of the opposite sign is frequent in synoptic analyses. These patterns are associated with well defined isolated pressure features.

It is instructive to find the area integral of H , that is

$$I = 2 \pi \int_0^{\infty} \rho H(\rho) d\rho \quad 2.56)$$

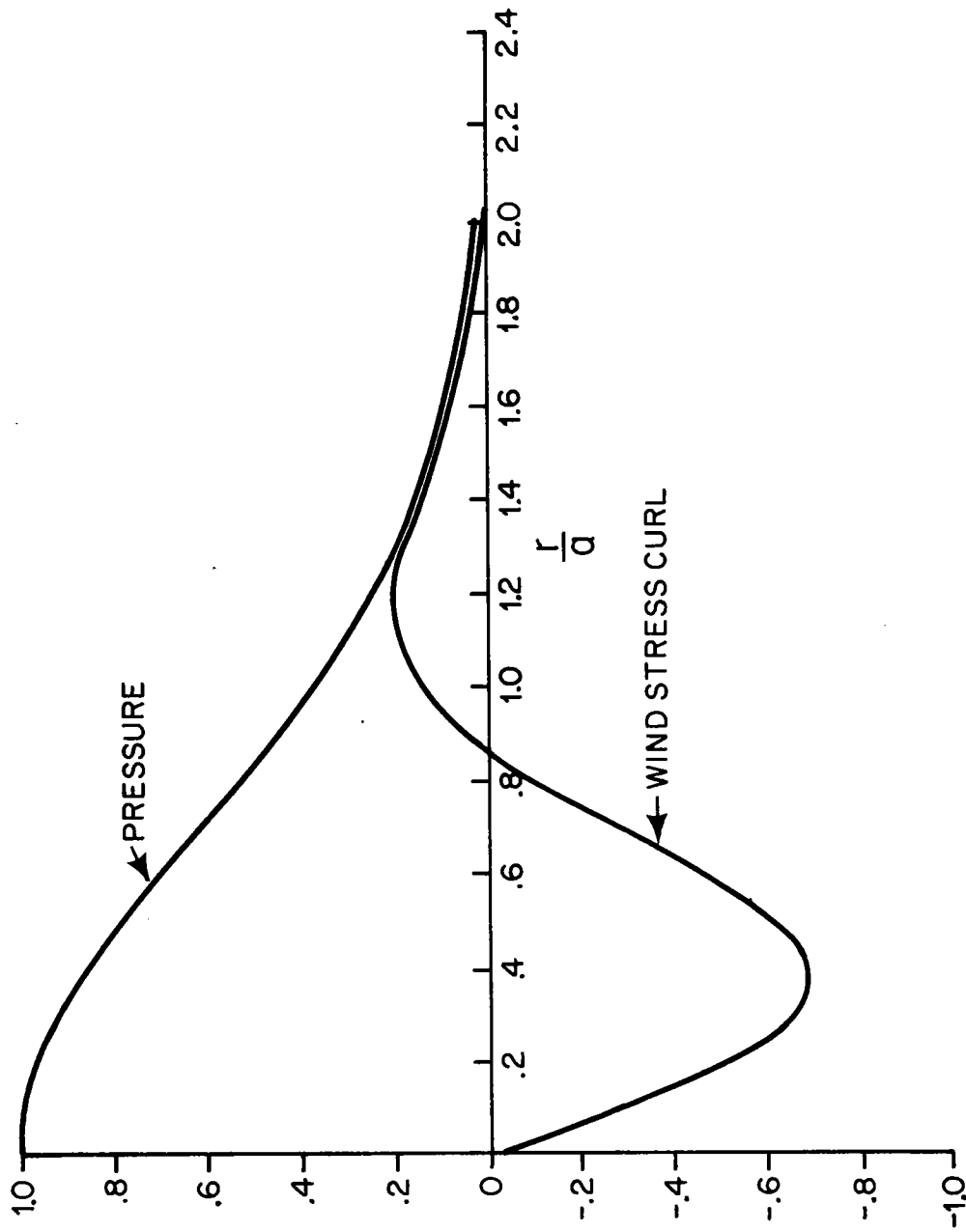


Figure 2.3. Normalized curves of 1000 mb height and wind stress curl for the example of a Gaussian pressure pattern as discussed in the text.

This quantity corresponds to the total integrated vertical motion beneath the Ekman layer due to a single pressure cell.

Accordingly, we write

$$I = 2\pi \int_0^{\infty} (4\rho^4 - 3\rho^2) \ell^{-2\rho^2} d\rho \quad (2.57)$$

or

$$I = 2\pi \left[4 \int_0^{\infty} \rho^4 \ell^{-2\rho^2} d\rho - 3 \int_0^{\infty} \rho^2 \ell^{-2\rho^2} d\rho \right]$$

A change of variables $y = \rho^2$ leads to

$$I = 2\pi \left[4 \int_0^{\infty} y^{3/2} \ell^{-2y} dy - 3 \int_0^{\infty} y^{1/2} \ell^{-2y} dy \right]$$

The first of these integrals can be integrated once by parts to give

$$I = 2\pi \left[4 \cdot \frac{3}{2} \cdot \left(-\frac{1}{2}\right) \left(- \int_0^{\infty} y^{1/2} \ell^{-2y} dy \right) - 3 \int_0^{\infty} y^{1/2} \ell^{-2y} dy \right] = 0$$

Thus the net integrated vertical velocity from a single isolated Gaussian pressure cell is zero.

This result is actually part of a more general result.

Consider equation 1.2

$$w(-\infty) = \hat{k} \cdot \nabla \times \left(\frac{\tau}{f} \right)$$

If we integrate this over a large finite area, we have

$$\iint w(-\infty) dA = \iint \hat{k} \cdot \nabla \times \left(\frac{\tau}{f} \right) dA \quad (2.58)$$

The right hand side is in the form necessary for application of Stokes' theorem yielding

$$\iint w(-\infty) dA = \oint \left(\frac{\tau}{f} \right) d\ell \quad 2.59)$$

where $d\ell$ is an element of the boundary of the area of integration. But in an isolated disturbance, one can draw a boundary line completely around it such that $\tau = 0$ on the line. Thus, for an isolated disturbance, we have

$$\iint w(-\infty) dA = 0 \quad 2.60)$$

This powerful result applies to any isolated disturbance, such as a hurricane, regardless of the mechanism of momentum transfer, the drag coefficient, R_s , and λ .

A similar result can be derived for the Sverdrup equation with some qualifications if we wish to compute the total Sverdrup transport (equation 1.3) over a zonal section of the ocean basin. Thus

$$T(y) = \frac{1}{\beta} \int_{\text{West coast}}^{\text{East coast}} \hat{k} \cdot \text{curl } \underline{\tau} dx \quad 2.61)$$

Suppose we have an isolated storm passage through the zonal section during a time period $t_1 < t < t_2$. Then the average transport through the section during this period is

$$T(y) = \frac{1}{\beta} \frac{1}{t_2 - t_1} \int_{t_1}^{t_2} \int_{\text{West coast}}^{\text{East coast}} \hat{k} \cdot \text{curl} \underline{v}(x, y, t) dx dt \quad (2.62)$$

Now if the storm remains of constant strength and velocity the time integral can be represented by a space integral representing the space locus of the zonal section during the time of the storm passage if the velocity of the zonal section is opposite to the storm velocity. The curl can thus be taken over this area and Stokes' theory applied to transform the integration over the boundary of the area. If this is done, the result is that the net transport at the western boundary due to the passage of an isolated constant strength offshore storm is zero. Contributions to the net transport occur if the pressure pattern is partly over land, if the pressure pattern becomes deeper or shallower, or if the velocity of the storm changes while the storm crosses the section.

Consider now a non-equatorial basin completely bounded by land. At the continental boundaries, we have postulated an "image" transport which has a horizontal component normal to the coast given by equation 1.8 and equation 1.9.

$$\underline{U}_I = (-\underline{U}_E \cdot \hat{n}) \hat{n} = [-\hat{S} \cdot \frac{\tau}{f}] \hat{n}$$

If we assume that this image transport is limited to boundary regions, it must be equal to an integrated vertical movement or upwelling in the coastal region. If the upwelling transport is given by

$$T_w = \int_{-\infty}^{\text{Coast}} W_I \hat{n} \cdot dr \quad (2.63)$$

where T_w is the horizontally integrated vertical upwelling per unit of coastal length, we have

$$\oint T_w \cdot dl = \oint -\frac{\tau}{f} \cdot \hat{S} \cdot dl \quad (2.64)$$

Now the interior Ekman pumping is given by equation 2.59. If we take the coastal boundary as the path of integration we have

$$\iint w(-\infty) dA = \oint \frac{\tau}{f} \cdot \hat{S} \cdot dl \quad (2.65)$$

By comparison of equation 2.64 and 2.65, we arrive at

$$\iint w(-\infty) dA = \oint T_w \cdot dl \quad (2.66)$$

This equation states that the total Ekman pumping over the interior of a bounded homogeneous ocean is identically balanced by the wind driven upwelling at the coasts.

These examples have been designed to indicate what we might expect from calculations of wind stress curl using the formula developed in this chapter. In the next chapter, the formula is applied to actual data. In addition, the geostrophic wind is calculated from the pressure data and compared to observed winds in several ways.

CHAPTER III

"It does not do to leave a live dragon out of your calculations, if you live near him" - J. R. R. Tolkien

At this point we have a body of data and a set of recipes for using the data to calculate numbers which supposedly correspond to physical quantities, in this case, the geostrophic wind and the wind stress curl. Before the recipes can be used with confidence, some idea of the expected results should be obtained. We need to gain a "feel" for the recipes.

In this case, we have potentially available an enormous quantity of numbers. For instance the weather bureau generates four surface pressure maps every day, each of which is analyzed at 1977 points (the NMC grid). We can obtain about 10 years of such data giving a total of $10 \times 4 \times 365 \times 1977 \approx 2.7 \cdot 10^7$ points. Furthermore some analyses, and we shall find at least one good reason for this, are being made at twice the linear resolution of the NMC grid resulting in a fourfold increase in the rate of number production.

With this quantity of data, one cannot hope to become well enough acquainted with each individual point to judge it on its own merits. An alternative is to calculate some

statistics from the points and judge the statistics. Fortunately, the existence of a large number of points, which brought on the problem in the first place, is exactly the requirement for obtaining reasonable statistics.

A statistical study was undertaken for the 1968 NMC data before the significance of the shape amplitudes, S, B, and C, discussed in chapter 2 was understood. The main results of this study are histograms and mean values of geostrophic wind speeds and wind stress curls over various ocean areas. These histograms do give a certain amount of feel for the data, but by no means constitute a complete study.

The first quantity for which histograms and means were computed is geostrophic wind speed. Values of the mean wind speed for 10° latitude bands of the North Atlantic and North Pacific are plotted as figure 3.1 for January and July of 1968. From this figure, it is apparent that annual variations are greater in the middle and high latitudes than in the low ones. Also, there is a distinct minimum of mean wind speed in both oceans in the 30°N to 40°N latitude band in the summer but not in the winter. The maximum is at 40°N to 50°N in the Pacific for both January and July while in the Atlantic it is in, or north of the 50°N to 60°N band. Each of these features is in agreement with the U. S. Weather Bureau Atlas of Climatic Charts of the Oceans (1938). This qualitative

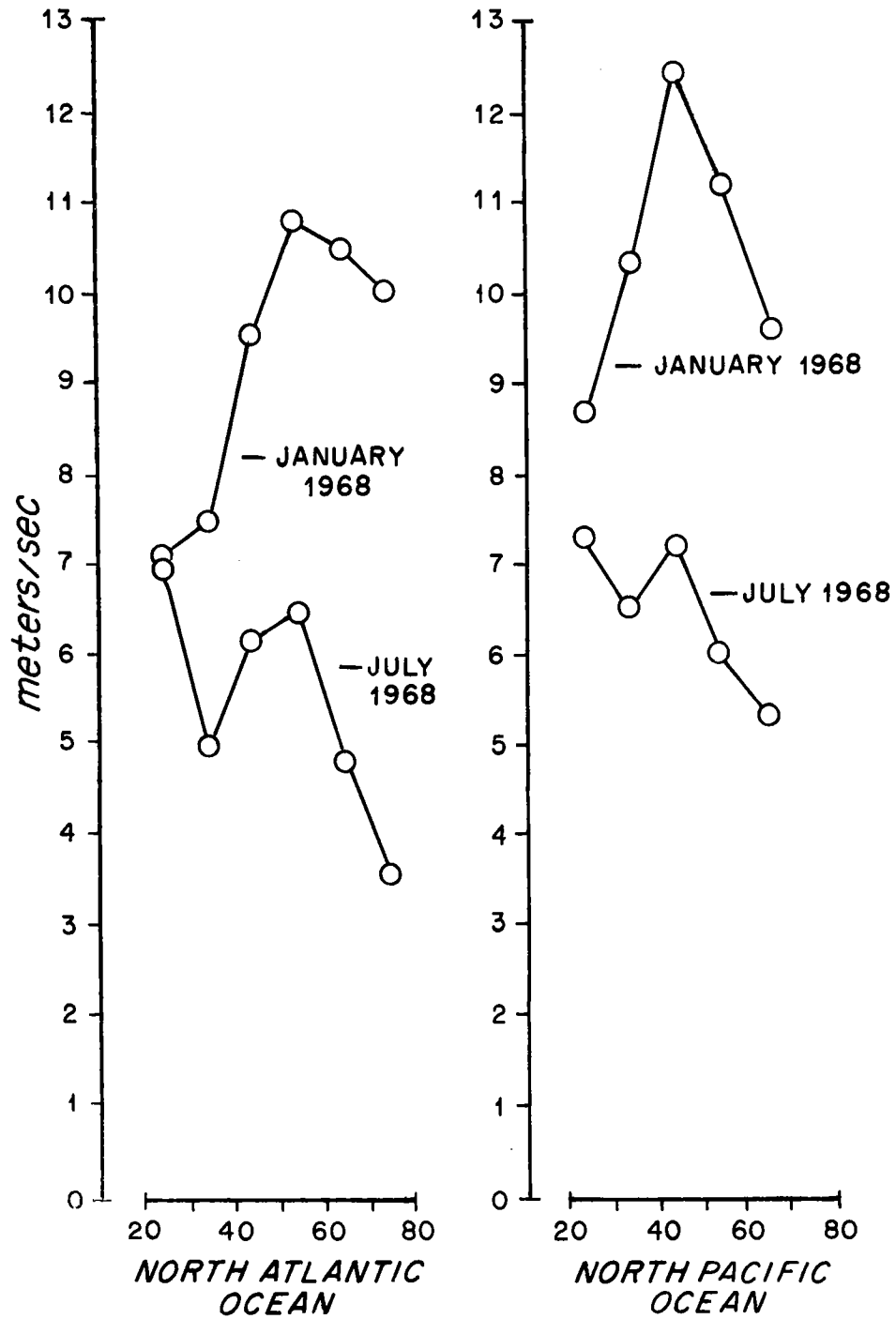


Figure 3.1. Zonally averaged estimates of monthly averaged geostrophic wind speed for January and July, 1968. The areas covered are the North Atlantic Ocean and the North Pacific Ocean north of 20°N.

agreement of mean winds is encouraging both because it lends credence to the calculation technique and also because it indicates that 1968 was not a strongly atypical year.

As another test for the geostrophic wind calculations, a comparison was made between an anemometer record (2801) obtained by the W.H.O.I. buoy group at Site "D" and geostrophic winds calculated from pressure maps. This study is particularly interesting for several reasons. First, the wind record is completely independent of the weather maps. Wind records from weather stations, as a contrast, are used to estimate pressure gradients in the NMC objective analyses of pressure, and so a comparison between weather station winds and geostrophic winds computed from weather maps is likely to be biased. Record 2801 is also comparable to a second anemometer (2791) which was located on another buoy a mile distant from the first one for forty-one days. During this period the two records agree well enough that gross instrumental failures by either instrument can be ruled out. Finally, a comparable geostrophic wind calculation was performed for the same time period at Site "D" using pressure analyses every 12 hours on the diamond grid used in the Canadian Fisheries Research Board studies.

The first comparison between geostrophic and observed winds was made by vector averaging the observed winds over

12 hour intervals centered at the analysis times of the weather maps (00Z, 12Z) and computing for each of the resulting 85 points the values of R_s , the ratio of the observed to the calculated wind speed and λ , the difference of the observed from the calculated direction. The resulting numbers were then grouped in class intervals and are presented as histograms in figures 3.2 and 3.3. The vertical dotted lines are the values of R_s and λ used in the study of wind stress curls. The improvement gained by going to the smaller grid spacing is quite evident from this comparison, particularly in the definition of the direction of the wind.

The same data are again compared in figure 3.4 using progressive vector diagrams. To estimate the surface winds, the geostrophic winds are reduced in magnitude by .7 and veered 15° counterclockwise. The resulting series is presented in figure 3.4 as the computed surface winds, the two progressive vectors on the top. The corresponding observed progressive vectors are given below. The series is broken into two pieces because of missing NMC data between October 28, 1968 and November 2, 1968. The agreement between the two series is worst in the period November 6-13, during which time the observed wind turned through $2 \frac{1}{2}$ full circles.

For each 12-hour period, an error vector can be constructed. The amplitude of this error vector as a function

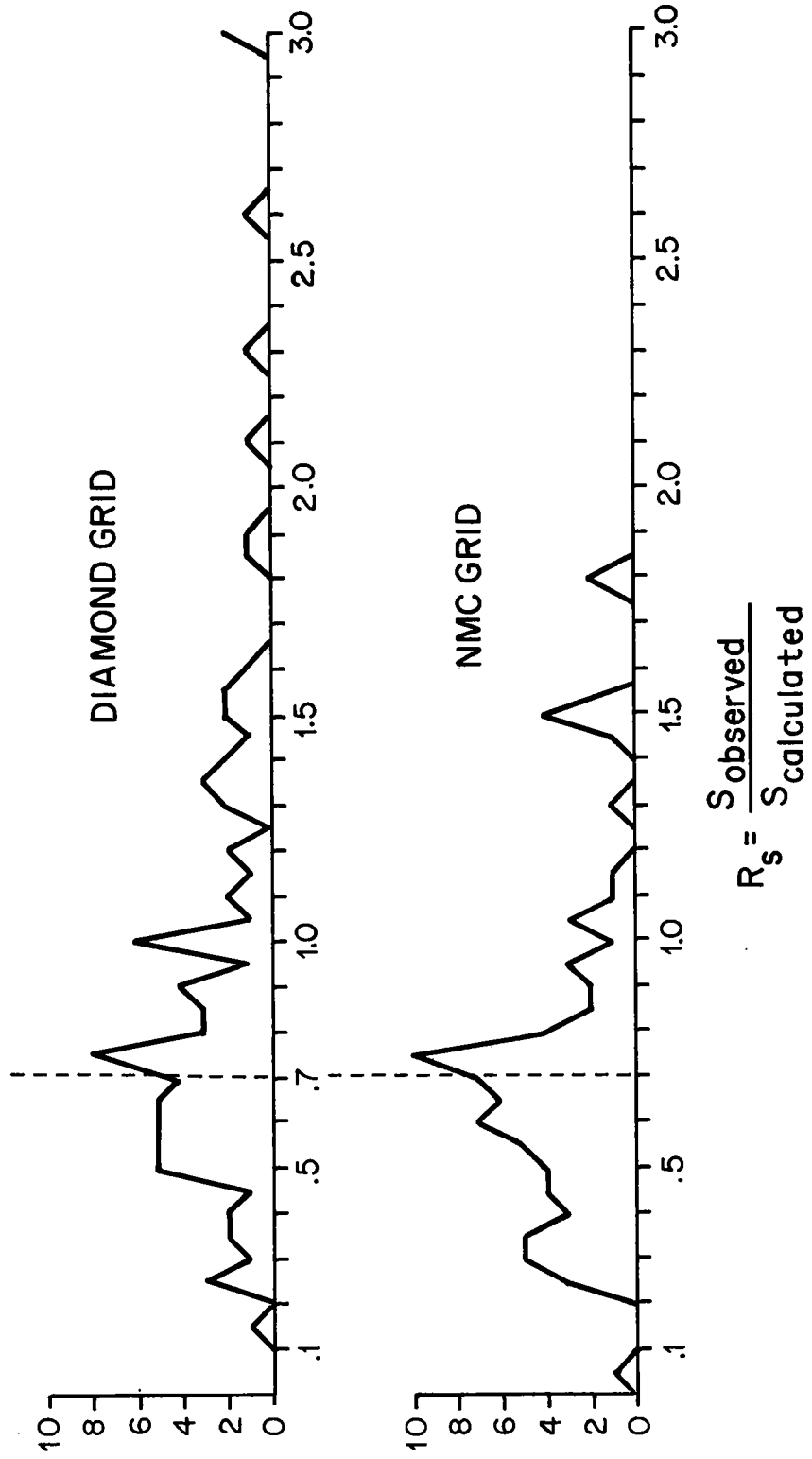
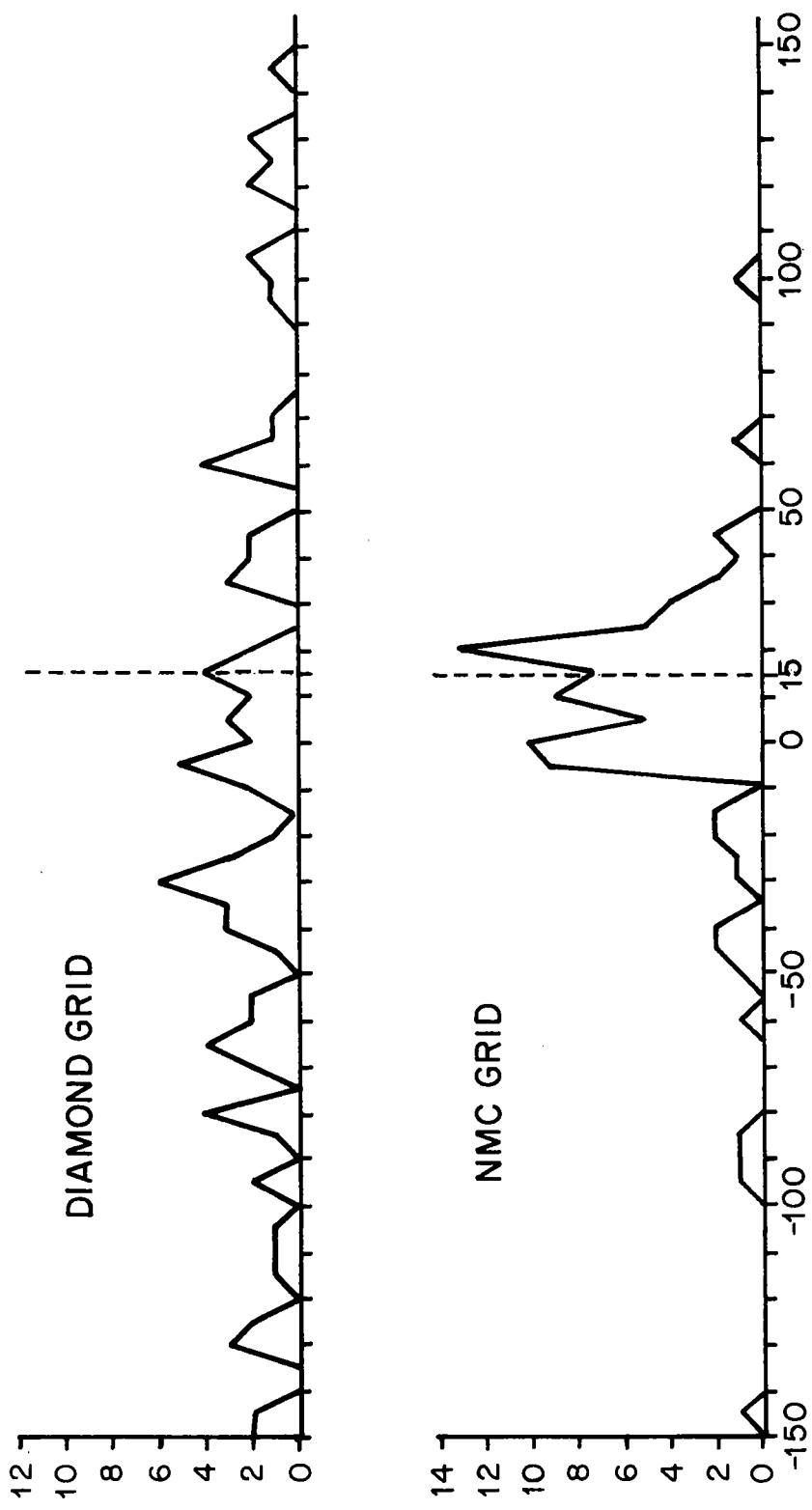


Figure 3.2. Histograms of ratio of observed surface wind speed to calculated geostrophic wind speed for W.H.O.I. wind record 2801. In the upper figure, the geostrophic wind is estimated using the diamond grid used by the Canadian Fisheries Research Board. In the lower figure, the NMC grid used in the present study is used. The vertical line at .7 marks the value of R_s used in the present study.



$$\lambda = D_{\text{calculated}} - D_{\text{observed}}$$

Figure 3.3. Histogram of veering angle between calculated geostrophic wind and observed surface wind for W.H.O.I. record 2801. The vertical line at 15° marks the value of λ used in the present study.

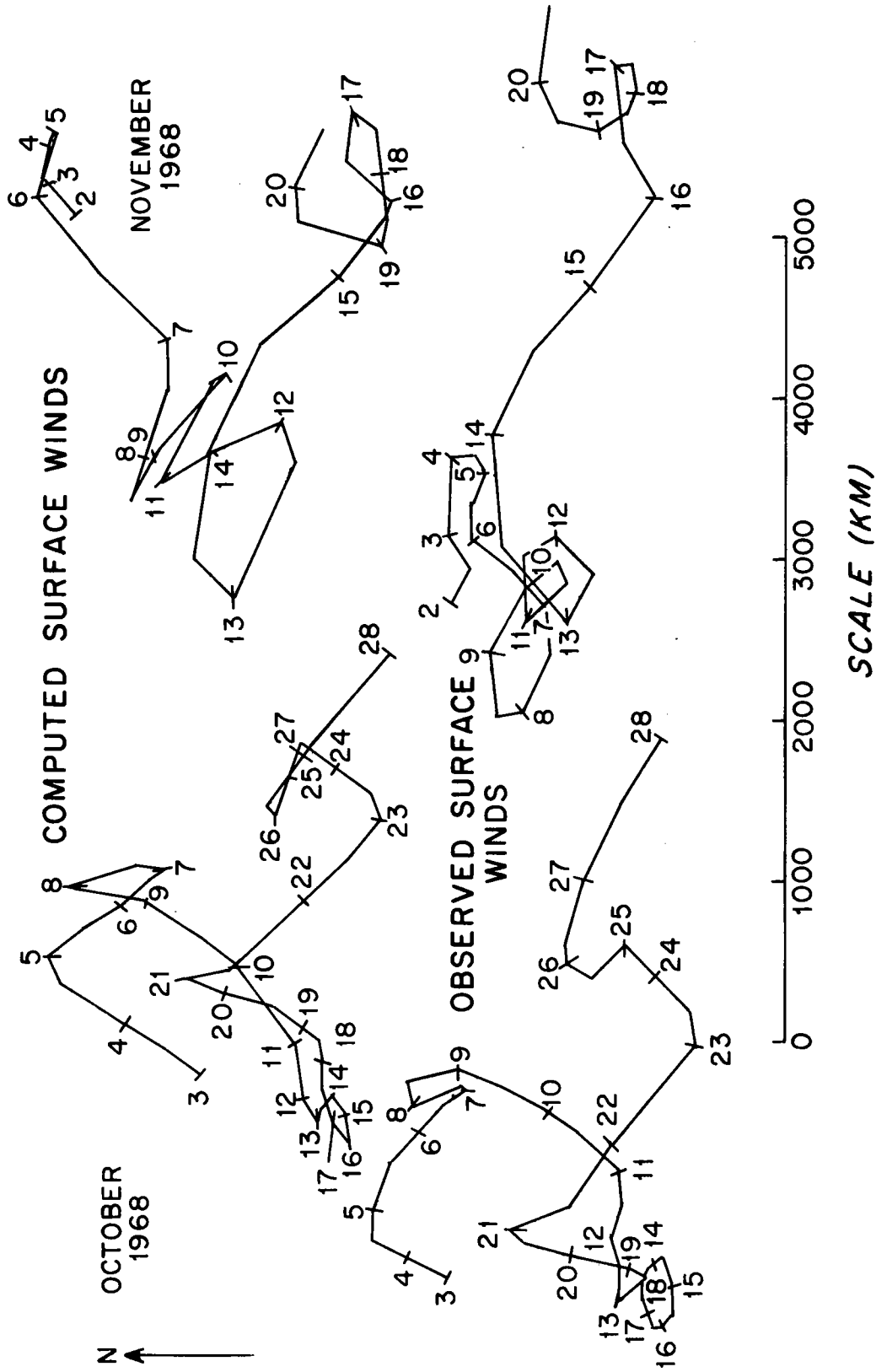


Figure 3.4. Progressive vector representation of computed and observed surface wind at W.H.O.I. site D for record 2801.

of time is shown in Figure 3.5. The median value for October is 2.0 m/sec while for November it is 3.1 m/sec. The rapidly turning wind from November 6-13 is seen clearly to produce the largest errors. The RMS vector error for the entire record is 3.7 m/sec. This can be compared to the RMS observed surface wind speed of 6.9 m/sec giving a reduction of variance of 71%.

Power spectra of the observed and computed surface winds are given for each segment in figure 3.6. The power of the observed wind is shown by circles while that of the computed wind is shown by squares. The shape of the computed power follows that of the observed power throughout the frequency range .1-1 CPD. There seems to be some overestimation of the 1 CPD power in both segments. As is expected, the discrepancy in the power between the observed and computed wind is greater in the November segment than in the October one.

The coherency between the observed and computed series is shown in figure 3.7. In order to gain statistical reliability, eight cross spectral estimates are used to compute each value. The eight pairs consist of two east and two north components in each of the two time segments averaged over bands of two adjacent frequencies. The coherence is high at all frequencies falling from about .97 at low frequencies to about .84 near 1 CPD with a low

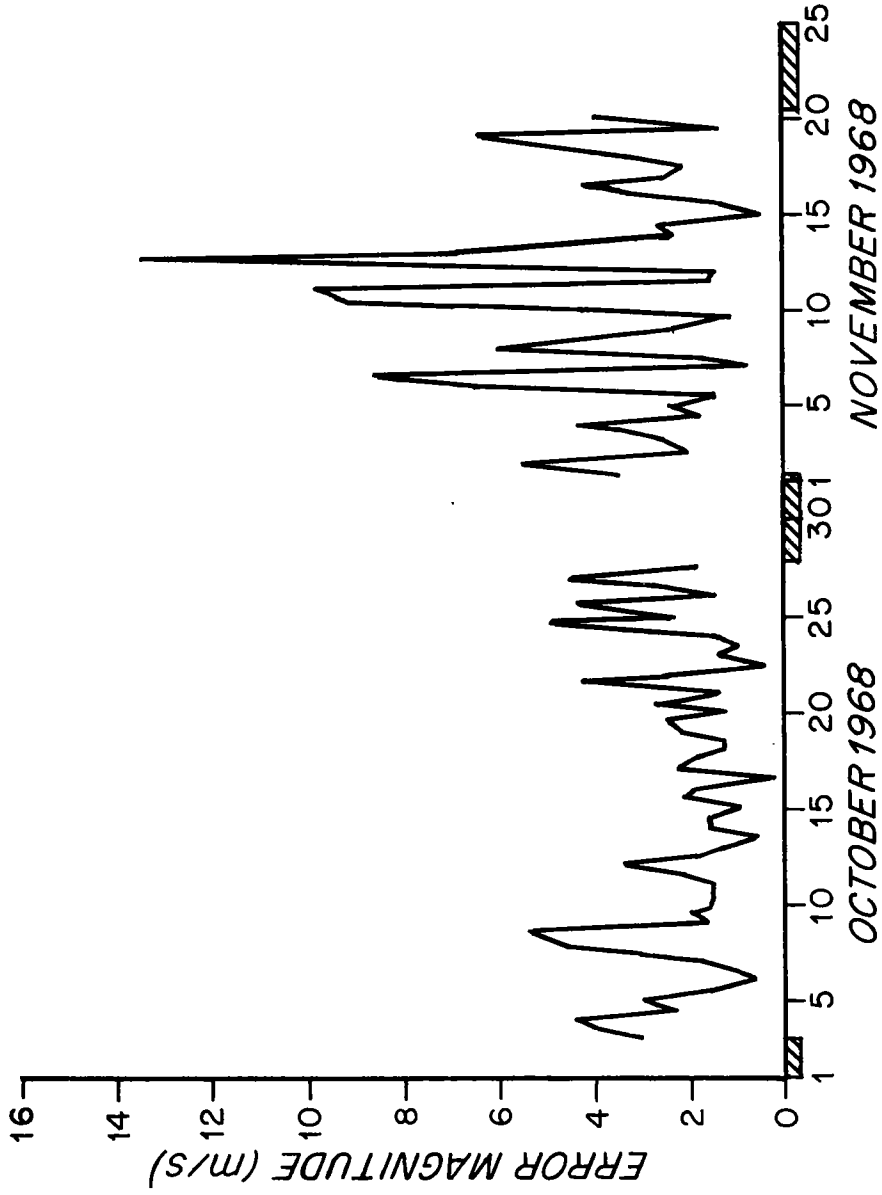


Figure 3.5. Magnitude of the error vector between estimated and observed surface wind for W.H.O.I. wind record 2801 at site D.

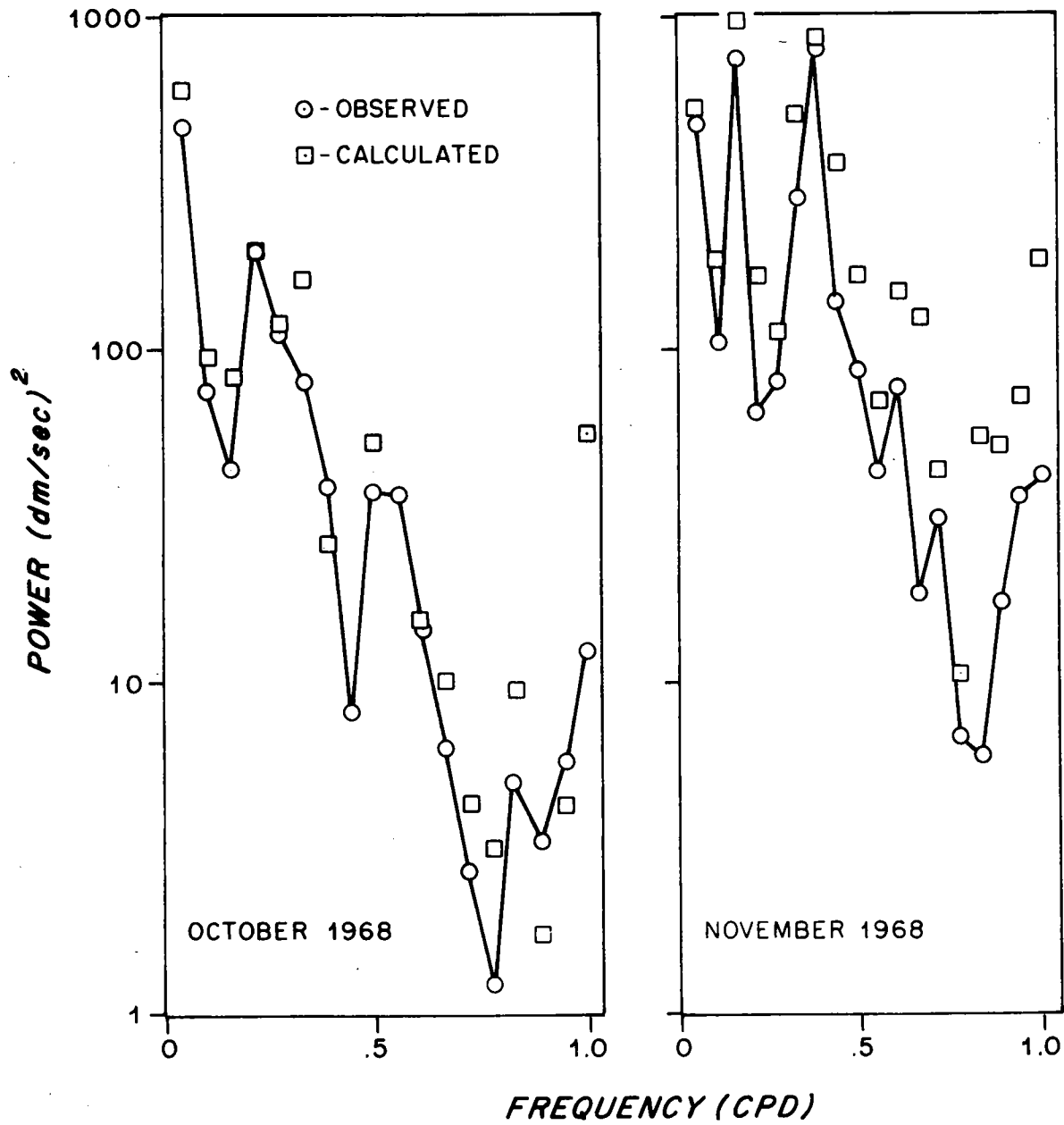


Figure 3.6. Unaveraged power spectra for observed and estimated fluctuating surface wind at site D for W.H.O.I. record 2801.

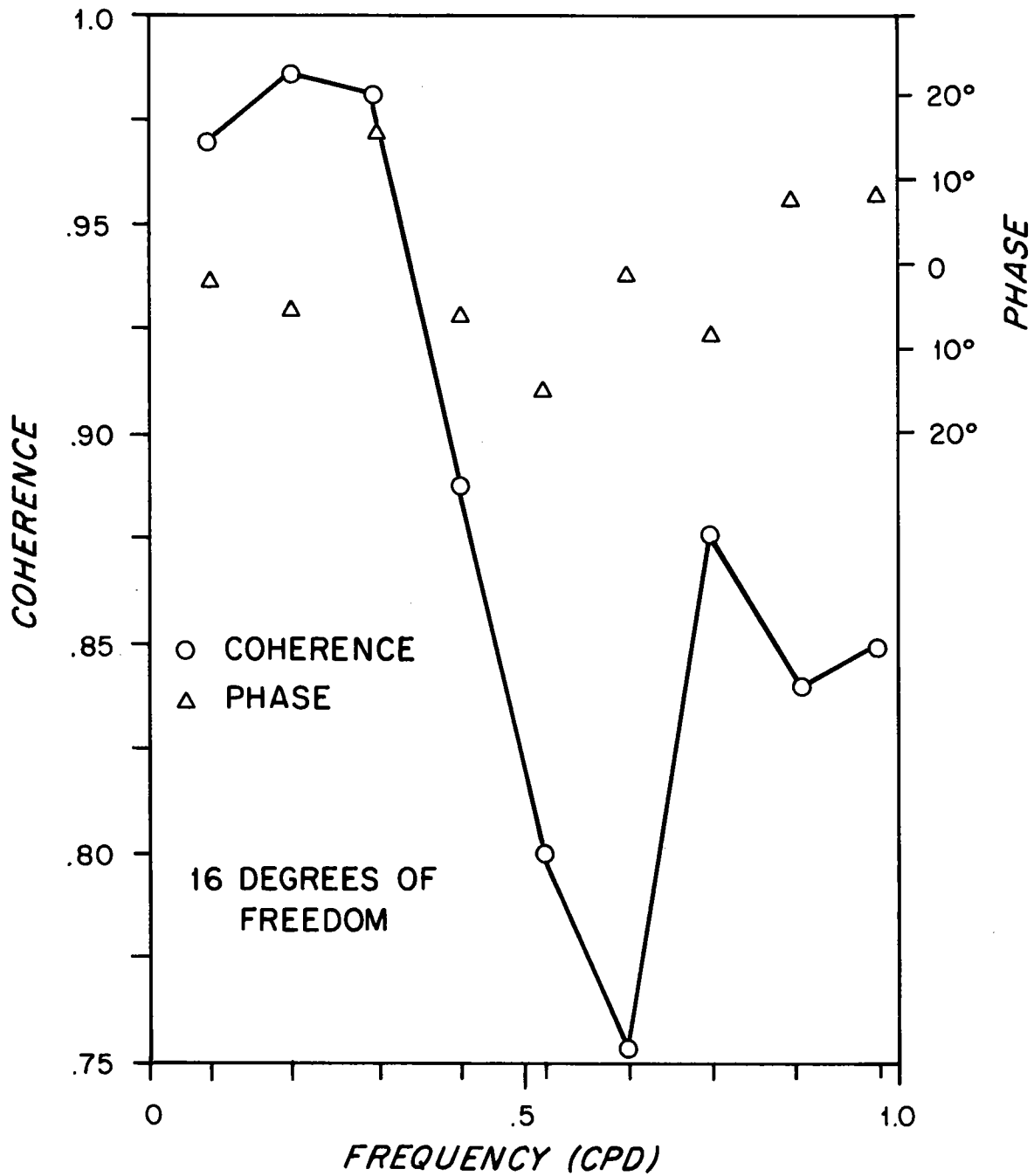


Figure 3.7. Coherency between observed and estimated fluctuating surface wind at site D for W.H.O.I. record 2801.

value of .76 at .6 CPD. The series are in phase at all frequencies.

As a final comparison, the observed winds and those computed from the NMC grid were vector averaged over the 85 half days of record 2801 for which comparisons could be made. From these averages, empirical values of R_s and λ were computed. These values are 0.75 and 17° respectively. If values of 0.70 and 15° for R_s and λ are used to estimate geostrophic winds from observed winds, the RMS vector error during record 2801 is 5.35 m/sec. This RMS error may be compared to the value of 3.2 m/sec for the weather bureau objective analyses quoted in chapter II.

The agreement between calculated and geostrophic wind is fortunate for another reason. The geostrophic wind is directly related to the slope amplitude S in the wind stress curl formula. The relation, as given in chapter 2, is of the form

$$S = (\text{function of latitude}) \times |\underline{U}_g| \quad 3.1$$

The probability distribution of $|\underline{U}_g|$ is then of some interest in estimations of the wind stress curl.

The geostrophic wind speeds calculated over the 30°N to 40°N latitude band of the Atlantic Ocean during January and July of 1968 were taken as examples to match by curve fitting and application of the χ^2 test (Bendant and Piersol,

1966) using the Rayleigh distribution. Wind speeds will have this distribution if the individual east and north components are uncorrelated and have Gaussian distributions with zero means and equal standard deviations.

If U is the wind speed and σ the standard deviation of the east and north components, the Rayleigh distribution is given by

$$\Pr\{S < U < S + \Delta S\} = \frac{1}{\sigma^2} \text{Se}^{-\frac{S^2}{2\sigma^2}} \Delta S. \quad 3.2)$$

The smallest values of χ^2 for the data described were obtained with a σ of 620 cm/sec for January 1968 giving a χ^2 of 185. For July 1968 the corresponding value for χ^2 was 123. Using 23 and 21 degrees of freedom respectively, such high values of χ^2 are unlikely to occur if the distribution actually is a Rayleigh distribution. The best fit curves and the data are shown in figures 3.8a and 3.8b. The likelihood for the parent distribution to be a Rayleigh distribution may actually be greater than indicated above because the samples used to construct the histogram are not independent. This dependence has the effect of decreasing the number of degrees of freedom and hence increasing the likelihood corresponding to a given value of χ^2 .

If the speed distribution is known for each direction, wind stress curl estimations from mean wind roses can be

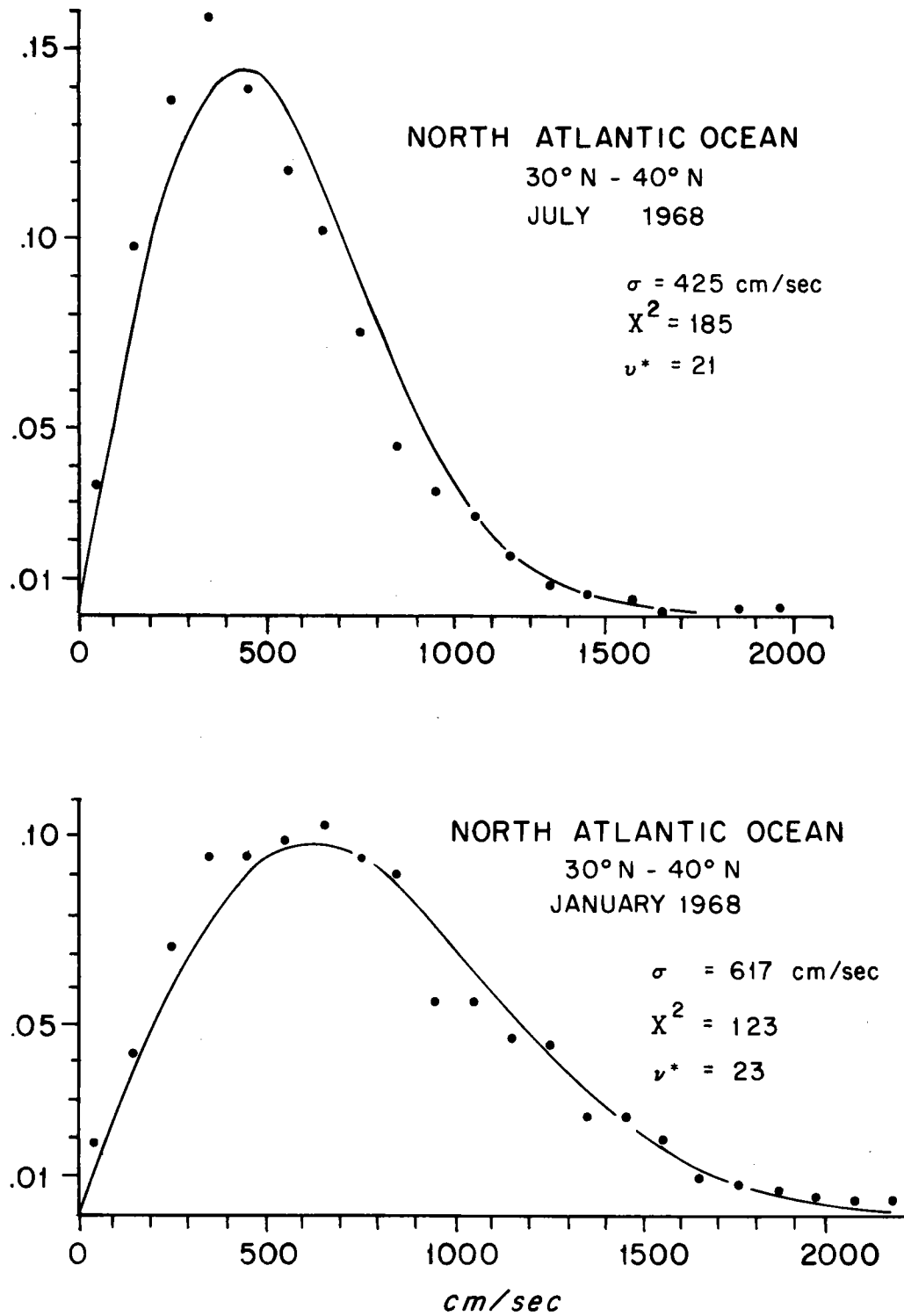


Figure 3.8. Histograms of estimated geostrophic wind speeds during January and July 1968 over a 10° wide zonal band of the North Atlantic Ocean. The histograms are compared to the best fit Rayleigh distribution.

corrected for the effects of variability. The technique was presented in the Scripps report (1948). If the winds are assumed to have a Rayleigh distribution for each direction class, the values of wind stress curl from studies such as that by Hidaka (1958) should be increased uniformly by 27% to account for the variability of the winds.

The first statistical study using the wind stress curl formula derived in chapter 2 was the production of histograms of the computed curls over various areas of the northern hemisphere north of 20°N. These areas included the entire NMC grid, the major oceans, and 10° latitude bands of the Atlantic ocean, the Pacific Ocean, and the Labrador Sea.

A typical histogram of estimates is given in figure 3.9a for the 30°N to 40°N latitude band of the Atlantic Ocean during January 1968. Each estimate represents a single calculation of wind stress curl from a single 12 point grid on a 12-hourly 1000 mb height analysis. The estimates are not statistically independent as each 1000 mb height value can be included in as many as 12 wind stress curl estimates. The horizontal scale on the histogram is chosen to have the same units as those chosen by Munk (1950) such that 1 unit corresponds to 10^{-8} dyne-cm⁻³. The histogram is clipped so that estimates which are off scale are included in the counts for the extreme values of the scale.

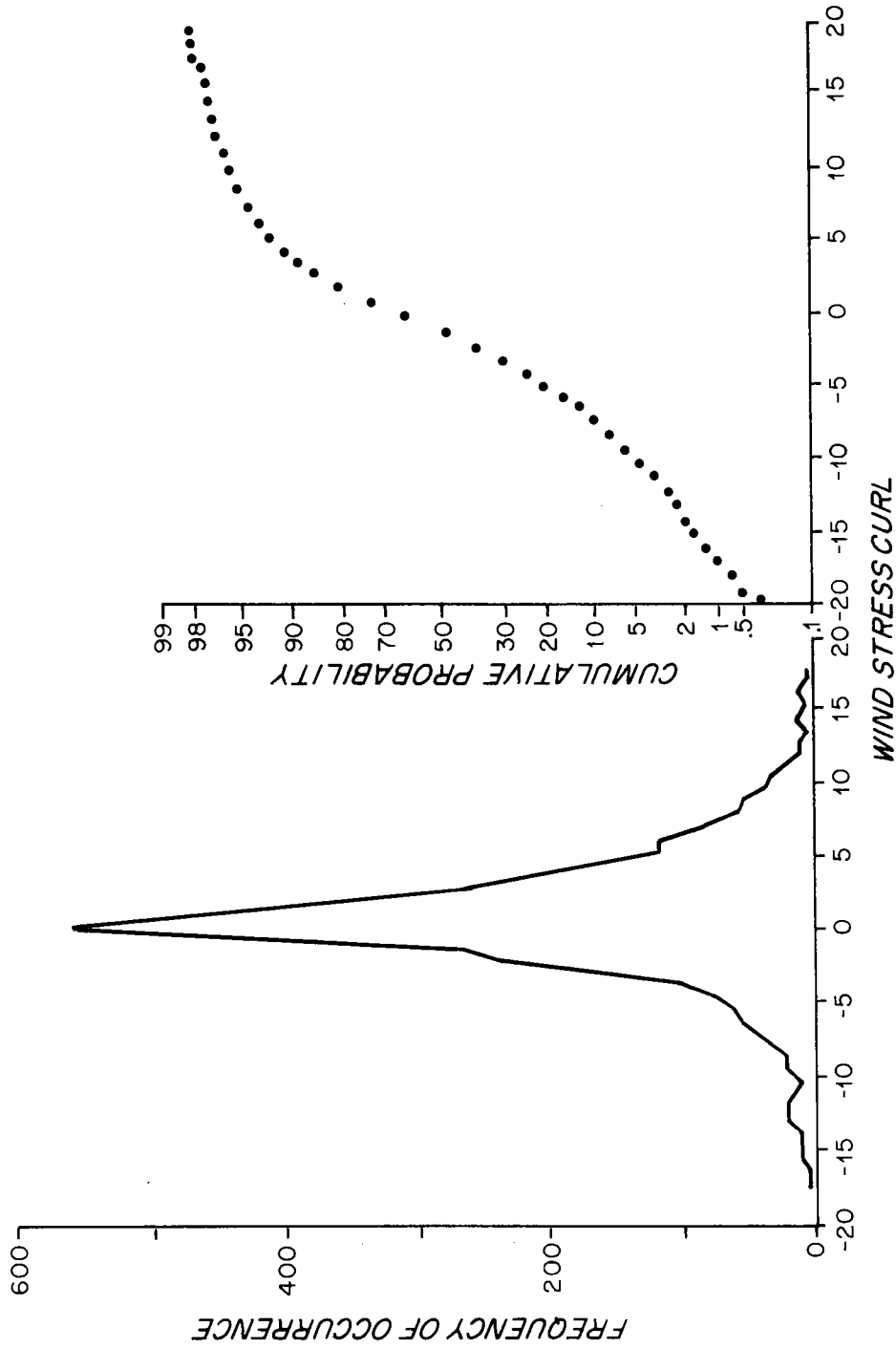


Figure 3.9. Typical histogram and associated cumulative probability curve of wind stress curl over a 10° wide zonal band of the North Atlantic ocean during a single month. This figure illustrates the non-Gaussian character of the wind stress curl distribution as discussed in the text.

Several things are quite striking about this histogram. The first is that the standard deviation of the clipped distribution is more than 10 times the value of the mean. The standard deviation of the unclipped distribution would be even greater. Although the central part of the distribution looks fairly symmetrical, the clipping is predominantly on the side of positive values resulting in a net bias. Inspection of individual estimates reveals numbers as high as 100×10^{-8} dyne-cm⁻³ on rare occasions. Another aspect of the curve, which is not quite so evident from the distribution itself, is that it is strongly non-Gaussian. To make this point more apparent, the cumulative distribution of wind stress curl is plotted in figure 3.9b vs. the error function $\times 100$. If the distribution were Gaussian, the resulting plot would be a straight line. An approximation to the best straight line may be the one tangent to the curve made by the estimated points at its inflection point. If this line is used, it is seen that a value of $+10 \times 10^{-8}$ dyne-cm⁻³ or greater occurs 5% of the time whereas if the distribution were Gaussian a value in this range would occur only 0.5% of the time. So at this level, extreme events occur 10 times as often as they would if the distribution were Gaussian. This accentuation of the extremes is the dragon which we must not leave out of our calculations.

To investigate the accentuation of extremes further, some trial curves were fitted to the histograms of wind stress curl. The curves all had the form of the Cauchy distribution:

$$P(x) = \frac{1}{\pi} \frac{\gamma}{[\gamma^2 + (x-x_0)^2]} \quad 3.3)$$

Here the two parameters γ and x_0 were chosen to give the best χ^2 fit. The trial functions were applied to the Atlantic Ocean between 30°N and 40°N for January and July of 1968. The best fit curves are shown relative to the data in figures 3.10a and 3.10b. The parameter γ is the half-width for this function rather than the standard deviation. With 41 degrees of freedom in each case, the χ^2 values obtained were 190 for January and 304 for July. The 50% point of the χ^2 distribution for 40 degrees of freedom is 39.3, and the 10% point, 51.8. Again, the fit may be better than indicated because the estimates are not independent.

The Cauchy distribution has an unfortunate property when it comes to estimating the mean of a quantity by the usual method. The usual method for estimating the variance of the mean is to relate it to the variance of the distribution using the formula

$$\sigma_{\text{mean}}^2 = \sigma_{\text{dist}}^2 / N^* \quad 3.4)$$

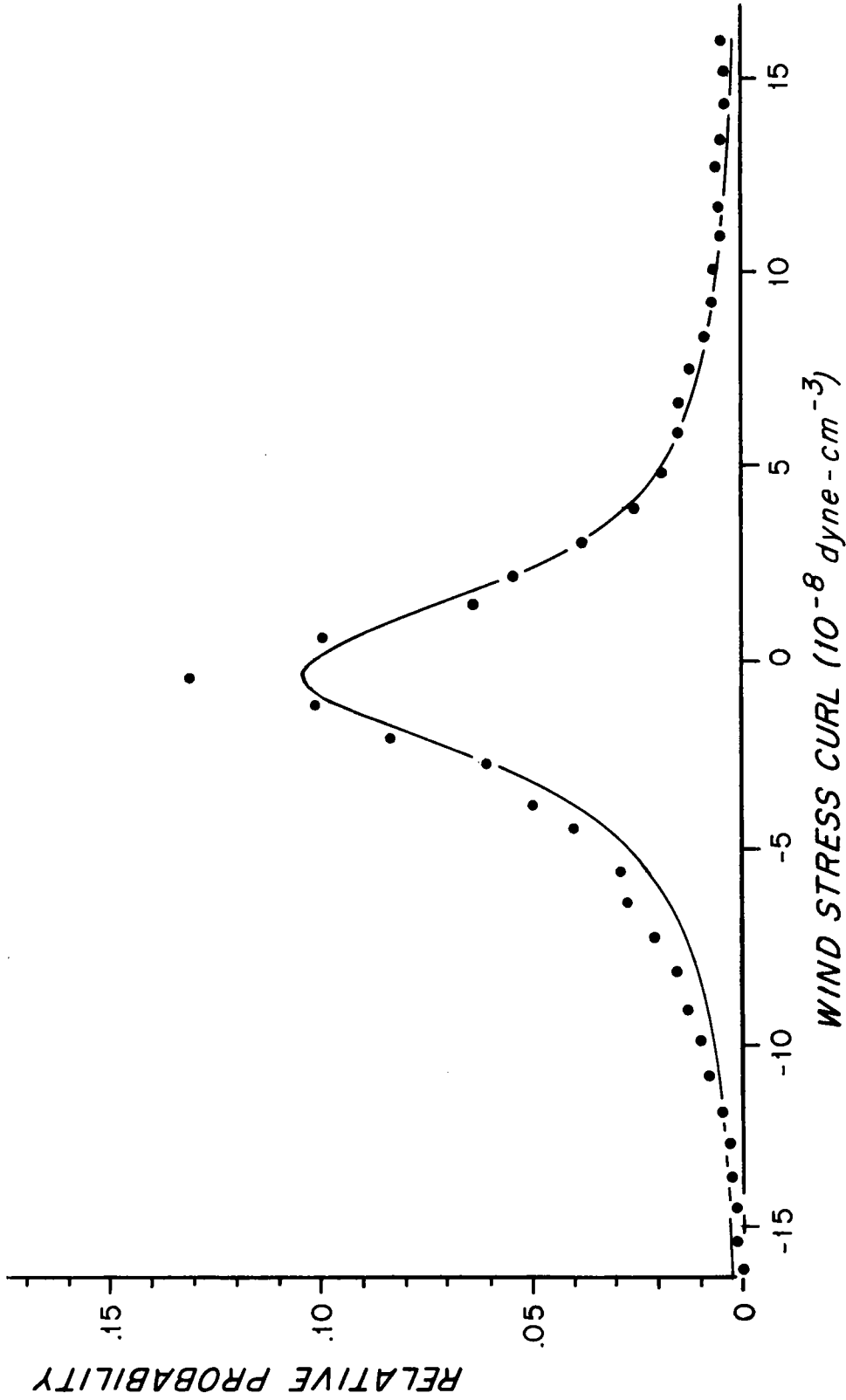


Figure 3.10a. Histograms of the estimated wind stress curl over the North Atlantic Ocean between 30°N and 40°N during January, 1968. The solid line shows the best fit Cauchy distribution as discussed in the text.

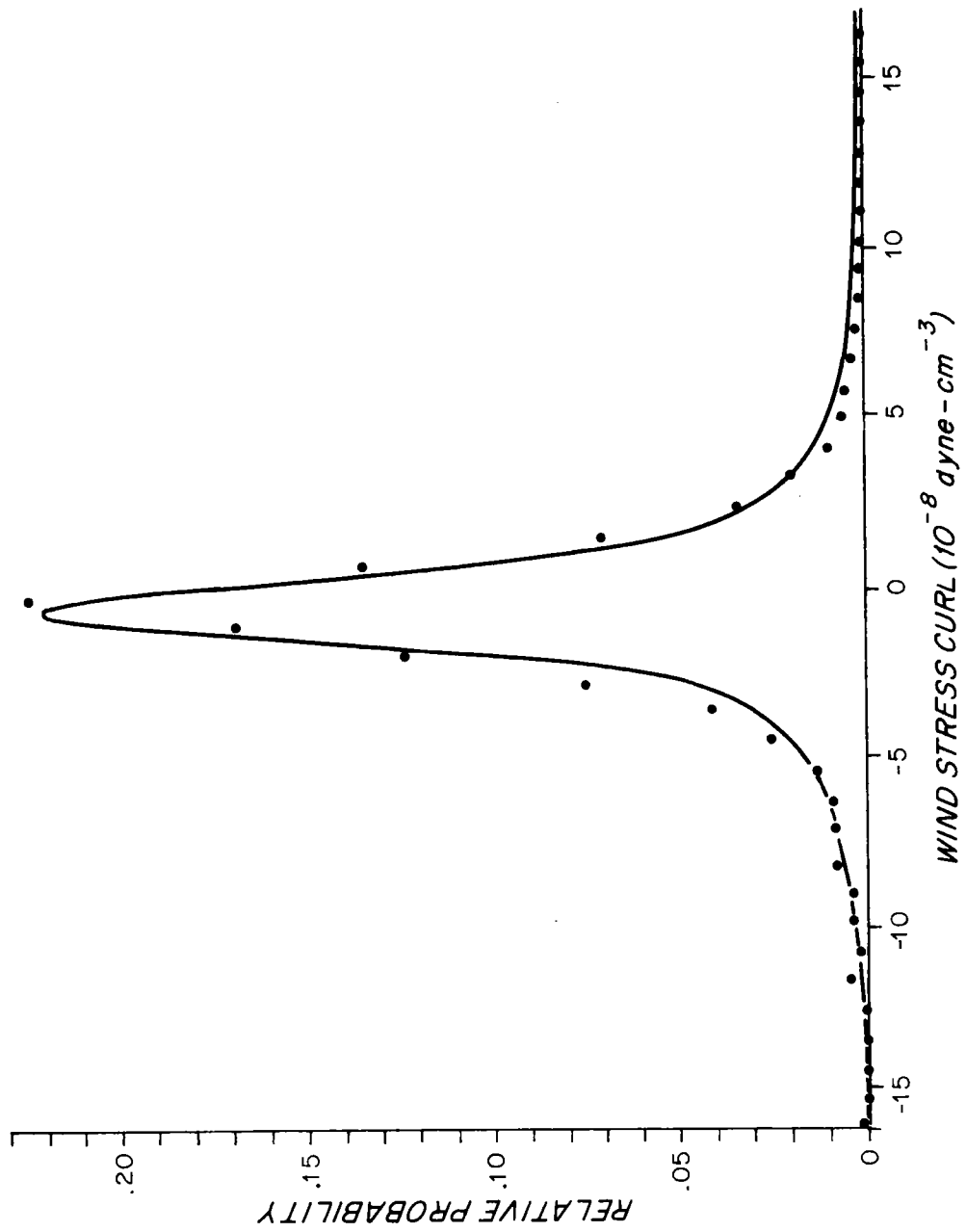


Figure 3.10b. Same as figure 3.10a for July, 1968.

where N^* is the number of independent estimates used in computing the mean. If $P(x)$ is the known probability distribution of the variate in question, the variance is formally given by

$$\sigma_{\text{dist}}^2 = \int_{-\infty}^{\infty} x^2 P(x) dx \quad (3.5)$$

where the variate in question is assumed to have zero mean for convenience. If this formula is evaluated with the Cauchy distribution, the result is

$$\sigma_{\text{dist}}^2 = \frac{\gamma}{\pi} \int_{-\infty}^{\infty} \frac{x^2}{\gamma^2 + x^2} dx \quad (3.6)$$

which is a divergent integral. Formally, then, it is impossible to estimate the mean value of a process which has a Cauchy distribution by the usual method.

Physically, of course, the wind stress curl cannot have a Cauchy distribution any more than the wind speed can truly have a Rayleigh distribution or atmospheric pressure have a Gaussian distribution. The reason for this is that all these mathematical functions admit a certain probability for arbitrarily large values of the variate. In all these cases, it is possible to establish absolute bounds on the variate using some physical reasoning. These

absolute bounds, however large, insure that the variance of any physical quantity will be finite. The important distinction between the Cauchy distribution and the other ones mentioned is that the variance of the bounded Cauchy distribution is a linear function of the bounding value while for the others, it becomes independent of the bounding value as that value becomes very large.

The most severe constraint resulting from the large variance of the wind stress curl distribution occurs in the estimation of climatological mean values. We may expect to require a much larger number of estimates of wind stress curl to specify a climatological mean value of wind stress curl to a given percentage accuracy than we would require to specify other quantities such as mean wind speed or mean surface pressure to the same accuracy.

On maps of wind stress curl estimates, the extreme values occur in groups and are generally associated with intense storms. The progress of the groups can be easily followed as they evolve in time over 12 hour samples. Figure 3.11 shows a 1000 mb height map typical of the Atlantic Ocean winter along with the oceanic pattern of wind stress curl associated with it. This particular map shows two areas of intense positive wind stress curl associated with winter storm centers along with several areas of smaller values associated with moderate pressure gradients.

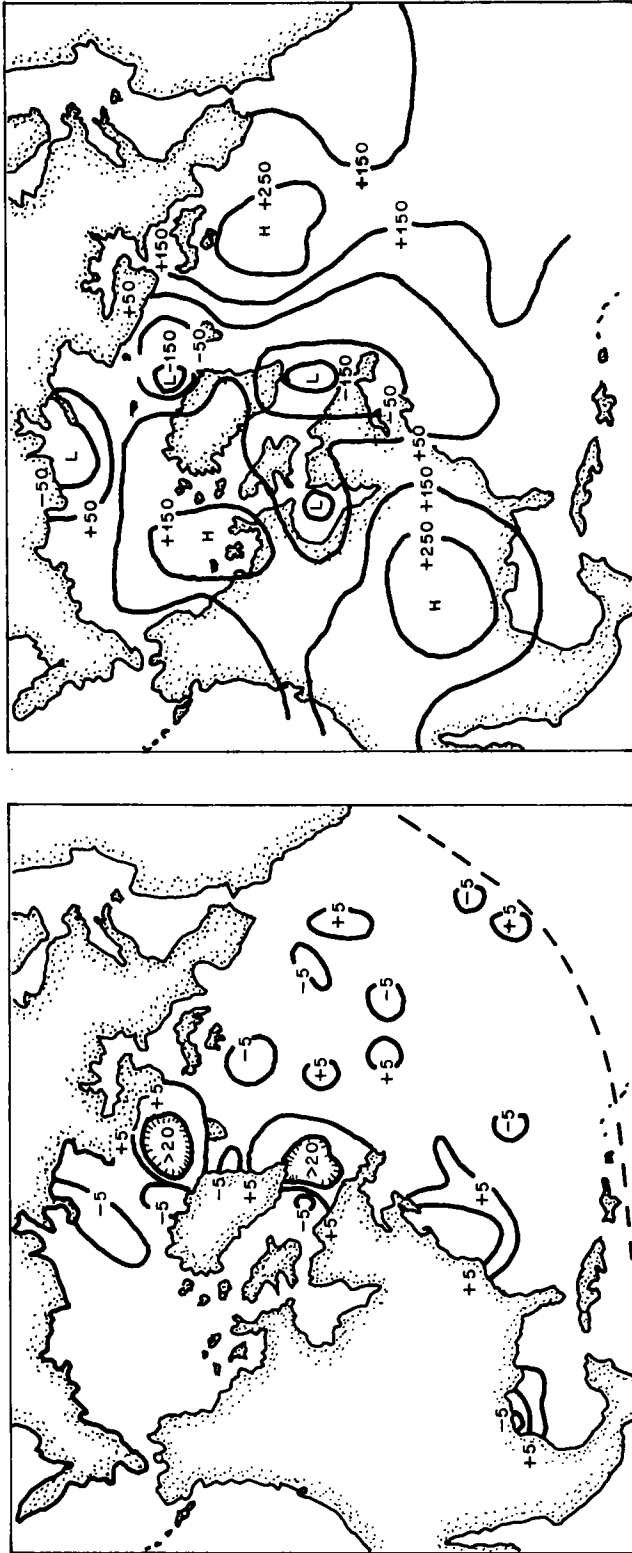


Figure 3.11. The right hand panel shows a typical winter 1000 mb height analysis over the Atlantic Ocean. The units are meters with a 100 meter contour interval. This particular analysis is for March 3, 1968 1200Z. The left hand panel shows the corresponding wind stress curl analysis with units of 10^{-8} dyne- cm^{-3} . An interpretation of these figures is given in the text.

By far the largest part of the ocean is occupied with wind stress curl estimates which are less than 5×10^{-8} dyne-cm⁻³ in absolute value. The character of the two maps is strikingly different. If these were topographic maps of different areas, a traveller would have little trouble distinguishing between them. The landscape corresponding to the pressure map would be gently rolling hills while that corresponding to the wind stress curl would be mostly flat, broken by high steep peaks and sudden deep holes.

The character of the synoptic wind stress curl map gives some insight into the unusual distribution of wind stress curl in a given area. Most of the contribution to the mean value of wind stress curl at a given point during a given month comes from the few events which have passed that point during that month. Thus, although sixty estimates are made during a month at a given point, one or two of these estimates, made when a storm passed over, are likely to account for most of the total monthly wind stress curl at that point. A monthly average at a point has only a few important independent estimates rather than sixty. This is the reason that it requires many more months to obtain a given number of important independent estimates than would be the case were the synoptic map more even.

If 12 hourly data are averaged over the period of a month, the average wind stress curl pattern becomes much

smoother, as shown in figure 3.12a for the North Pacific Ocean. Although smoother than the synoptic map, this monthly average does not look the way I expect climatological averages to appear. The averaging period is long enough for another effect to occur, however. This effect is the remarkable similarity between the pattern of wind stress curls calculated two different ways. Such a pair of patterns is shown in figures 3.12a and 3.12b expressed as meridional transport using equation 1.3. The first of this pair was calculated by averaging the 12 hourly computed maps of wind stress curl over a month. The second was calculated by averaging the values of 1000 mb height over the same month and computing the wind stress curl corresponding to the average 1000 mb height field. The major peaks in monthly average wind stress curl agree on the two maps. In fact, of the 85 separate estimates, only 10 disagree in sign, and those 10 are all adjacent to the contour of zero curl. If a response ratio is defined similar to the one constructed from the Aagaard study, it has a value of about 2 in the south increasing to about 3 in the northwestern corner. This remarkable similarity of patterns has remained one of the puzzles of this project. To date, no plausible reason for such a similarity has been discovered.

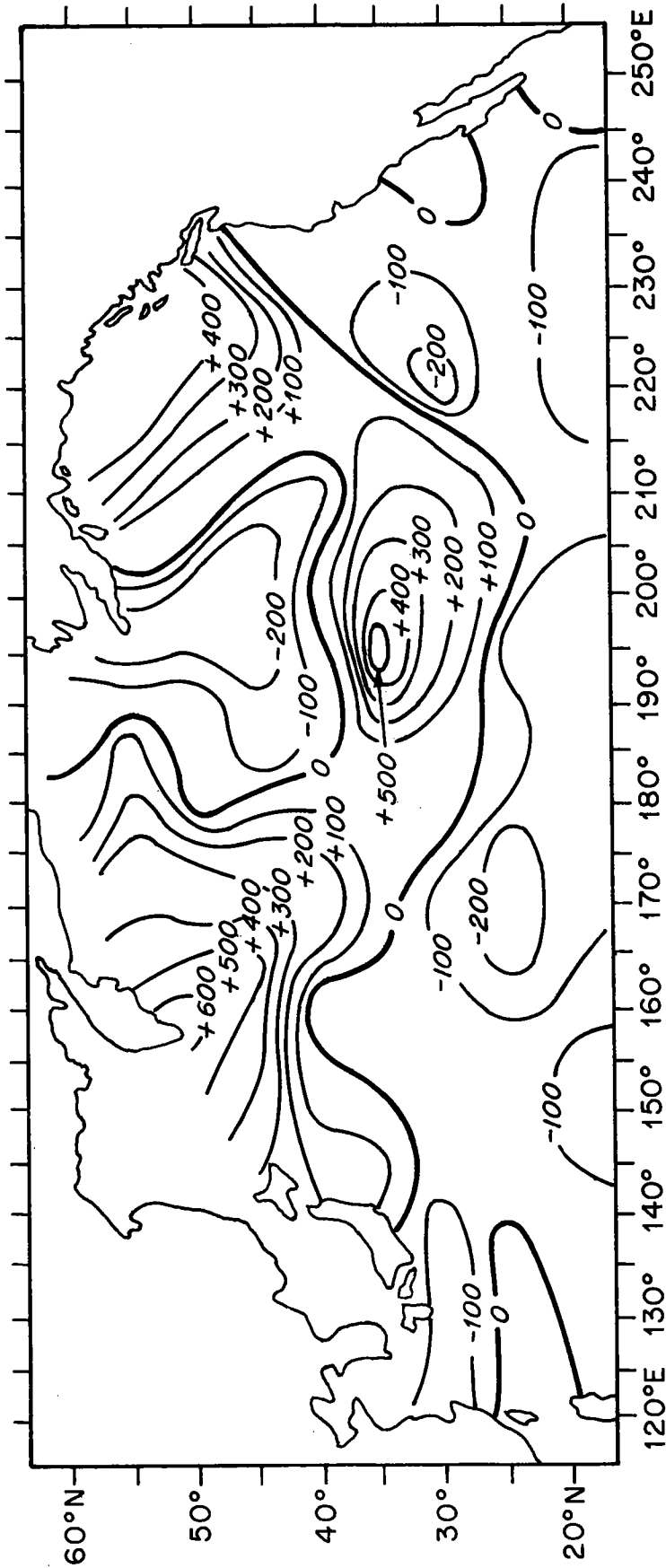


Figure 3.12a. Meridional Sverdrup transport over the North Pacific Ocean calculated from 1000 mb height analyses every 12 hours and averaged over January 1968. Contour interval is 10^{-2} Sverdrups/km.

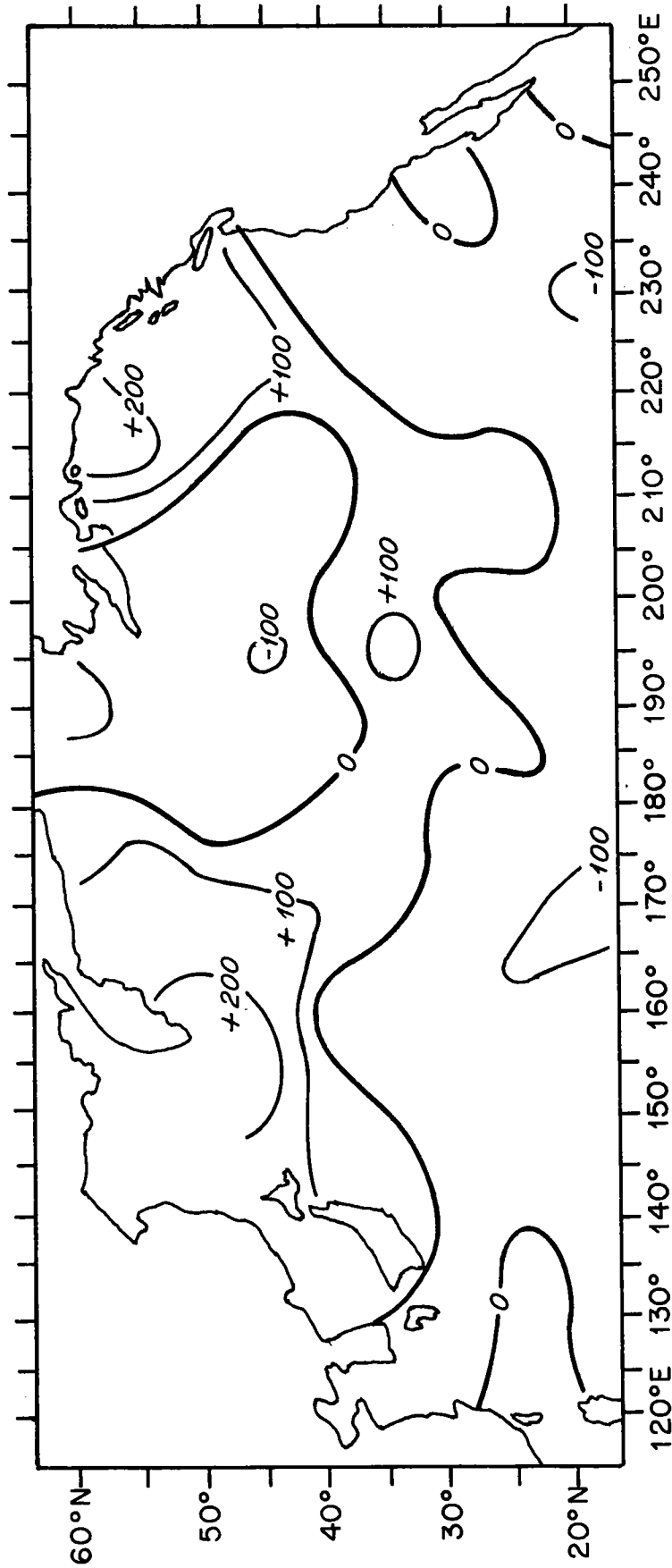


Figure 3.12b. Meridional Sverdrup transport over the North Pacific Ocean calculated from average monthly 1000 mb height analysis for January 1968.

In conclusion, the statistical study has had two objectives. The first has been to acquire some confidence in the data by studying a quantity, the geostrophic wind, which could be readily related to an observable quantity, the surface wind. The success of this comparison is best shown in the high value of coherence between the observed surface wind and the computed estimates. The second objective of the study has been the examination of the statistical properties of the wind stress curl field as estimated by the curl formula. The synoptic field of wind stress curl was found to be dominated by relatively few "events" of high absolute value surrounded by large areas of low absolute value. This structure was shown to produce a non-Gaussian distribution with strong emphasis on extreme values. The difficulty in estimating climatological means from such a distribution was discussed. Finally, a remarkable similarity between monthly averaged wind stress curls and wind stress curls calculated from monthly averaged pressure was noted in the Pacific Ocean. Such a similarity, apparent in the study of the Greenland Sea by Aagaard (1970) remains a puzzle.

The wind stress curl formula developed in these first three chapters is applied to several problems in the following chapters. First, it is used in a discussion of mean wind-driven transports. Then it is compared to fluctuations of the Bermuda sea level using the technique of time series analysis. Finally, it is compared to a time varying western boundary current as defined by the drift of icebergs in the Labrador Current.

CHAPTER IV

Equation 1.3) expresses the total meridional transport in a given location due to wind stress. If it is integrated across a zonal section of an ocean basin, the result is the total transport crossing the section due to wind driving. If the basin is closed off to the north of the section, continuity demands that the net flow across the section be zero. In this case, the wind driven flow to the north must be returned by some other mechanism. One such mechanism is a narrow western boundary current of the kind described by Stommel (1948) or Munk (1950). Because narrow boundary currents of considerable magnitude do exist in the North Atlantic and North Pacific Ocean, it is tempting and convenient to express the zonally integrated Sverdrup transport in terms of western boundary transport. This idea was first suggested by Munk (1950).

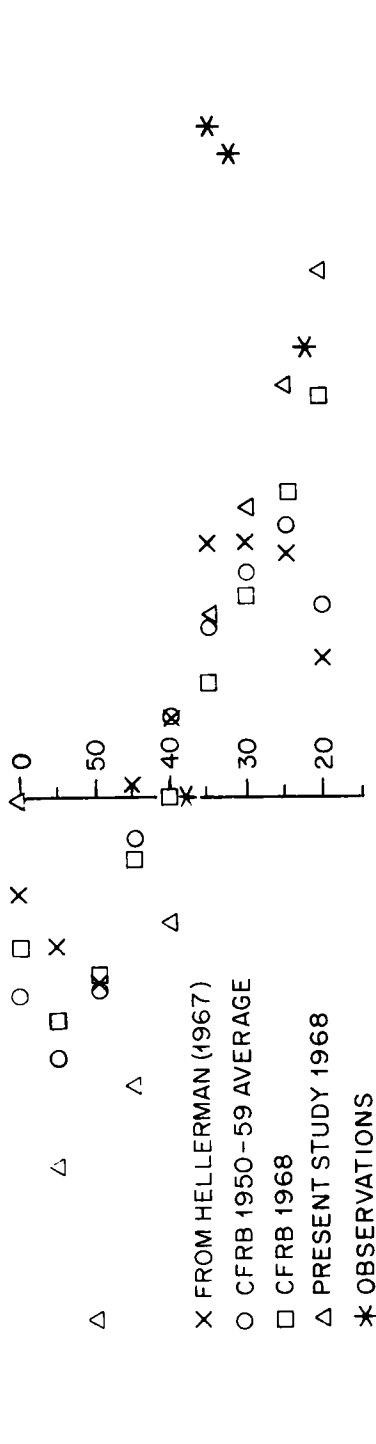
In applying Munk's suggestion, the assumption of no net flow must be examined. For instance, the East Australian current transport need not balance the wind driven transport between South America and Australia because the northward transport can easily return by circulating around the continent of Australia. Similarly, the Atlantic and Pacific Oceans exchange some water through the Arctic Ocean and Bering Strait. As this flow is only about 1 Sverdrup (Worthington, 1970),

it may be neglected in balancing the wind driven transport of the North Atlantic and North Pacific Oceans.

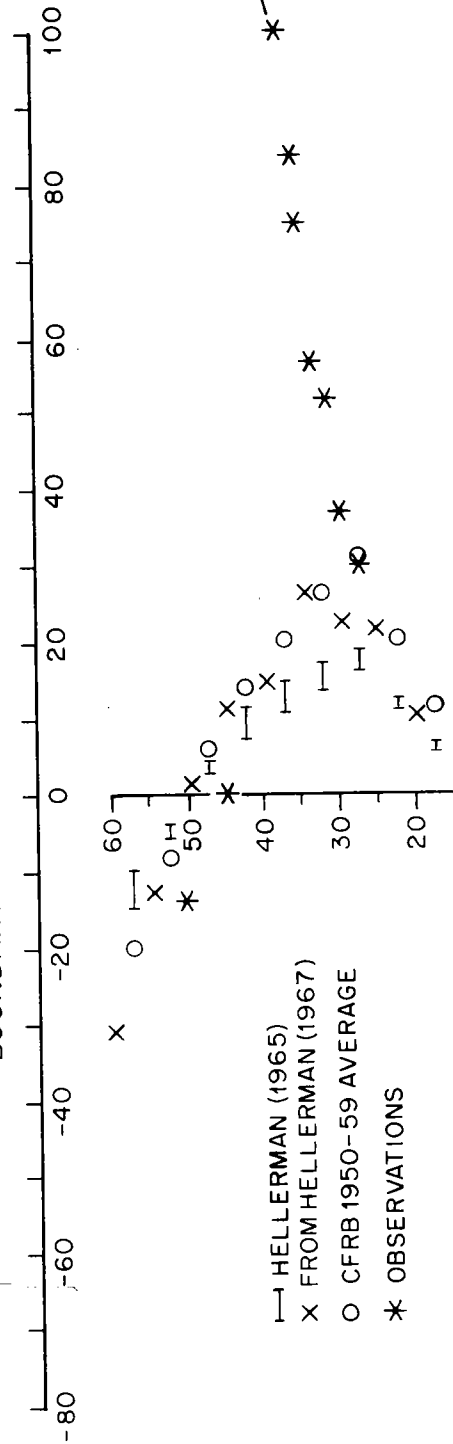
We can, then, apply Munk's suggestion to the wind stress in the North Atlantic and North Pacific Oceans. The resulting boundary transport is illustrated in Figure 4.1 for several different wind stress calculations. In the North Atlantic, estimates are shown from Hellerman (1965), from calculations using the data of Hellerman (1967) and from the Canadian Fisheries Research Board 10 year average (Fofonoff and Dobson, 1963a). Western boundary measurements are plotted from Knauss (1969) and Worthington (1969). In the North Pacific, estimates are made using calculations from the stress estimates of Hellerman (1967), the Canadian Fisheries Research Board 10 year means (Fofonoff and Dobson, 1963b), the Canadian Fisheries Research Board estimates for 1968 (Wickett, 1969), and the annual average for 1968 from the present study. Estimates of transport in the Kuroshio are obtained for comparison from Worthington and Kawai (in press). Estimates of latitudes of zero net transport (gyral boundaries) are taken from the surface current charts of Sverdrup, Johnson, and Fleming (1942).

In comparing the various calculated transport profiles to the observed profiles, one marked point of agreement and two points of strong disagreement may be noted. The

NORTH PACIFIC OCEAN



BOUNDARY TRANSPORT IN SVERDRUPS



NORTH ATLANTIC OCEAN

Figure 4.1. Western boundary transport in the North Atlantic and North Pacific Oceans as observed and estimated in several different studies from estimated wind stress.

agreement is between the sign of the calculated and estimated transports. In particular, the important latitude of the gyral boundary is well estimated in both Atlantic and Pacific Oceans.

In both oceans, the calculated and observed transports agree to within a factor of two from the southern limit of the calculation to the point where the calculated transports reach a maximum of about 30 to 50 Sverdrups. Between that point and the gyral boundary, the calculated net transport decreases smoothly while the observed transports continue to increase. At the gyral boundary, the net observed meridional transports decrease abruptly to zero. In both southern gyres, the maximum observed transports are significantly greater than the corresponding maximum calculated transports.

The situation in the northern gyres is somewhat different. Here the observed transports are smaller than the calculated transports. In fact, the maximum calculated transports of southward flow in the north are about as large as those of maximum calculated northward flow in the south. This means that if the "adjustable" parameters in the wind stress curl formula are set far beyond their normally quoted ranges to match the observed transport in the southern gyres, the flow in the northern gyres is grossly overestimated. Short of requiring the adjustable parameters to be strong functions of latitude, a procedure

for which there is little physical support, it is not possible to match these mean wind driven transport profiles with the observed ones.

An additional factor was considered in the present study which could have an effect on the values of calculated transport vs. latitude curve. The radius of a small storm can be just a few hundred kilometers and thus a few gridpoints. The entire area of positive wind stress curl from a Gaussian low pressure cell is located within 1 radius scale of the center. The same small storm may have the largest magnitude of local wind stress curls associated with it. Because the RMS value of wind stress curl is so much larger than the mean value, the numerical errors resulting from calculations on a finite difference grid may systematically bias the integrated transport calculations. This systematic bias would be different in the southern, central and northern portions of the oceans studied. In other words, a spatial response factor analagous to the temporal response factor discussed in chapter I may exist and the grid spacing of the NMC grid may not be fine enough to estimate the full value of the mean wind stress curl. Such an effect has been shown to exist for a numerical example of Gaussian pressure.

In order to present a direct comparison between calculations of wind stress curl from actual data using different areal densities, the NMC pressure data were averaged over periods of 1 month during the year 1968 and average annual transports were calculated (as a function of latitude) for the north Pacific Ocean. This calculation is directly comparable to the Canadian Fisheries Research Board calculations for 1968 (Wickett, 1969). Accordingly, figure 4.2 shows the annual average transport for the Pacific Ocean calculated several different ways. The two calculations described are plotted along with the 10 year averages from the Canadian Fisheries Research Board and the 1968 annual average from the twice daily wind stress curl calculations. The first feature of this graph is that 1968 was an unusual year in the southern part of the Pacific Ocean in that the mean transport in all estimates increased towards the south beyond the 10 year average maximum at 25°N. This indicates that the calculated value of 70 Sverdrups from the twice daily calculations may be unusually large and not comparable to the 1965 hydrographic sections from which the observed transport was calculated. The other feature of note is that the effect of using the finer grid mesh seems to bias the Canadian Fisheries Research Board results towards negative transport values in both gyres. This means that rather than reduce the discrepancy between observed and estimated transports, the finer grid mesh actually increases the discrepancy.

NORTH PACIFIC OCEAN

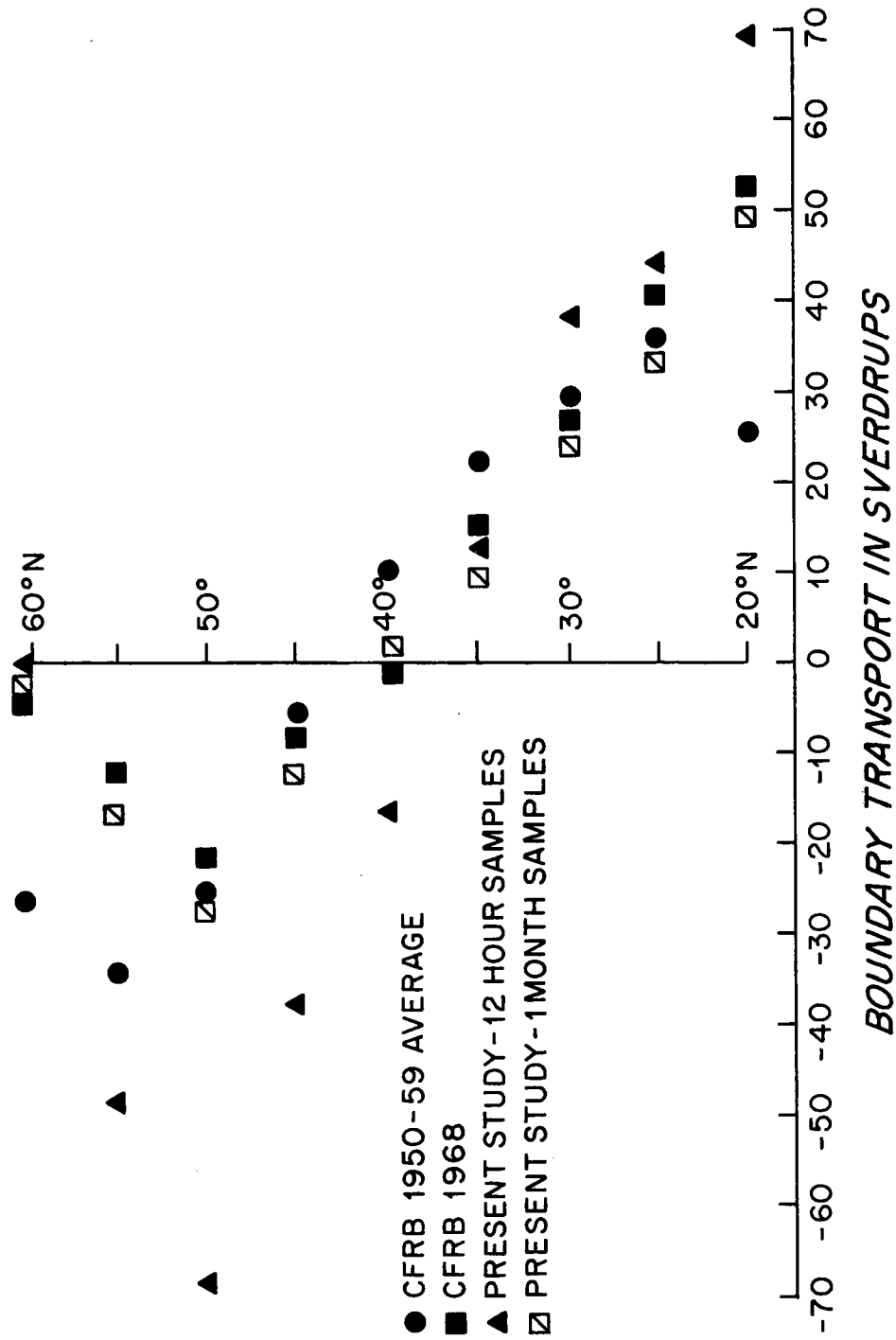


Figure 4.2. Western boundary transport for the North Pacific Ocean calculated several different ways as discussed in the text.

The result of the investigation of mean transports following the suggestion of Munk is that the mean meridional transport in the North Atlantic and North Pacific Oceans is not entirely driven by the mean wind stress curl. Although the gyral boundary is well estimated by the mean wind stress curl, the observed meridional transport to the south of the boundary is too large and to the north of the boundary too small to balance the mean wind stress curl. The effect of increasing the areal density of analysis, thus improving the calculation of the wind stress curl field, is to reduce a southward bias in the transport calculations and apparently aggravate the discrepancy between observed and calculated transports.

CHAPTER V

The study of mean values using the wind stress curl estimation formula has shown that the formula produces results which, when averaged over a month, agree with estimates of average wind stress curl using other methods. The value of the formula for estimation of oceanic driving terms will be greatly increased if it can be shown that the formula produces physically meaningful results on a much shorter time scale than a month, perhaps as short as 1 day. To this end an experiment was performed using time series analysis techniques to compare calculated wind stress curl to observed sea level fluctuations at Bermuda. The object of this experiment was to discover a significant coherence between the calculated wind stress curl and the observed sea level.

This particular experiment and data set were chosen for several reasons. Bermuda is in many ways an isolated island. It is not specifically associated with any major ocean currents or any large scale geological features, such as the mid-Atlantic ridge system. It is also a small flat island. Thus, it is likely to interfere as little with the atmospheric and oceanic

pressure and velocity fields as any island one might choose for such a study. During 1968, a high resolution (.01 ft) tide gauge was in operation on the island. This tide gauge provided a moderate quality high resolution time series of an oceanic variable (sea level) with a duration of over a year. Such records are relatively rare in oceanography. Although it is geophysically isolated, Bermuda is frequently visited by many ships. This is important because the analyses of atmospheric pressure which form a data base for this study are constructed from a combination of extrapolations and weather observations from ships. The analyses will be better in regions from which many ship reports are received than those with few ship reports. Because Bermuda has a high density of shipping, the pressure analyses are likely to be as good there as in any open ocean area. Thus at Bermuda, geophysical solitude is combined with a high resolution sea level record and high quality synoptic specification of the pressure field.

For this particular comparison, a strong noise component is included in the non-tidal sea level fluctuations. This noise is due to the inverted barometer effect. Because of this noise component, coherence between sea level and wind stress curl can be considered

significant only if it is unrelated to the coherence between sea level and atmospheric pressure. Thus, the actual experiment consists of a time series analysis of three fluctuating quantities, analyzed 1000 mb height (atmospheric pressure), estimated wind stress curl, and observed sea level.

There are two data bases used in this calculation, the data recorded by the automatic tide gauge at Ferry Reach, Bermuda and the 1000 mb height analyses made by the U. S. National Meteorological Center (NMC). The wind stress curl, calculated from the 1000 mb heights using a non-linear formula, is treated as a third independent time series.

The sea level data were supplied on punched cards for the period from January 1968 to July 1969. The numbers are recorded at hourly intervals. Because the tide gauge was newly operative in 1968, the data supplied contain both errors and gaps. The first editing done was to plot the data out in time series form. In this form, the regular diurnal and semidiurnal tidal cycles were quite apparent. Errors consisting of single or a few misplaced points during a cycle were also quite apparent. Such erroneous values were changed so that a smooth line drawn through the neighboring points would pass through the corrected value. A total of

75 errors were detected in this manner. Sixty-nine corrections were made and a single portion of the record totalling 48 hours was judged to be uncorrectable by this method. The sea level data thus consisted of corrected hourly values with some gaps between them. The next step was to process the data using a convolution filter developed by Groves (1955) for the specific purpose of discriminating against diurnal and semidiurnal periodicities. The filter is 37 hours long and reduces the principal semidiurnal and diurnal amplitudes by at least two orders of magnitude. The resulting series was then resampled at every twelfth point to match the sampling frequency of the NMC analyses. One problem associated with this procedure is that the length of each of the gaps is increased by four resampled points. The resulting sea level series is 1030 half-days long and has 179 missing points grouped in 20 gaps.

The 1000 mb height values for Bermuda were obtained from the NMC analyses. Fortunately, the position of Bermuda is nearly in the center of a square formed by the four grid-points nearest to the island. The values of 1000 mb height at these four points were averaged with equal weighting to produce the 1000 mb height time series. These data also had gaps in them resulting from missing analyses. There are a total of 60 missing

analyses grouped in 18 gaps.

The wind stress curl was calculated using the 12 point formula previously described. A single estimate was made from each analysis. This estimate was centered very nearly at the island. The resulting series has gaps corresponding to the gaps in the pressure data, and was left unfiltered.

Because of the gaps in both records, the analysis was performed by averaging over spectral estimates obtained from short time segments of the data rather than averaging over frequency estimates in bands obtained from a single spectrum analysis of the entire time series. The final analyses were done on 16 segments each of which contained 32 points spaced at 12 hour intervals. In order to reduce noise from spectral components of frequencies lower than $1/16$ cycles per day (CPD), the lowest resolvable frequency, the best fit straight line was removed from each of the 48 individual time series before the spectral decomposition was performed. The individual analysis frequencies thus lie between 0 and 1 CPD at 16 uniform intervals of $1/16$ CPD. The calculations were not done for the 0 CPD frequency estimate or the $15/16$ and $16/16$ CPD estimates.

The power spectrums of the three variables are shown in figure 5.1 for the remaining 14 frequencies.

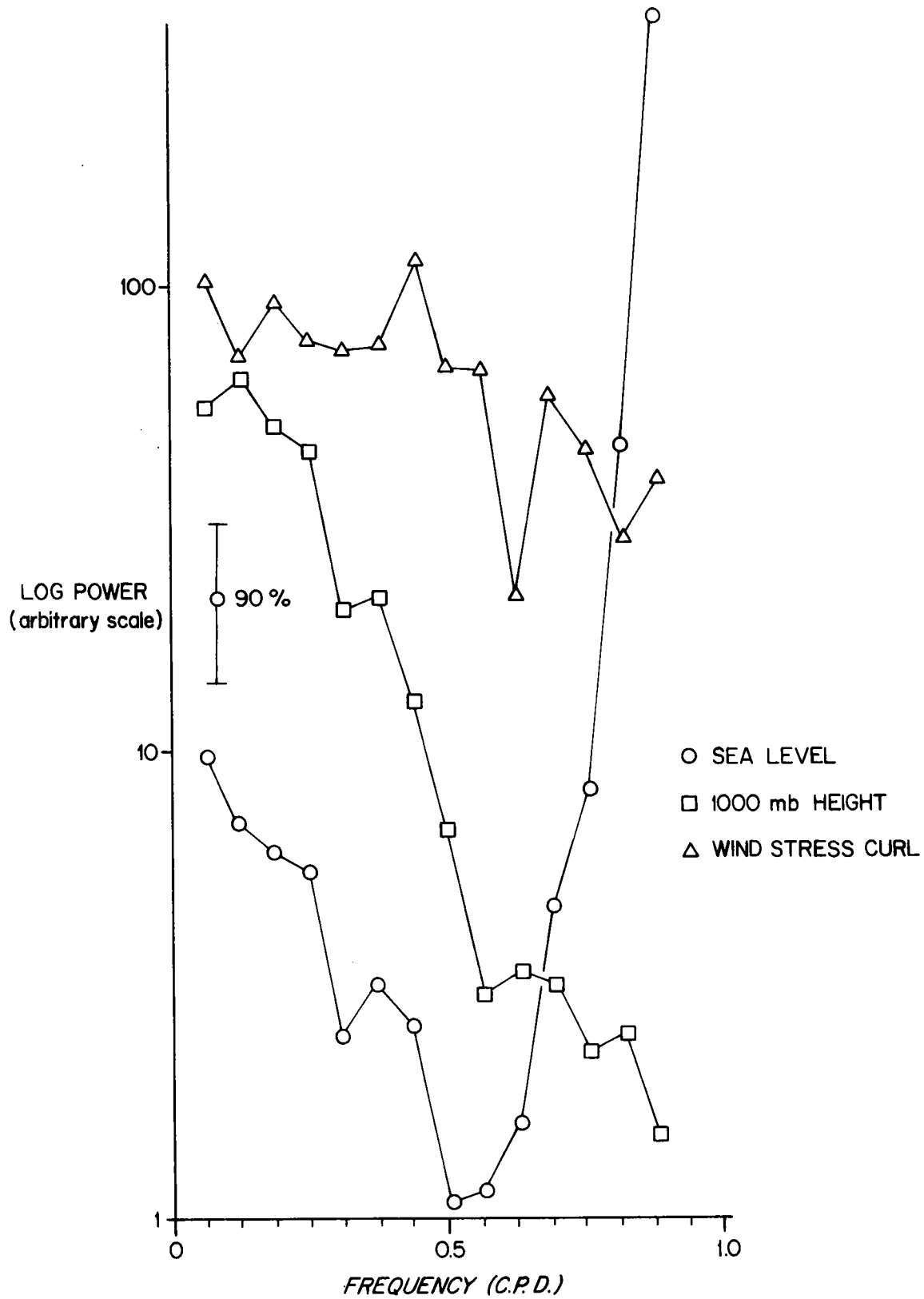


Figure 5.1. Power spectra of variables used in the Bermuda sea level experiment.

The sea level power has been corrected for the filtering attenuation at high frequencies. The rapid rise at frequencies approaching the diurnal tide starts at lower frequencies than a similar rise in a study of sea level at Bermuda over the 8 years 1953-1960 (Wunsch, 1972). This power is attributed to aliasing of the resampled series from non-tidal power at high frequencies. Because of this aliasing, 9/16 CPD appears to be the highest frequency at which the coherence for which we are looking can be found. At lower frequencies, the slope is similar to that presented in Wunsch (1972) so that this part of the spectrum is probably representative of actual conditions. In the 1000 mb height, the spectrum is seen to be a red one dropping off slightly faster than the sea level spectrum above .2 CPD and flattening out at lower frequencies. This qualitative behavior agrees with that of Wunsch (1972). Finally, the spectrum of the wind stress curl is a good deal flatter than the pressure spectrum, although it is still a red spectrum.

The next step in the study was to perform a linear regression of 1000 mb height and wind stress curl on sea level. The details of the method used are given in Groves and Hannan (1968) as are the estimates of statistical significance for the multiple and partial

coherences. The method used for calculating partial coherences was obtained from Bendant and Piersol (1966) while estimates of statistical significance for coherence were obtained from Amos and Koopmans (1963). The regression relation sought was of the form

$$\hat{y} = a_1 \hat{x}_1 + a_2 \hat{x}_2 + \hat{n} \quad 5.1)$$

where \hat{y} is the Fourier transform of the sea level record, \hat{x}_1 is the Fourier transform of the 1000 mb height and \hat{x}_2 , the Fourier transform of the wind stress curl. The a's are the complex regression coefficients. They are obtained by a least squares minimization of $\hat{n}\hat{n}^*$, the residual power.

Figure 5.2 shows the values of the regression coefficients obtained from this study. The 1000 mb height coefficient amplitude is close to the inverted barometer level and the phase is close to the inverted barometer phase of 180° from the low end of the spectrum to the frequency at which the sea level record is aliased. The phase stays near 180° even at higher frequencies. In the frequency range where the aliasing is not severe, these results are consistent with those of Wunsch (1972). The wind stress curl coefficient

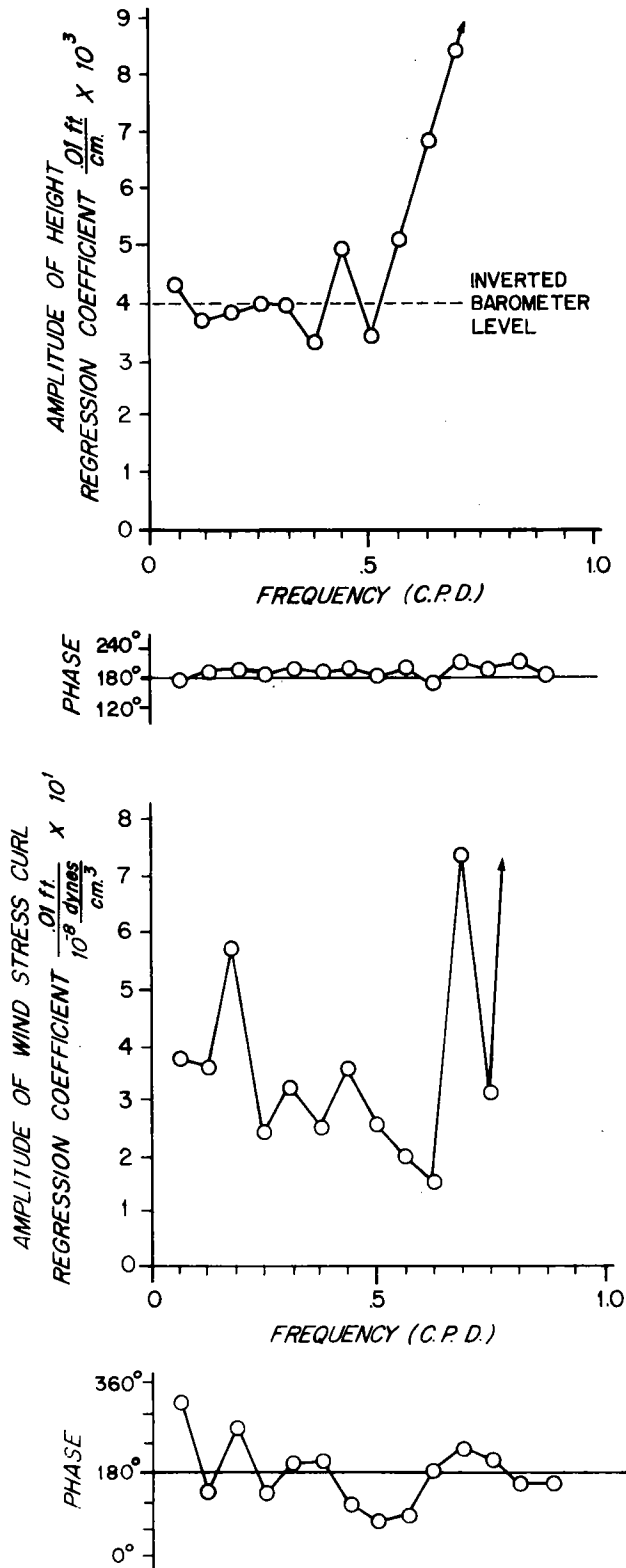


Figure 5.2. Linear regression coefficients of sea level on wind stress curl and 1000 mb height for the Bermuda sea level experiment.

is possibly random at low frequencies with slight evidence of stability between 4/16 CPD and 10/16 CPD. By itself, the value of the regression coefficient is not very informative. For the present purposes, the value of the partial coherence coefficient is of more value.

Before computing partial coherences, we calculate how successful the model of equation 5.1 is at describing the data. The measure of success is given at each frequency by the coefficient of multiple coherence, C_m as

$$C_m^2 = 1 - \frac{\hat{n}\hat{n}^*}{\hat{y}\hat{y}^*} \quad 5.2)$$

Here the astrisk denotes a complex conjugate. A graph of C_m as a function of frequency is presented as figure 5.3. From the figure, it is apparent that the linear regression fits the data well in the frequency range from 1/16 to 7/16 CPD. Above 7/16 CPD, the fit suddenly gets worse. Because the frequency of the first low coherence estimate is below the frequency of the severe aliasing, the cause of the sudden drop in coherence is probably something other than the aliasing of the sea level record.

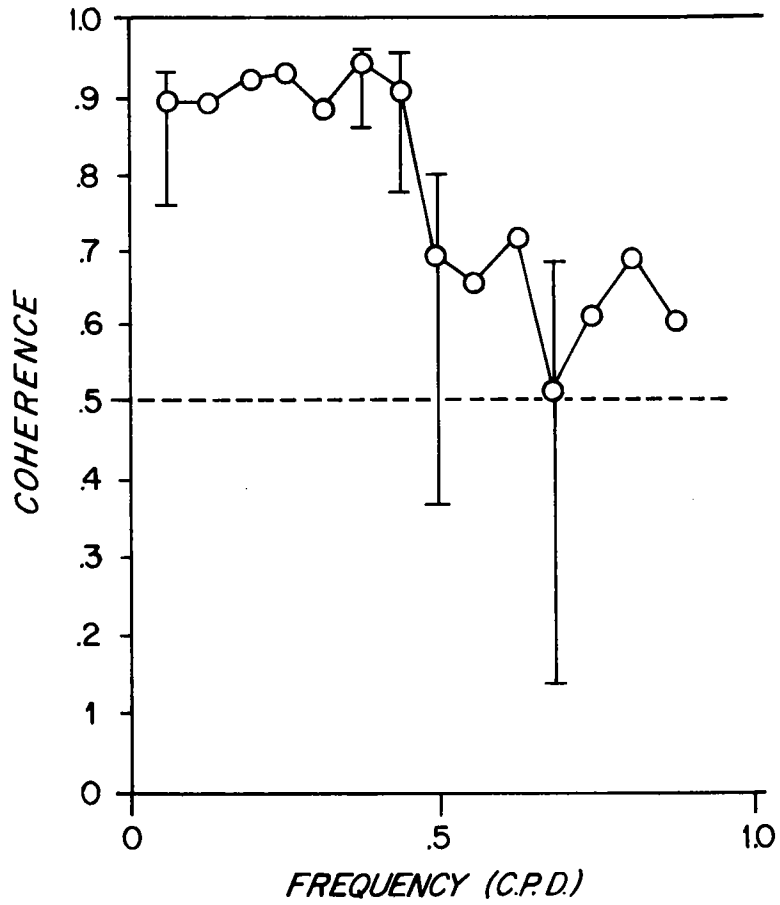


Figure 5.3. Multiple coherence of the linear regression model for the Bermuda sea level experiment.

The final figures 5.4 a, b are the partial coherences. These show that the low frequency success of the model is due to the 1000 mb height and the inverted barometer effect. This is consistent with the results of Wunsch (1972) who demonstrates that as much as 80% of the variance of the sea level in this frequency range can be related to the atmospheric pressure.

At higher frequencies, the wind stress curl has a peak of significant partial coherence. This peak occurs just at the frequency where the linear regression model starts to fail. It is only in the region of this peak that the regression coefficients for the wind stress curl series have any meaning. This peak is, in fact, the significant relation which this experiment was designed to find.

The peak in partial coherence between wind stress curl and sea level at Bermuda is the kind of response which would be produced by a trapped island oscillation mode which was being driven at its natural frequency. Such oscillations can exist around islands at frequencies below the local inertial frequency as shown in Rhines (1969). Such waves can exist when the oscillations advect the fluid across contours of constant depth. At Bermuda the constant depth contours are not symmetrical around the island, as the slope to the southeast of the

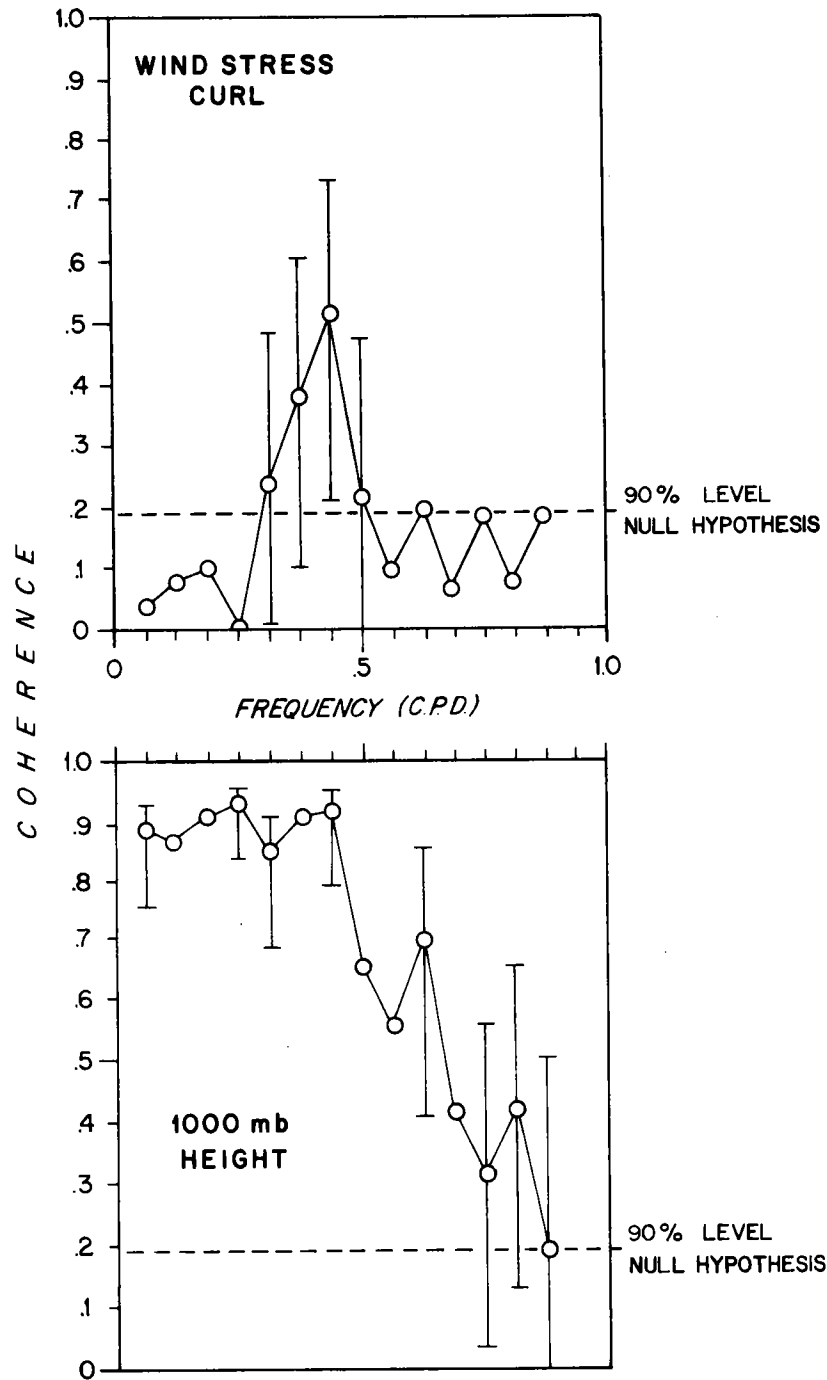


Figure 5.4. Partial coherence coefficients of 1000 mb height and wind stress curl with sea level for the Bermuda sea level experiment.

island is much greater than that to the northwest. Thus, an isotropic forcing can produce the motion of fluid across constant depth contours which is necessary for topographic waves. Thus it is plausible, although not conclusive that the wind stress curl is exciting a topographic wave around Bermuda resulting in the partial coherence peak.

The conclusion of this experiment is that the wind stress curl as estimated by the method developed in this thesis does estimate a physically significant quantity other than the atmospheric pressure from which it is derived. It is plausible that the estimated quantity is actually wind stress curl. A convincing demonstration would require an elaborate mathematical theory along with an extended experimental study designed to discriminate between alternatives. Such a demonstration is beyond the scope of this work.

In the next chapter, the wind stress curl formula is assumed to estimate wind stress curl. The estimated values are used in conjunction with a very simple theory to calculate currents rather than sea level. The currents thus calculated are compared to observations of iceberg drifts in the Labrador Sea.

CHAPTER VI

ICEBERG EXPERIMENT

A time dependent verification of the curl formula as applied through Sverdrup Transport was attempted using icebergs in the Labrador Current essentially as current drogues. The rationale for this assumption is that the effect of the current on the iceberg drift is able to dominate the local wind effect in this small region of relatively high current velocities. The behavior of icebergs for the year 1959 in the Labrador Current system on the slope of the Grand Banks was particularly well documented by the International Ice Patrol. It was also varied enough to provide a test for a time-dependent theory. Pressure analyses compatible with my existing programs were also directly available from NCAR for the same period. The calculations were made under the assumption of immediate response in the western boundary current to the Sverdrup Transport in the entire section from the Grand Banks to Europe. The actual dynamical reason why such a simple calculation gives the good agreement that is found is somewhat of a mystery, but the claim is made that essentially correct time variability of the wind stress curl field is a necessary condition for the good agreement between calculated and observed results.

Figure 6.1 shows the rough geographical relationship of the area in question, the NCAR calculation grid, and a schematic iceberg trajectory. A typical iceberg is formed from the Greenland ice cap and enters the ocean somewhere on the east coast of Greenland. It travels south in the East Greenland Current and rounds Cape Farewell to be carried north an unknown and variable distance in the Labrador Sea. The Labrador Sea is thought of as a reservoir of icebergs, which are frequently associated with polar sea ice. Some time later, it is caught up in the southward flowing Labrador Current and begins a rapid trip down the coast of Labrador to its eventual destruction in the warm waters of the North Atlantic Current. On reaching Newfoundland, it has several paths. It may ground on the Grand Banks or be carried around to the eastern slope of the Grand Banks where it can continue to the east or the south. If it goes south, it may leave the eastern slope at any time or even continue on around the southeastern corner to head west. In general, it is destroyed by melting in a fairly short time (about 10 days for a large berg) after encountering warm water. The only portion of the path with which this calculation is concerned is the southerly track along the eastern slope of the Grand

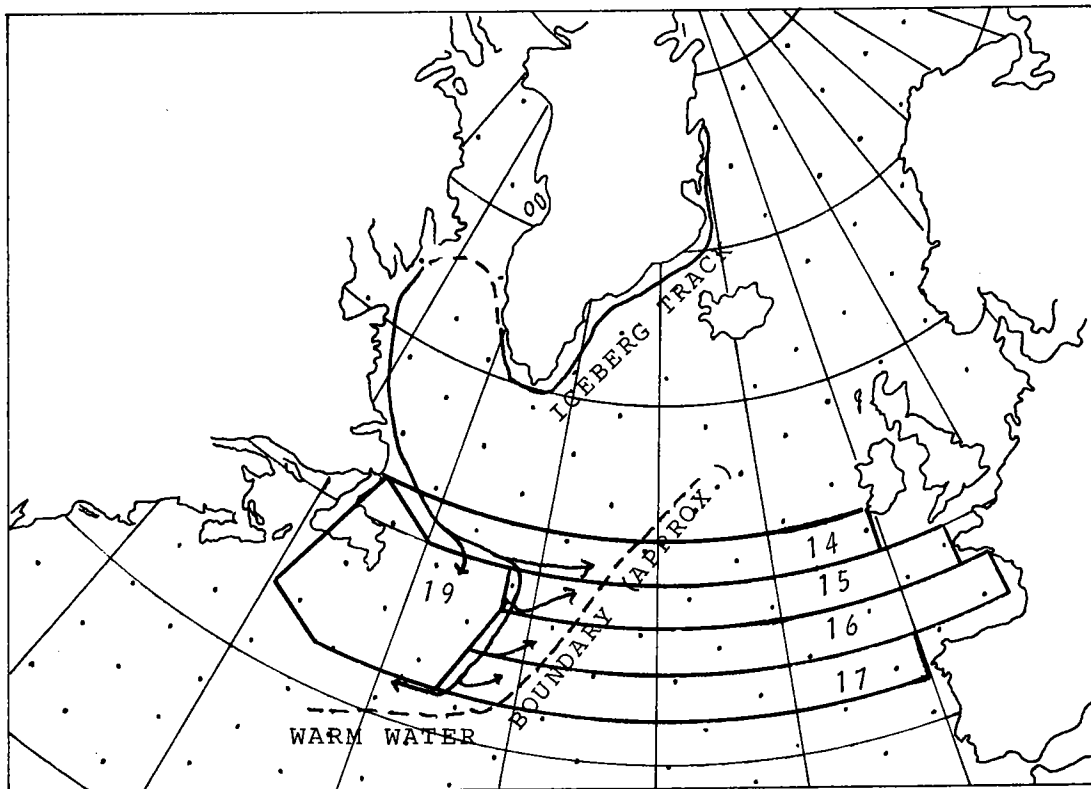


Figure 6.1. The geography relevant to the iceberg study. A schematic iceberg track is presented including the various paths an iceberg can take in the vicinity of the Grand Banks (region 19 on the chart). Regions 14-17 are $2\frac{1}{2}^\circ$ wide zonal sections over which the average value of wind stress curl was calculated. The dots give the location of NMC gridpoints in this region.

Banks where the current dominated trajectory assumption is likely to be valid.

Figure 6.1 also shows the latitude bands over which the calculations were made. The equation used was

$$V(\phi) = - \frac{R^2}{2\Omega\rho} (\theta_2 - \theta_1) \overline{\hat{k} \cdot \text{curl} \tau}^\theta \quad (6.1)$$

These calculations were made at 12 hour intervals at the sections marked 14, 15, 16 and 17. In addition, the estimates of the inflow or outflow of the Labrador Current were made by taking differences between adjacent sections of V . Thus, estimates of southward or outward transport were made at twelve hour intervals throughout the ice-berg season (January 1 to August 30) of 1959.

Figure 6.2 shows a typical integrated transport calculation over a period of eight months. Perhaps the most striking feature of this graph is the extreme spikiness of the signal. It is also clear that the spikiness and amplitude are both greater in the winter than in the summer. The spikiness may well be due in large part to the aliasing of the first derivative estimates which was mentioned in chapter I. Accordingly, the raw series was averaged over six estimates (three days) with even weighting and resampled at every sixth sample. The resulting series is shown as figure 6.3.

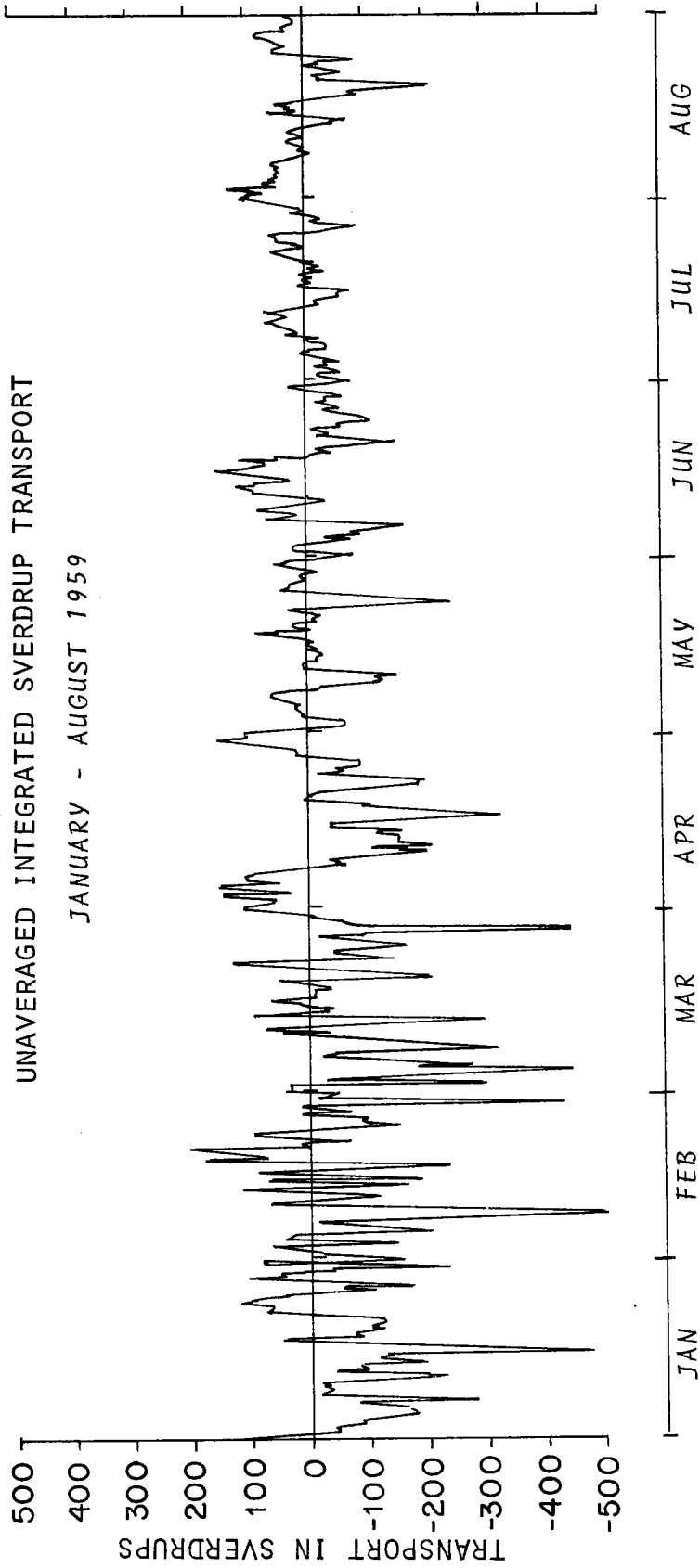


Figure 6.2. Labrador current transport calculated at 12 hour intervals across section 14 as discussed in text during the iceberg season of 1959.

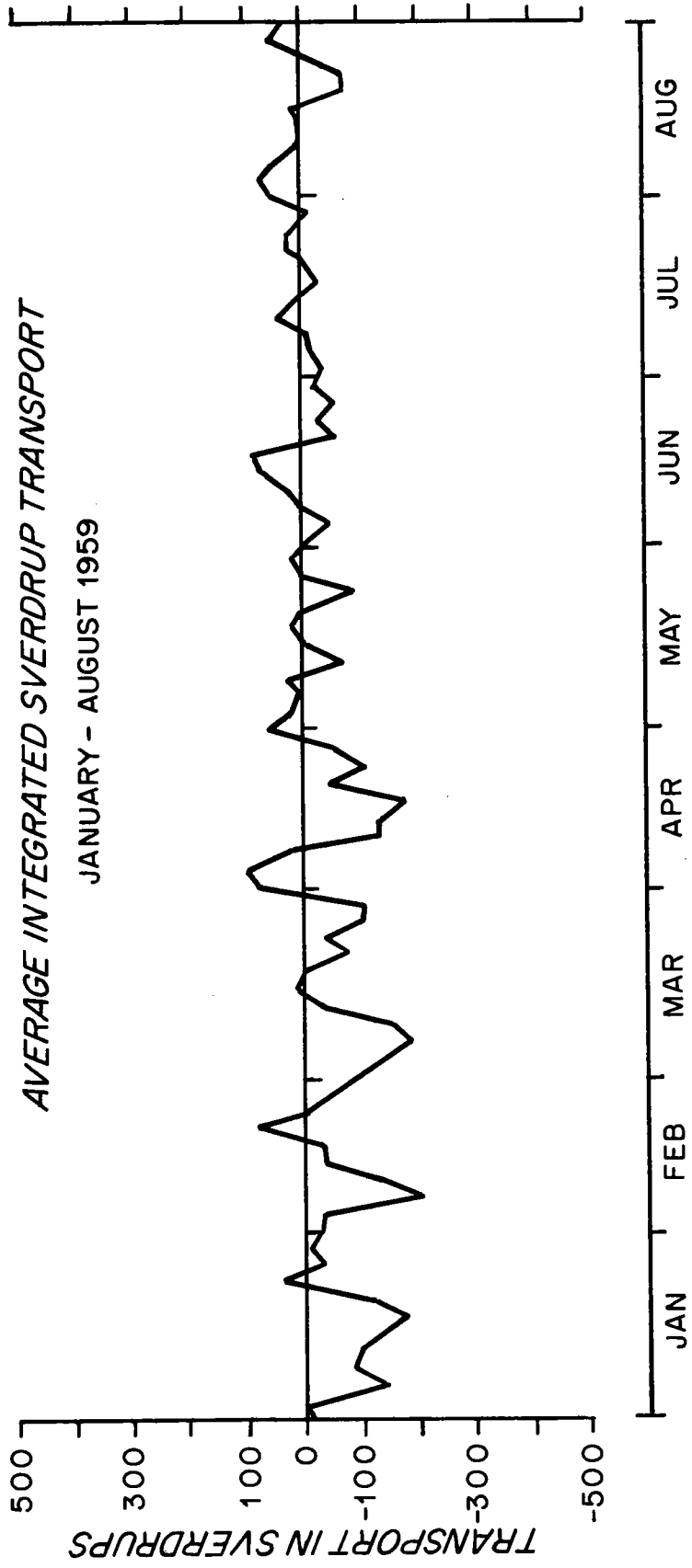


Figure 6.3. The same as figure 6.2 averaged over successive three day intervals.

The data used in the 1959 pressure calculations were originally analyzed to half the resolution of the 1968 data and then interpolated to the density of the 1968 data in order to be compatible with computer programs handling the 1968 data. For this reason, results obtained using the 1959 data can not be considered strictly comparable to those obtained using the 1968 data. As a general check on the comparability, some of the general statistical runs which were performed on the months of January and July for 1968 were rerun for the same months in 1959. The 1959 curl distribution had about 25% less (monthly) standard deviation over all the areas relevant to the study. This indicates that the re-interpolation did entail a certain amount of information loss. The effect this loss has on time mean values is difficult to ascertain as the high wavenumber response is most affected by such a smoothing procedure. My guess is that the mean estimates would probably be biased towards negative values. Such a bias correction would not bring the 1959 monthly means closer to the 1968 monthly means, but it must be pointed out that the reason iceberg data for 1959 are available is that 1959 was a particularly severe year for icebergs. This severity indicates that, in at least one particular, 1959 was an atypical year.

It is just this severity that led to the establishment of a surface ice patrol and an unusually large

quantity of position and drift data being taken during 1959. These data are presented in Coast Guard Bulletin #45 entitled International Ice Observations and Ice Patrol Service in the North Atlantic Ocean-Season of 1959, excerpts from which are given in appendix III. These data are presented in three places in the report and in two forms. In using them, one must think of the report as an historical rather than as a scientific document. The first source of data is a general summary of the year's activities. The next is a detailed month-by-month account of all kinds of ice in the Ice Patrol area. The third source is a set of charts of ice sightings and a single chart of iceberg drift tracks. (These tracks are illustrated individually for clarity in appendix III. In order to obtain a quantitative index of the amount of data contained in the first two sections, the following procedure was used. First, as many statements about ice as could be identified were given an index number. Then all statements or combinations of statements which could be used to make estimates of iceberg movements in the area of interest were collected and the estimates thus made were compared to the estimated integrated contemporary wind stress curls. The data contained in the iceberg track chart, with redundant information removed and contradictory information noted, was also used to compare to the calculated results.

Time sections of the results appear in figure 6.4a and figure 6.4b. In all, there are 171 statements about ice in the body of the report and 29 iceberg tracks. From these, a total of 26 deductions about iceberg movements were made which could be verified by the calculations. Of the 26, 20 agreed with the calculations and 6 disagreed. If the month of July is not included, the score is 18 and 3. The detailed scoreboard appears in appendix III.

The scoreboard approach looks good on the surface, but it is not the most convincing demonstration of the agreement. The single most convincing event will be presented here both for its own value and as an example of the deduction process used in constructing figures 6.4a and b. In appendix 3, the statement with index number 85 reads,

"Through the first week in April, a rapid recession of the ice limits gave the impression of an abrupt and early ending."

Statement number 87 reads, in part,

"The boundary was again on 11 April found to be moving southward and this trend continued....."

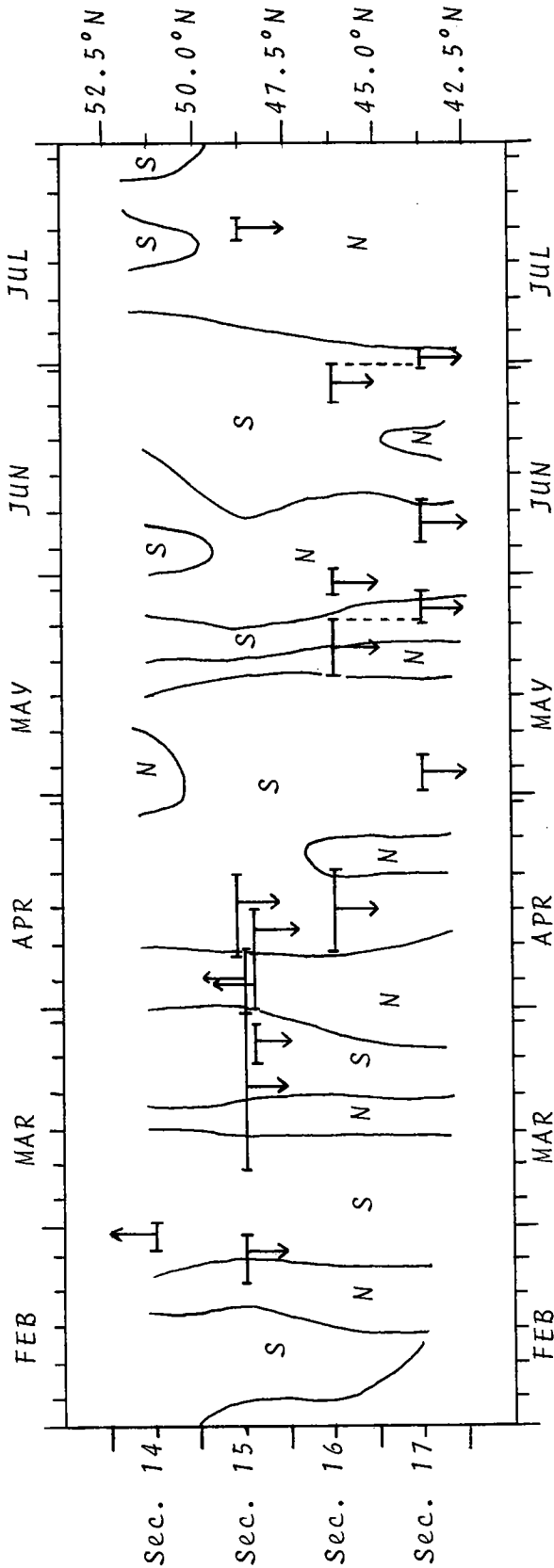


Figure 6.4a. Time section for Labrador current transport during the iceberg season of 1959 calculated according to the text. The iceberg motions deduced from the data are represented by the superimposed arrows and line segments. The periods over which the deductions are made is shown at each latitude by the extent of the horizontal segment. The vertical arrows indicate the direction of deduced motion, an upward pointing arrow denoting a northward drift and a downward pointing arrow denoting a southward drift. A broken vertical line indicates that a single iceberg has moved to a new section.

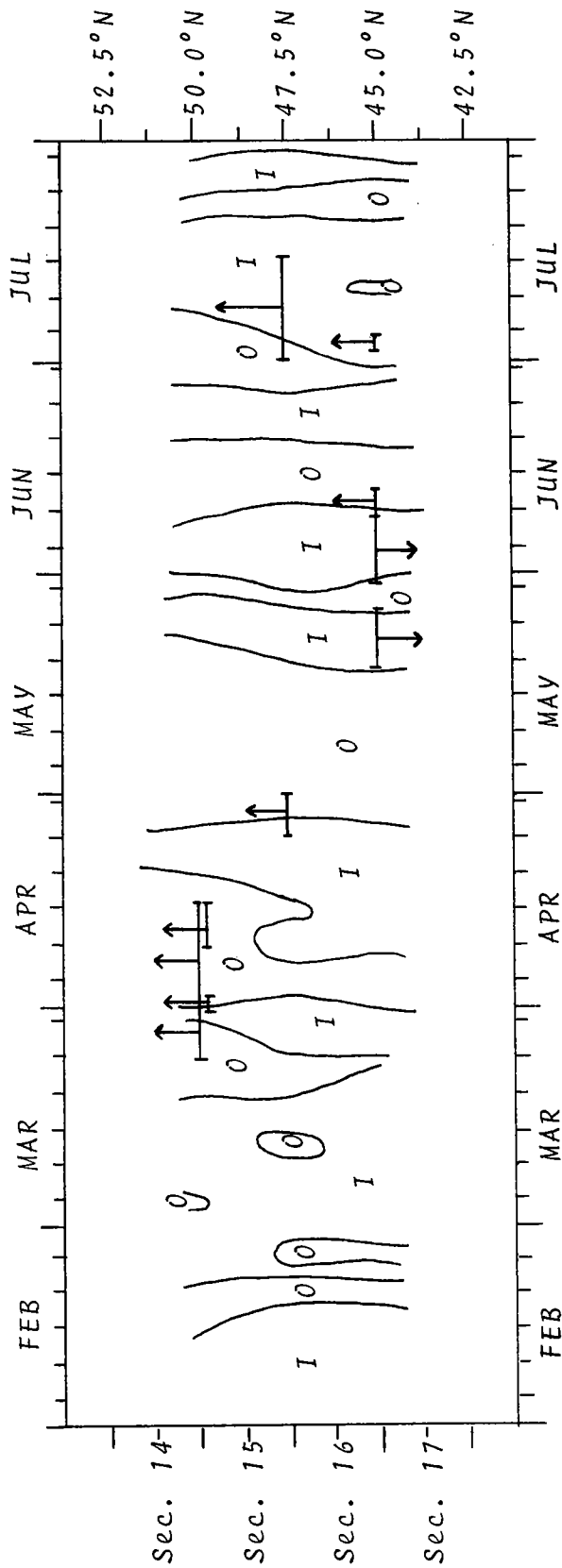


Figure 6.4b. Time sections for the horizontal divergence of the Labrador Current calculated according to the text and compared to deduced iceberg motions. The deduced motions are indicated as in figure 6.4a with upward pointing arrows denoting divergence and downward pointing arrows denoting convergence.

These two statements refer to the southern limits of the pack ice field. Going on further in the report, we find statements number 99 and 100, which read,

"During the first week in April, the several icebergs which led the movement southward along the eastern slope of the Grand Banks appeared to have been an isolated group the main body of bergs was still within the field ice limits north of 49° Latitude."

Statement number 107 is,

"Aerial Ice Reconnaissance on 9 April showed the main body of bergs was just reaching latitude 49°N and still concentrated well offshore."

Statement 109 is, in part,

"By 20 April Large numbers of bergs had crossed the 48th Parallel"

Finally, statement number 111 reads,

"The arrival of the berg multitude over the Grand Banks corresponded closely with the advance of the Arctic sea ice pack described in the second paragraph of the discussion for this month."

From these statements, we infer that the ice movement, which had started freely during March (statement number 82), was blocked from about April first or second until the tenth or eleventh of April. Then, the ice which had accumulated behind the block was released and overran the Grand Banks. Now refer to figure 6.2, the unaveraged transport for section 14. (The graph for section 15 is similar). During the period from the first to the ninth of April, the calculated transport is entirely to the north, the abnormal direction. Such a long unbroken string of northward transport estimates is not again exceeded until the middle of the summer. If we consider it to be a single highly unusual event, we cannot say statistically that it should not coincide with the abnormally rapid ice limit recession. That two such unusual events which can be physically associated by a simple theory do coincide is a very convincing situation when it is found in nature. In my opinion, it is more convincing than the scoreboard.

In order to emphasize the long period motions, a monthly mean transport time section, figure 6.5, was constructed. This seems to show an unusually strong transport for the month of March, one month before the actual peak of the iceberg season. It also shows a net transport to the north during some summer months. It turns out that April was the heaviest iceberg month for 1959, a not un-

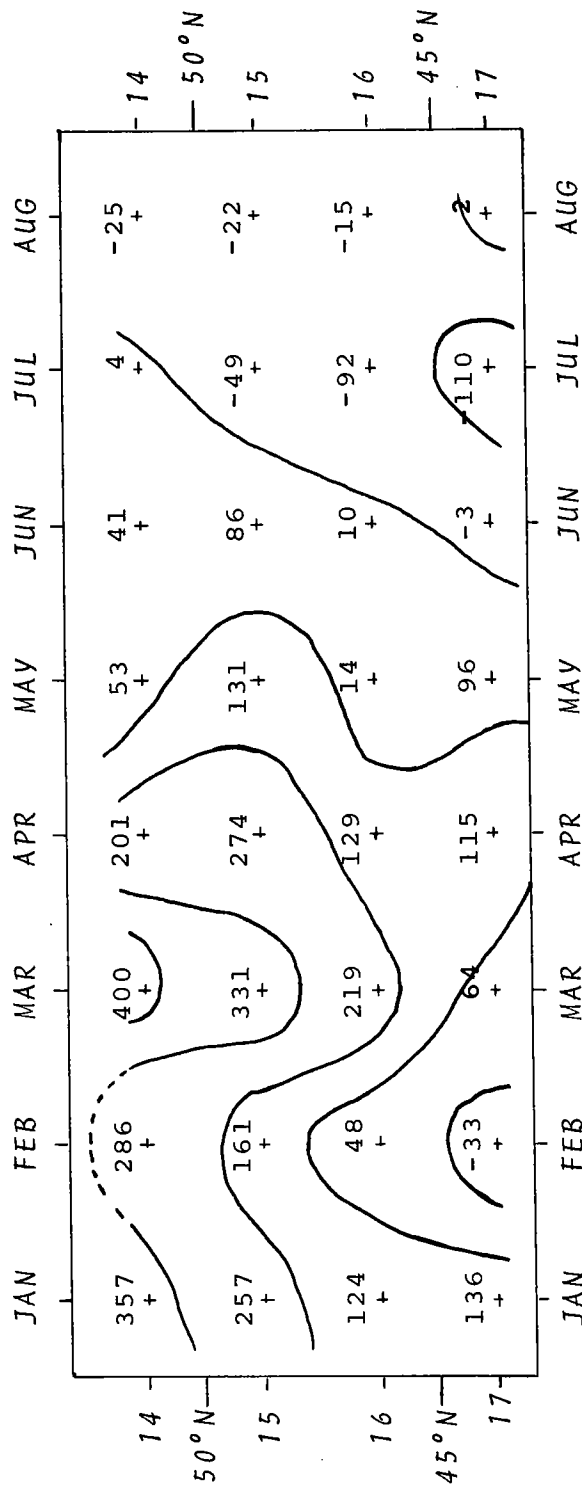


Figure 6.5. Time sections of monthly averaged calculated Labrador Current transports for January through August 1959. Units are 10⁻¹ Sverdrups with a contour interval of 10 Sverdrups.

usual occurrence. It was, however, the fifth most severe April since 1900. It may be that the severity of April is related to the particularly strong transport in March. It is also interesting to note that some current meters placed to the north of this area in the summer of 1970 by the Coast Guard showed a net northward displacement during the period of their deployment from August 21 to September 4. These two points are presented in a most tentative manner. They are suggestive rather than conclusive and serve only to point to features which may well be worthy of further study.

The conclusions of this experiment are then as follows. The time variable nature of the Labrador Current as evidenced by iceberg drifts is such that it agrees well with concurrent Sverdrup Transport calculations for the sections extending from the Grand Banks to Europe. Whatever the dynamics of the situation, an essential ingredient for the good agreement is that the signs both of the calculations in each section and the signs of the differences between adjacent sections must be essentially correct. This strongly supports the theory and method leading to the values of wind stress curl.

An example of good agreement is probably the best place to stop and try to examine what has been accomplished. This research has consisted of further development of a tool, in this case the method for calculating wind stress curl proposed by Montgomery and developed by Fofonoff, and some initial attempts to apply the tool to oceanographic problems. The remarkable success of these crude attempts indicates that the method is well enough developed to be of some utility in an area of oceanography which has been noted for its elusiveness and costliness, the time-dependent calculations of oceanic motions. This potential utility is the most compelling argument in favor of presenting the results of this research at this point rather than polishing the details to a high gloss. It is my hope that the potential utility becomes actual.

APPENDIX I

STEREOGRAPHIC PROJECTION FORMULAS

This appendix continues the development of formulas relating the spherical coordinates of the earth to the computer coordinates of the stereographic projections.

The transformation formulas are

$$I = 31 \tan \left(\frac{90^\circ - \phi}{2} \right) \cos (\theta - 10^\circ) \quad (\text{I-1})$$

$$J = 31 \tan \left(\frac{90^\circ - \phi}{2} \right) \sin (\theta - 10^\circ) \quad (\text{I-2})$$

with inversions

$$\phi = 90^\circ - 2 \tan^{-1} \left[\frac{(I^2 + J^2)^{\frac{1}{2}}}{31} \right] \quad (\text{I-3})$$

$$\theta = 10^\circ + \tan^{-1} \left(\frac{J}{I} \right) \quad (\text{I-4})$$

In order to select the correct quadrant for θ the following sign convention is used

I	J	$\tan^{-1} \left(\frac{J}{I} \right)$
+	+	0 - 90°
-	+	90° - 180°
-	-	180° - 270°
+	-	270° - 360°

In these formulas θ is the east longitude, ϕ the north latitude, and I and J are the rectangular coordinates on the stereographic projection.

Coordinates can be defined which are identical to FORTRAN array indices (I*,J*) by translating the origins

$$\begin{aligned} I^* &= I + 24 \\ J^* &= J + 26 \end{aligned} \tag{I-5}$$

provided that an array is used such as the NMC 47 x 51 grid illustrated in figure 2.1b.

The scale factors for the transformation are the same for both I and J directions and are given by

$$h_I = h_J = \frac{62R}{I^2 + J^2 + 961} = \frac{R}{31} (1 + \sin \phi) \tag{I-6}$$

where R is the radius of the earth.

Trigonometric functions of latitude become algebraic functions of the new coordinates and are given by

$$\sin \phi = \frac{961 - I^2 - J^2}{961 + I^2 + J^2} = \frac{961 - r_I^2}{961 + r_I^2} \tag{I-7}$$

$$\cos \phi = \frac{62(I^2 + J^2)}{961 + I^2 + J^2} = \frac{62r_I^2}{961 + r_I^2} \tag{I-8}$$

$$\tan \phi = \frac{961 - I^2 - J^2}{62(I^2 + J^2)} = \frac{961 - r_I^2}{62r_I^2} \tag{I-9}$$

The combination $I^2 + J^2$ occurs so frequently that it is convenient to abbreviate it r_I^2 .

There are eight possible first partial derivatives given by

$$\frac{\partial \phi}{\partial I} = - \frac{62I}{r_I(961 + r_I^2)} \quad (\text{I-10a})$$

$$\frac{\partial \phi}{\partial J} = - \frac{62J}{r_I(961 + r_I^2)} \quad (\text{I-10b})$$

$$\frac{\partial \theta}{\partial I} = - \frac{J}{r_I^2} \quad (\text{I-10c})$$

$$\frac{\partial \theta}{\partial J} = \frac{I}{r_I^2} \quad (\text{I-10d})$$

and

$$\frac{\partial I}{\partial \phi} = - \frac{I(961 + r_I^2)}{62r_I^2} \quad (\text{I-11a})$$

$$\frac{\partial J}{\partial \phi} = - \frac{J(961 + r_I^2)}{62r_I} \quad (\text{I-11b})$$

$$\frac{\partial I}{\partial \theta} = - J \quad (\text{I-11c})$$

$$\frac{\partial J}{\partial \theta} = I. \quad (\text{I-11d})$$

The Jacobian of the transformation is

$$J \left(\begin{matrix} I, J \\ \phi, \theta \end{matrix} \right) = - \frac{r_I(961 + r_I^2)}{62}. \quad (\text{I-12})$$

These derivatives can also be expressed in terms of the latitude and longitude ϕ and θ , but the frequently occurring combinations $\alpha = \frac{90^\circ - \phi}{2}$ and $\beta = \theta - 10^\circ$ will be used instead.

Thus

$$\frac{\partial \phi}{\partial I} = - \frac{2}{3I} \cos^2 \alpha \cos \beta \quad (\text{I-13a})$$

$$\frac{\partial \phi}{\partial J} = - \frac{2}{3I} \cos^2 \alpha \sin \beta \quad (\text{I-13b})$$

$$\frac{\partial \theta}{\partial I} = - \frac{1}{3I} \cot \alpha \sin \beta \quad (\text{I-13c})$$

$$\frac{\partial \theta}{\partial J} = \frac{1}{3I} \cot \alpha \cos \beta \quad (\text{I-13d})$$

and

$$\frac{\partial I}{\partial \phi} = - \frac{3I}{2} \sec^2 \alpha \cos \beta \quad (\text{I-14a})$$

$$\frac{\partial I}{\partial \theta} = - 3I \tan \alpha \sin \beta \quad (\text{I-14b})$$

$$\frac{\partial J}{\partial \phi} = - \frac{3I}{2} \sec^2 \alpha \sin \beta \quad (\text{I-14c})$$

$$\frac{\partial J}{\partial \theta} = 3I \tan \alpha \cos \beta \quad (\text{I-14d})$$

with

$$J \left(\frac{\phi, \theta}{I, J} \right) = - \frac{2}{96I} \cos^2 \alpha \cot \alpha \quad (\text{I-15})$$

Using these formulas and the scale factors, vector derivative formulas can also be expressed in computer coordinates. In these expressions the derivatives with respect to computer coordinates will be expressed with the subscript I while those with respect to the earth will have no subscript. R is the radius of the earth. So

$$\nabla f = \frac{961 + r_I^2}{62R} \nabla_I f \quad (\text{I-16})$$

$$\nabla \cdot \underline{\alpha} = \frac{961 + r_I^2}{62R} \nabla_I \cdot \underline{\alpha} - \frac{1}{31R} r_I \cdot \underline{\alpha} \quad (\text{I-17})$$

$$\hat{k} \cdot \nabla \times \underline{\alpha} = \frac{961 + r_I^2}{62R} \nabla_I \times \underline{\alpha} - \frac{1}{31R} r_I \times \underline{\alpha} \quad (\text{I-18})$$

If a vector \underline{A} is written in components either of latitude and longitude (A_θ, A_ϕ), or in computer coordinates (A_I, A_J), it can be transformed to the other system with the following equations:

$$A_I = - A_\theta \sin \beta - A_\phi \cos \beta \quad (\text{I-19a})$$

$$A_J = - A_\theta \cos \beta - A_\phi \sin \beta \quad (\text{I-19b})$$

or

$$A_{\theta} = -A_I \sin \beta + A_J \cos \beta \quad (\text{I-20a})$$

$$A_{\phi} = -A_I \cos \beta - A_J \sin \beta \quad (\text{I-20b})$$

where we have $\cos \beta = \frac{I}{r_I}$ and $\sin \beta = \frac{J}{r_I}$.

APPENDIX II

FORMULA VALIDITY CHECK

The wind stress curl formula was first derived in the form of equation 2.13, which is fairly complicated. In order to check for mistakes, equation 2.51, another complicated expression was derived and the results of the two expressions compared for various grids and wavenumbers. The approach was to generate a pressure field and the exact expression for the wind stress curl field corresponding to that pressure field. The curl field was then calculated using the finite difference scheme from the pressure field and the two curl fields were compared using ratios and differences. The ratios and differences were calculated for each point in the NMC grid north of 10°N , in order to avoid the numerical problems at the equator. This might not have been necessary as the pressure formula was purposely chosen to have a $\sin x/x$ character in the resulting geostrophic wind speed at the equator. At the time the test was done, no plans were made to use the calculation in extreme tropical regions, in part because the geostrophic approximation becomes invalid there.

The differences and ratios at each point were displayed both as histograms and also as printer generated contour maps over the entire grid. Because the artificial pressure field was cylindrically symmetric around the pole, having no λ dependence, the printer maps proved an extremely sensitive and selective diagnostic tool for locating errors. Several errors in both the exact pressure formula and the finite difference approximations were located using this technique and corrected. An error common to both formulations remained undetected until quite recently, the error causing a factor of 10 scale change in both estimates.

Even when both formulations had been freed of obvious errors, the agreement was not perfect, the estimated values being consistently lower than the exact values. This is because the finite difference formula can only approximate a given bump, the approximation getting worse as the bump gets smaller horizontally. An estimate of the wavenumber response for a given finite difference scheme can be obtained by putting various values of k , the meridional wavenumber into the pressure formula and running the comparisons.

The zonal wavenumber in the study was always zero, the formula for a two wavenumber response being even more complicated than equation 2.51. The extra work

needed to develop some kind of orthogonal function expansion was considered not worth the benefit gained because the principle of superposition is not valid when dealing with non-linear formulas. Instead of specifying the modal responses out of which the response for an arbitrary forcing can be built, they become a series of special cases. The study actually done was itself a special case, perhaps not as appropriate as a bumpy one, but a lot easier to calculate. Also, because the pressure field is cylindrical while the overlaid grid is square, the local grid is presented with a nearly plane wave in pressure at many angles of incidence encompassing the whole circle.

The wavenumber response study allowed me to choose between various sets of finite difference grids. Two general criteria were developed for choosing between examples which looked symmetrical to the eye. The first was the behavior of the mean response curve as a function of wavenumber. The second was a measure of the unevenness of response around the map, the standard deviation of the ratios divided by the mean. The first is called response ratio and the second, noise ratio. Graphs of these, given as a function of wavenumber, are shown in figure II.1.

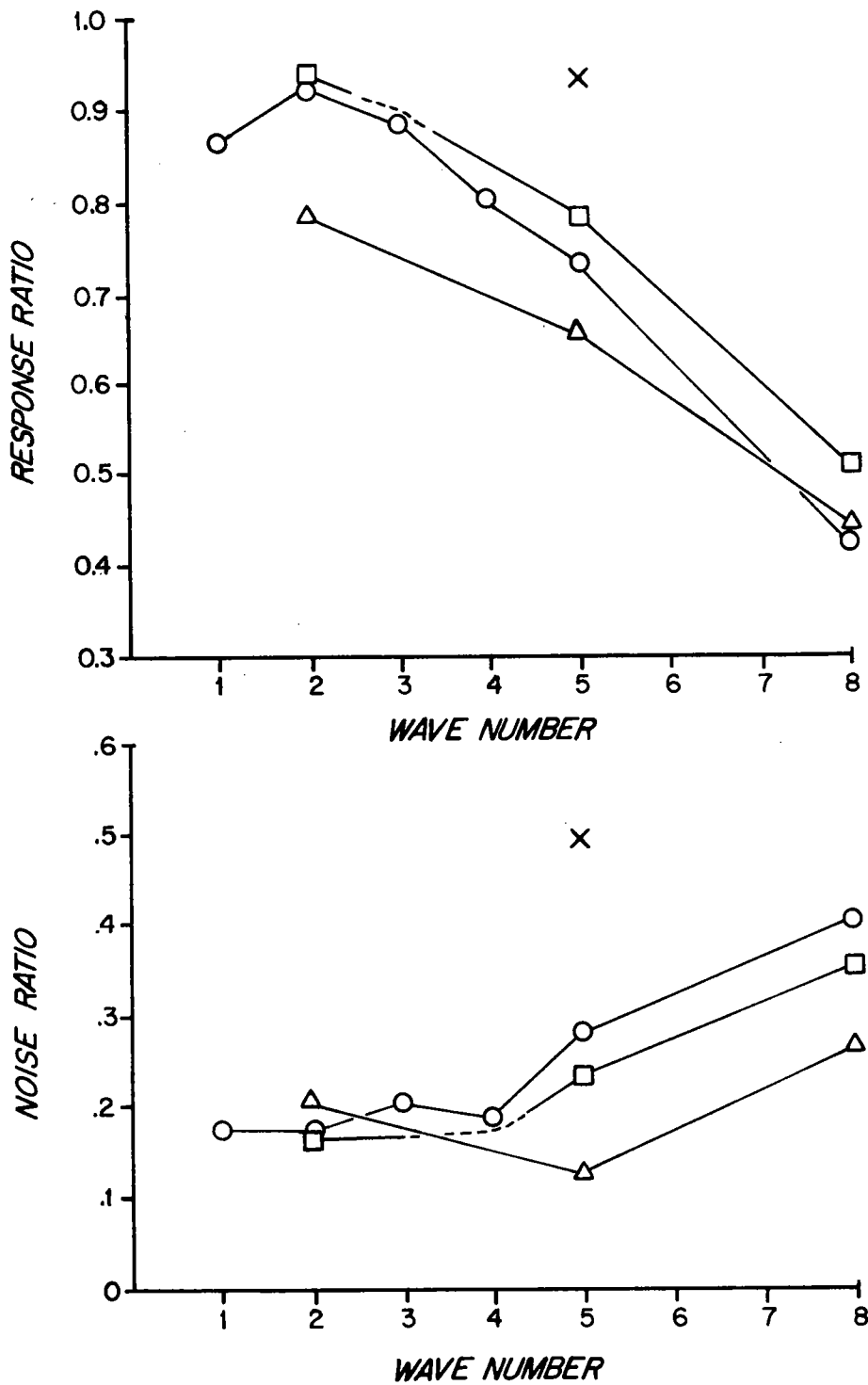


Figure II.1. Figures of merit for various finite difference schemes as discussed in the text.

The first grid studied was the square 9 point, least squares pressure grid. This is represented in figure II.1 by circles and serves as a starting point from which to compare changes. As I suspected systematic underestimation of the first derivatives as a cause of the rapid fall-off of the response ratio at high wavenumbers, a second try was made at wavenumber 5 by substituting the minimum possible first derivative formula, the non-symmetrical off-center three point formula. This single run, denoted by an X in figure II.1, raised the response ratio almost to 1.0, but the noise ratio was raised too much for comfort. As a compromise, the smallest symmetrical first derivative formula was chosen consisting of the four points nearest to a central point. This time, the response ratio and noise ratio were both improved, as shown by the squares in figure II.1. Encouraged by this improvement, I reasoned that the smallest symmetrical first derivative grid possible consisted of the four points around a single grid square. This grid is centered not on a gridpoint but on the center of a grid square. If symmetry were to be preserved, the smallest grid meeting the criteria for both symmetry and minimum number of points was a 12 point grid consisting of the four points making up a grid square and their eight nearest neighbors. Accordingly, the least

squares pressure derivation was applied to the 12 point grid and the resulting second derivative formulas used with the small four point formulas used for the first derivative estimates. The resulting points on the graph are given by triangles.

The resulting response ratio for the 12 point grid is lower than for the 9 point grid, but it falls off more slowly at high wavenumbers. Also, the noise ratio is smaller at high wavenumbers. A check with the printer maps shows that the low wavenumber degradation occurs mostly south of 20°N , so the low wavenumber response is actually better than indicated in the middle and high latitudes. As I was looking for a recipe to use at middle and high latitudes, I chose the "hopped up" 12 point formula.

As a matter of interest, the 20% to 30% level of the noise ratio indicates that the problem associated with the choice of a finite difference grid are as important to the accuracy of the formula as those associated with the accuracy of the basic pressure field. Perhaps more improvement can be gained by trying to estimate the shape, amplitudes and angles directly rather than the Taylor series derivatives.

APPENDIX III

ICEBERG DATA

This appendix contains all the information necessary to make the inferences about ice motions which are contained in figures 5.4a and 5.4b in the text. It consists of four parts.

The first, Section III.1, contains all the statements in Coast Guard Bulletin No. 45 which refer to ice. These statements are all assigned index numbers.

The second consists of five figures, Figure III.1a - III.1e, on which are shown the iceberg tracks to which the simple theory can be applied. These are all taken from figure 15 in the Coast Guard Bulletin and presented as separate figures both to make each track clear and to show the coherence of the flow during any given time.

The third and fourth parts are single tables. These present the statements about ice motions which are deduced from the information in the first and second parts and which are also tests of the simple theory. In Table III.1, the statements are listed by the index numbers of the statements in the report from which they are deduced. In Table III.2, the statements are grouped under the families of tracks from which they are deduced.

Section III.1

EXCERPTS
fromU.S. TREASURY DEPARTMENT
COAST GUARD
Bulletin No. 45International Ice Observations and Ice Patrol Service
in the North Atlantic Ocean-Season of 1959

Index No.	Page No.	Line No.	STATEMENT
1	1	6	The 1959 iceberg year was a severe one. Approximately 693 bergs drifted southward of the 48th parallel of Latitude during the year thus making it the 12th most active in records dating back to 1900 and the second heaviest since 1945.
2	1	27	Ice Patrol vessels maintained a constant guard of the southern limits of ice between 20 April and 11 July.
3	2	4	Ice conditions necessitated that Extra Southern Track "A" of the North Atlantic Lane Routes be placed into effect 13 May - 3 June. All other track shifts became automatic on scheduled dates.
4	2	16	Pre-season aerial ice observation in January and February indicated light iceberg conditions. None were sighted during these months south of the Strait of Belle Isle.
5	2	18	Newfoundland, however, was experiencing its worst winter in many years and local sea ice severely hampered coastwise shipping.
6	2	22	Ships attempting to use the Cape Race Track "F" during its period of non-scheduled use (1 Dec. - 15 May) often found it necessary to divert southward from course to avoid pack ice over the northern slope of the Grand Banks.

Index No.	Page No.	Line No.	STATEMENT
7	2	26	The Gulf of St. Lawrence found itself in the grip of a notably heavy ice season which had closed shipping at the middle of December 1958.
8	2	27	By mid-January ice was reported to be drifting seaward through Cabot Strait.
9	2	29	This ice (see 8) reached an extreme seaward limit at the end of February when ice fields extended from near Sable Island on the south to St. Pierre in the east.
10	2	45	At the beginning of March, Newfoundland and Labrador pack ice in its annual southward drift had encroached on the northern slope of the Grand Banks.
11	3	4	The first icebergs to be reported for the year were by Belle Isle Radio on 26 February.
12	3	5	A more southward advance, however, was indicated when USCGC Humboldt sighted three large bergs on 1 March near Lat. 51°31'N. longitude 18°30'W.
13	3	11	Field ice over the Grand Banks reached its greatest southward extent for the year during the middle of March when it covered the entire northern slope of the Banks. These conditions are considered to be about average for the Grand Banks regions.
14	3	16	Icebergs made their appearance on the Banks during the last week in March which is a relatively late date for this occurrence.
15	3	18	By the middle of April, however, increasing numbers of bergs arriving and drifting south along the eastern slope of the Grand Banks made it apparent that a severe year was at hand.
16	3	36	Icebergs were sighted on Track "C" on 13 April and remained until 1 July, the very day it once again became effective.

Index No.	Page No.	Line No.	STATEMENT
17	3	39	Field ice in the Cabot Strait and Gulf of St. Lawrence broke up during April.
18	3	44	Especially hard hit was the Newfoundland west coast where ice blocked the ports of Stephenville and Corner Brook until large United States and Canadian icebreakers attempted to convoy supply ships into these ports met with unexpected resistance from heavy ice and often were brought to a standstill.
19	4	3	During the period 10-12 May the Grand Banks were swept by a storm of whole gale proportions where northwest winds of Force 11 and greater were reported.
20	4	8	That this blow (see 19) had an extreme effect on ice distribution became apparent on 12 May when SS Esso Camden reported a large berg in 41°25'N. 49°W. This berg was later found to be the same one that 36 hours before was at a position 90 miles north-northwest of where it was found by the Esso Camden whose position was verified by the SS Hillcrest a short time later.
21	4	14	By the following day, 13 May, at least four bergs had been sighted in Track "B".
22	4	17	This marks but the fourth time since the establishment of the International Ice Patrol in 1913 that the use of Track A has been required.
23	4	23	The Androscoggin remained with the largest and southernmost of the bergs until 21 May when it melted in position 40°05'N. 48°20'W. During this period it was located directly on Track "A" but air observation had shown this to be the only ice endangering that track.
24	4	31	From 19-25 May the Patrol cutter, now the Acushnet, remained with the last survivor of the 12 May eruption. This was the final berg blocking Track "B" but it was not

Index No.	Page No.	Line No.	STATEMENT
		(cont.)	until 1 June that every report could be checked and berg drifts evaluated so that Track "B" once again could be recommended for use.
25	4	37	Field ice remained present over the northern slope of the Grand Banks through April.
26	4	40	By the beginning of May all pack ice had receded northward of latitude 48°N.
27	4	42	At the end of May the Newfoundland coast and Strait of Belle Isle was clear.
28	4	43	There was, however, a large belt of close pack ice which extended southward from Labrador but well offshore out of visual range of the coastal reporting stations at Belle Isle and the Newfoundland Coast. This tongue of sea ice averaging about 75 miles broad and protruding southward at times as far as latitude 50°15'N. persisted until the middle of June.
29	5	9	By 15 July all field ice was gone from the eastern approaches to the Strait of Belle Isle and that route was in wide use.
30	5	10	High numbers of bergs were present on Track "G" from the 1,000-fathom line to the Strait but this is a usual condition which ships using the Strait of Belle Isle must expect.
31	5	14	During April and May a high concentration of bergs grounded on the northern slope of the Grand Banks and off the southeast coast of Newfoundland.
32	5	16	Shipping through this area (see 31) reported sighting more bergs than have been encountered in recent years.

Index No.	Page No.	Line No.	STATEMENT
33	5	21	In May and June numerous bergs in the Cape Race vicinity drifted westward and several entered Placentia Bay. This is a most unusual occurrence as bergs are seldom seen west of the 54th meridian.
34	5	24	During June, the nearest encroachment occurred on the 15th when a large berg under the guard of the Androscoggin reached position 12°N. 48°30'W. just 30 miles from the eastbound lane before it recurved northeastward under the influence of the Atlantic Current.
35	5	28	The last berg to achieve any significant southward drift melted on 1 July in 13°N. 48°35'W. which was the day that Track "C" passing through this point, became effective.
36	5	31	Until 11 July the presence of the patrol cutter was required to stand by several bergs drifting between latitudes 45°N. and 44°N. and not too distant from eastbound Track "C".
37	5	33	By 11 July no ice existed south of the 46th parallel and the surface patrol was terminated.
38	5	35	Icebergs all over the Grand Banks deteriorated rapidly in late June and early July so that by mid-July only a remaining few were grounded in the area east of the Avalon Peninsula of Newfoundland and there were none on the eastern slope of the Banks.
39	5	12	The tragic loss during the year of the Danish motor vessel Hans Hedtoft with 95 passengers and crew cannot go unobserved. This ship struck an iceberg on 30 January 1959 in position 59°05'N. 43°00'W., 40 miles south-southeast of Cape Farewell, Greenland. This ship was proceeding through regions known to be infested with ice year round and was especially constructed for ice navigation and equipped with the latest electronic devices.

Index No.	Page No.	Line No.	STATEMENT
40	6	44	On that date (28 April) icebergs lay within 40 miles of westbound lane Track "B" and the need for a continuous patrol was obvious.
41	11	2	Since the middle of December (1958) the Gulf and River St. Lawrence had been ice bound.
42	11	3	On 27 December an aircraft had reported the Strait of Belle Isle blocked with heavy pack ice.
43	11	5	By 15 January heavy sea ice extended northward along the Newfoundland and Labrador coasts from latitude 51°N. and eastward to longitude 53°40'W.
44	11	7	On 16 January fields of loose ice were reported drifting seaward in Cabot Strait reaching as far out as 46°N. 57°W.
45	11	9	Throughout the month patches of block and brash ice hampered coastwise shipping along Newfoundland.
46	11	10	This was all local ice due to the extremely cold winter and was not of the Arctic pack.
47	11	12	No icebergs were reported south of latitude 54°N. during the month.
48	11	13	The month of February was marked by extremely heavy local pack ice conditions along the Newfoundland coast.
49	11	14	By the end of the first week a heavy ice field extended eastward from the Newfoundland coast along the 48th parallel to longitude 50°W. thence turning north-northwestward.
50	11	17	Small fields and patches of loose pack ice existed all around the Avalon Peninsula of Newfoundland.

Index No.	Page No.	Line No.	STATEMENT
51	11	18	For the first time in many years shipping was hampered in Placentia Bay, normally an ice-free access to Newfoundland.
52	11	25	Throughout the latter half of February the boundary of the heavy pack ice remained very nearly the same as the first week...
53	11	25	...the only significant change being a southeastward extrusion during the last week to about latitude 47°50'N. longitude 48°40'W. evidencing a transport by the Labrador Current.
54	11	30	Fields of loose sea ice persisted around the coast of the Avalon Peninsula through the end of the month, diminishing somewhat, however, the later half.
55	11	32	The greatest southward penetration occurred on 17 February when a field of ice of nine-tenths ice cover of the sea surface extended from Cape Race southward to latitude 46°15'N.
56	11	35	Ice in the Cabot Strait and the Gulf of St. Lawrence became heavier as the month wore on.
57	11	38	However, no ice was reported during the month south of latitude 44°50'N. or east of longitude 57°W.
58	12	3	The first of the Arctic ice was reported on 26 February by Belle Isle Radio which stated that 8 miles to the north had been sighted "...the edge of the Arctic ice pack with many icebergs in pack".
59	12	9	March witnessed the peak of the Cabot Strait and Grand Banks field ice and the beginning of the iceberg menace to the shipping tracks.

Index No.	Page No.	Line No.	STATEMENT
60	12	11	During the first 2 weeks, the sea ice off eastern Newfoundland resembled a huge boot with the heel at St. John's and the toe pointing eastward to longitude $47^{\circ}30'W$. and the leg extending northward between longitude $50^{\circ}W$. and the Newfoundland coast.
61	12	14	All the ice south of latitude $50^{\circ}N$. was non-Arctic in origin.
62	12	16	Ice to the east of the Avalon Peninsula eased somewhat the first week of March.
63	12	17	However, during the second week and under the influence of strong northerly winds sea ice again was carried southward past Cape Race and reached its greatest extent of the year on 14 March when it protruded southward from Cape Race and Cape Pine to about latitude $46^{\circ}N$.
64	12	21	This ice (see 63) quickly deteriorated so that 21 March no more was reported south of Cape Race.
65	12	22	By the 24th of the month the coast of the Avalon Peninsula was free south of Cape St. Francis and remained so.
66	12	24	To the eastward, over the northern slope of the Grand Banks, field ice persisted changing little during the second half of March. Throughout this period it extended from the Newfoundland coast north of latitude $48^{\circ}N$. outward along the 100-fathom isobath to about longitude $47^{\circ}W$.
67	12	28	The peak of the field ice over the Grand Banks for the year was reached between 15-22 March and represented about average conditions.
68	12	32	During the first week in March, Cabot Strait was bridged with ice and the seaward limits became definite and remained throughout the month at approximately a line extending from Cape Ray, Newfoundland, to St. Pierre to about $45^{\circ}N$. $58^{\circ}W$. thence recurving northward to Cape Breton Island.

Index No.	Page No.	Line No.	STATEMENT
69	12	36	The greatest southward drift of the year was reported on 5 March when the ice edge was sighted near Sable Island, and the farthest east were patches and strings of loose ice at 46°N. 54°40'W. on 27-28 March.
70	12	39	By the end of the month, though, the seaward limits were receding and the western reaches of the Gulf between Cape Gaspe and Anticosti Island were reported open.
71	12	41	But the "ice bridge" between Cape Breton Island and Cape Ray caused by the piling up of the huge amount of outward drifting ice remained fast.
72	13	5	The first icebergs to approach the Grand Banks area were sighted by the U. S. Coast Guard Cutter Humboldt en route to Ocean Station Bravo from Boston, Massachusetts. Five large bergs were reported between latitudes 51°30'N. and 53°N. at about longitude 48°40'W. These bergs were considerably offshore, free of the pack ice and not the same bergs reported by Belle Isle Radio on 26 February.
73	13	11	Prevailing westerly winds throughout February had placed them eastward of the axis of the Labrador Current where they experienced a continued eastward drift.
74	13	13	This group of few bergs, perhaps numbering less than ten, was not followed by any replacements and by the middle of March all had melted in the general area of 50°N. and 46°W.
75	13	16	Thereafter bergs were from inside the pack and in their southward approach to latitude 50°N. were rarely east of the 50th meridian.
76	13	19	Prevailing westerly winds, nevertheless, had carried the ice edge and accompanying main body of icebergs a greater than usual distance offshore.

Index No.	Page No.	Line No.	STATEMENT
77	13	21	By 8-9 March the van of the berg movement was at about 50°N . 50°W .
78	13	25	The first bergs to drift across the 48th parallel did so on about 24 March.
79	13	26	At this time there was a well-defined limit of iceberg positions which resembled a sharp wedge pointing southeastward and bounded by a line from Belle Isle to 48°N . $48^{\circ}30'\text{N}$. 51°W . Within this wedge were several hundred large icebergs and almost none without.
80	13	30	At the month's end this wedge (see 79) was still in evidence but with bergs drifting from the apex. Several continued to the southeast and east but most curved southward and followed just seaward of the 100-fathom isobath which corresponded to the axis of the Labrador Current.
81	13	35	The southernmost berg to be reported in March was by the SS Statensingel (Neth.) on 31 March at $46^{\circ}50'\text{N}$. $47^{\circ}15'\text{W}$.
82	13	37	Altogether it is estimated that 14 icebergs drifted south across latitude 48°N . during the month.
83	13	39	At the beginning of April sea ice over the Grand Banks was bounded by a line from 48°N . 53°W . to $47^{\circ}20'\text{N}$. $47^{\circ}39'\text{W}$. to about 52°N . $52^{\circ}30'\text{W}$. South of latitude 49°N . the ice was in fields, patches and strings of small floes and blocks of concentrations varying between one-tenth and five-tenths ice cover of the sea surface.
84	14	1	At no time during the remainder of the month or year did pack ice penetrate any farther south than at this time.
85	14	3	Through the first week in April a rapid recession of the ice limits gave the impression of an abrupt and early ending.

Index No.	Page No.	Line No.	STATEMENT
86	14	4	The boundary on 9 April lay roughly along latitude 50°N . between longitude 54°W . and 50°W . It seems, however, that most of the ice previously to the south had been chiefly non-Arctic winter and bay ice and that this new boundary was the southern extremity of older, heavy Arctic ice which each year makes its annual visitation into these waters.
87	14	9	The boundary was again on 11 April found to be moving southward and this trend continued until the 23 April when it reached its southernmost advance at the 48th parallel between longitude 52°W . and 48°W .
88	14	13	During the last week in April destruction of the field ice due to spring warming was in evidence and the pack edge showed positive signs of retreating.
89	14	15	At the month's end the ice boundary extended no farther offshore than longitude 50°W . and all sea ice south of latitude 50°N was in rapid deterioration.
90	14	18	Ice conditions during the first week in April remained severe in Cabot Strait and the eastern Gulf of St. Lawrence.
91	14	19	Ten-tenths ice cover continued from Cape North, Nova Scotia, across to Cape Ray, Newfoundland. The seaward limit extended to about a line from 45°N . $58^{\circ}30'\text{W}$. to St. Pierre.
92	14	27	By the middle of April conditions has eased considerably in Cabot Strait and lanes of open water were appearing through the Strait.
93	14	29	Heavy ice persisted, however, between Cape Ray, Newfoundland, and the Magdalen Islands.
94	14	32	At that time (20 April) the seaward ice limits had shrunk to a line from Cape Breton to Cape Ray and consisted of loose strings and patches of rapidly rotting winter ice.

Index No.	Page No.	Line No.	STATEMENT
95	14	36	The west coast of Newfoundland including the ports of Stephenville and Corner Brook remained icebound.
96	14	38	On 24 April only a small patch of loose ice remained in the Cape Breton area.
97	14	39	Cabot Strait and the main body of the Gulf were ice free after a notably heavy season.
98	14	40	Ice continued to block St. Georges Bay, Newfoundland, and the northeast arm of the Gulf of St. Lawrence throughout April.
99	14	42	During the first week in April, the several icebergs which led the movement southward along the eastern slope of the Grand Banks appeared to have been an isolated group.
100	14	44	...the main body of bergs was still within the field ice limits north of latitude 49°.
101	14	45	This advance group (see 99 and 100) melted mostly within the area between 45°-46°N. latitude with the southernmost survivors being last reported on 12 April by the SS Media (Brit.) at 44°07'N. 48°39'W.
102	15	2	No more bergs reappeared this far south until 20 April although a growler was reported on 19 April near 42°20'N. 49°18'W.
103	15	6	The period 1-15 April witnessed another group of bergs, also early arrivals, which drifted to the eastward between latitude 47°30'N. and 49°N. ...they often exceeded 30 miles per day, unusual for this region.
104	15	10	The location, however, is a commonly observed feature during the early part of the iceberg season.
105	15	11	A rapidly melting large growler was sighted by SS Beavercone (Brit.) 14 April at position 48°N. 42°18'W. This position is

Index No.	Page No.	Line No.	STATEMENT
		(cont.)	farther to the east than any piece of glacial ice has been sighted in this latitude in over 27 years.
106	15	14	No more bergs this season north of Flemish Cap followed a path to the eastward.
107	15	16	Aerial Ice Reconnaissance on 9 April showed the main body of bergs was just reaching latitude 49°N . and still concentrated well offshore.
108	15	17	One lone, large berg was sighted this day (9 April) near Cape Freels, Newfoundland, at $49^{\circ}20'\text{N}$. $52^{\circ}55'\text{W}$. Except perhaps for the Strait of Belle Isle region, this was the first berg to arrive at the Newfoundland coast. It was to be followed by almost record numbers more.
109	15	22	By 20 April the pattern for the year was clear. Large numbers of bergs had crossed the 48th parallel and were drifting southward along the eastern slope of the Grand Banks with the leaders at about latitude 44°N .
110	15	25	North of 49° latitude large concentrations of bergs were arriving at and coming south along the east coast of Newfoundland.
111	15	28	The arrival of the berg multitude over the Grand Banks corresponded closely with the advance of the Arctic sea ice pack described in the second paragraph of the discussion for this month (85, 86, 87).
112	15	31	The last week found a relatively stable condition over the southeastern slope of the Banks.
113	15	32	Bergs carried southward in the cold and narrow stream of the Labrador Current would either escape to the east between latitude 46°N . and 43°N . and be carried northward again to a quick destruction by

Index No.	Page No.	Line No.	STATEMENT
		(cont.)	the warm waters of the Atlantic Current, or else those surviving a drift to the Tail-of-the-Bank would dissipate in a mixed water eddy centered at about 43°N. 48°49'W.
114	15	38	Other bergs had penetrated and grounded over most of the northeastern half of the Grand Banks...
115	15	39	...but with none encroaching beyond a line between Cape Race and the Tail-of-the-Bank.
116	15	41	Along the Newfoundland east coast, however, conditions were far from steady. Greater numbers of bergs were appearing daily hazarding coastwise and St. John's shipping.
117	15	44	Approximately 266 bergs drifted across the 48th parallel during April. This is the fifth highest on record since 1900 and the greatest since 1932.
118	15	46	The average figure is 95 (see 117).
119	16	1	East of Newfoundland a rapid recession of pack ice occurred during the first week in May so that by the 8th only rotting patches remained south of latitude 49°N. and this was restricted to Trinity and Bonavista Bays.
120	16	4	Moderate to heavy field ice remained north of Cape Freels but extended no further east than longitude 54°W. ...
121	16	5	...except for a belt of heavy pack protruding eastward along the 50th parallel as far as longitude 51°40'W.
122	16	7	This easterly belt appears to be a common feature to this region especially during the period when the ice limit is retreating.
123	16	13	Ice in the northeast arm of the Gulf of St. Lawrence also receded rapidly during the first week in May.

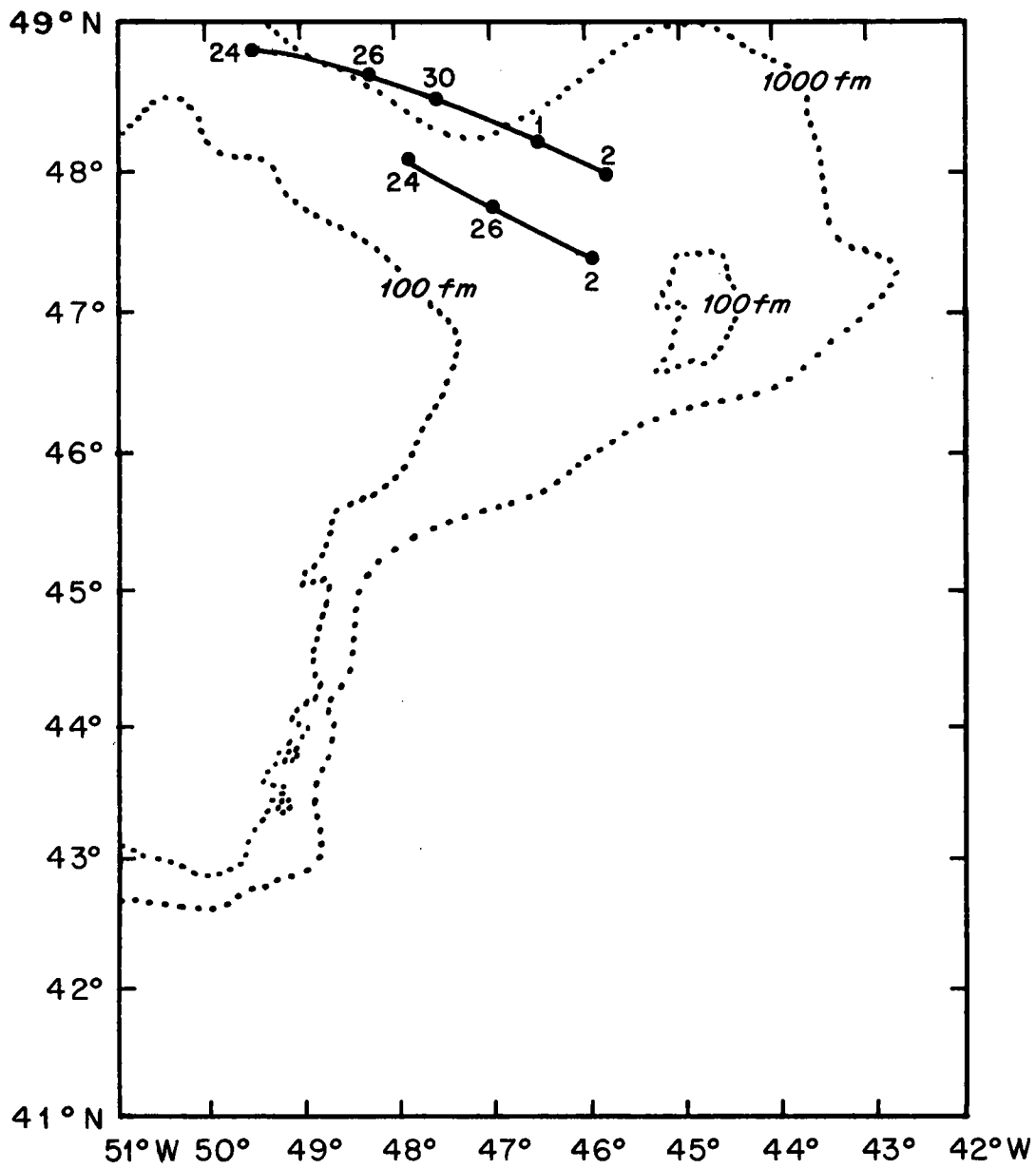
Index No.	Page No.	Line No.	STATEMENT
124	16	14	By the 9th all Newfoundland west coast ports south of latitude 50°N. were open and by the 20th the entire Gulf and western approaches to the Strait of Belle Isle were clear.
125	16	17	On 20 May aerial observation showed that field ice south of Belle Isle along the east coast had shrunk into a coastal zone lying north of latitude 50°N. and west of longitude 55°W.
126	16	19	Northward of Belle Isle the pack remained heavy, its boundary extending approximately northeast from Belle Isle to as far seaward as longitude 52°W.
127	16	22	A severe cyclonic storm 22-25 May brought strong northerly winds which backed to the west.
128	16	23	The result of this storm (see 127) was that the ice in the Notre Dame and White Bays of Newfoundland was driven seaward and again drifted southeasterly part Cape Freels and reached its greatest extent about 28 May at position 49°N. 52°40'W.
129	16	26	Greater consequence of the blow (see 127), however, was a sudden southward movement of field ice off the Labrador Coast from about latitude 52°30'N. on 22 May to 51°N. on 28 May.
130	16	29	The Strait of Belle Isle, Newfoundland, and southern Labrador coasts had been cleared of ice at the month's end...
131	16	30	...but large field ice lay offshore out of sight of the coastal stations whose reports were conveying ice-free impressions.
132	16	33	Iceberg drifts the first week in May remained much as they had been in the latter part of April.
133	16	34	The northern slope of the Banks continued to fill up with bergs.

Index No.	Page No.	Line No.	STATEMENT
134	16	35	At the end of the first week in May many bergs were reported to be rounding Cape Race and drifting to the westward.
135	16	36	About a dozen bergs drifted south of the 43rd parallel during this week and for the most part remained in the vicinity of the Tail-of-the-Bank.
136	16	38	At least three rounded the Bank and commenced a westward drift on the opposite slope.
137	16	39	Such a drift is relatively common and in some years the majority of bergs arriving at the southern extremity have recurved to the westward. But these few were the only such occurrences in 1959 and all other bergs reaching the southeastern slope this season drifted to the eastward.
138	17	1	From 7-10 May one exceptional large berg, about 275 feet high and 1,000 feet long, was observed to be grounded in a position 42°50'N. 50°W. at a depth of 90 fathoms.
139	17	3	The inactivity of several other large bergs nearby strongly suggests that they too may have been grounded.
140	17	5	During the period 10-12 May an intense cyclonic storm swept the Grand Banks with northwesterly winds of Force 11 and greater.
141	17	10	On 12 May a large iceberg subsequently identified as the previously described grounded one (see 138), was reported by SS Esso Camden (Pan.) and SS Hillcrest (Brit.) to be near 41°25'N. 49°W. This location was 90 miles south-southeast of its position on 10 May and represents a minimum drift of 60 miles per day.
142	17	14	The following day, 13 May, an Ice Patrol aircraft relocated this berg at 59 miles farther SSE in 40°40'N. 48°10'W.

Index No.	Page No.	Line No.	STATEMENT
143	17	17	This berg melted at position 40°05'N. 48°20' W. on 21 May. This remarkable drift is noteworthy for two reasons: first, it represents the southernmost penetration of ice during 1959 and second, it is only the berg during the year drifting southeastward which failed to recurve to the northward with the Atlantic Current.
144	17	22	This latter occurrence is perhaps due to the berg's being driven through and across a northern branch of the Atlantic Current and into slower moving water.
145	17	30	Two other bergs were sighted 13 May near 40°40'N. 48°10'W. and
146	17	31	...a third in position 41°45'N. 48°15'W.
147	17	31	A lone berg was found to the west on 12 May by SS Neptune (Lib.) in 41°53'N. 52°14'W and again on 13 May by SS Tarakan (Neth.) in 42°20'N. 52°20'W.
148	17	33	Last located by Ice Patrol aircraft the next day in position 42°N. 42°W. it had recurved to the east and was well under the destructive influence of the Atlantic Current.
149	17	37	Prior to the storm, on 9 May, bergs over the Grand Banks had encroached to about a line from Cape Pine, Newfoundland, to 44°N. 50°W.
150	17	39	On 14 May this line now approximated the 100-fathom contour of the southwestern slope. This represents an average advance of about 65 miles over the entire Grand Banks.
151	17	45	By 20 May, however, most of the effects of the extreme drifts had disappeared except for the large berg sighted 13 May in 41°45'N. 48°15'W.
152	18	1	...and relocated 19 May by SS Bellair (Ital.) near 41°42'N 47°13'W.

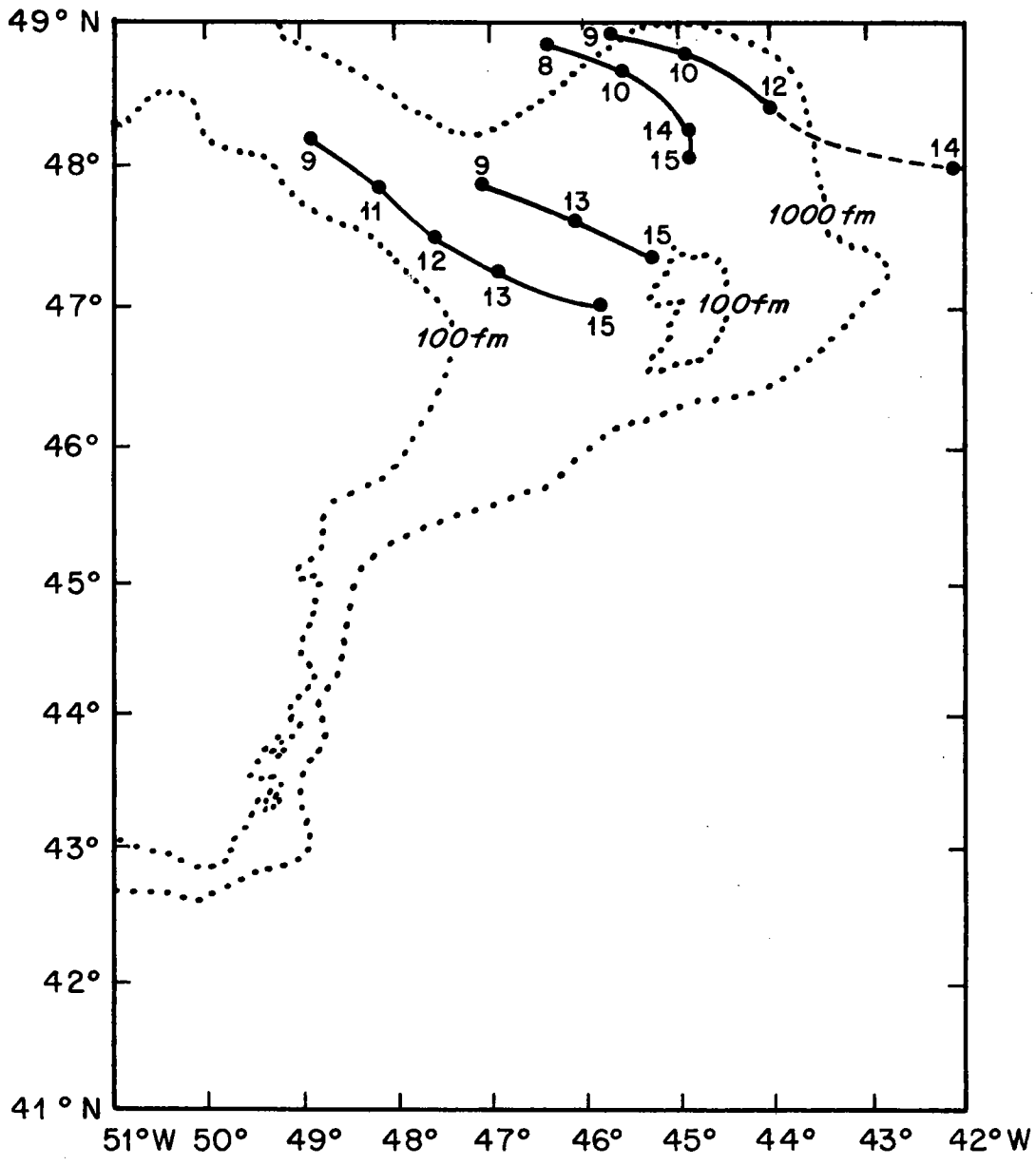
Index No.	Page No.	Line No.	STATEMENT
153	18	2	This berg (see 151) drifted northward and melted on 24 May near position 44°20'N. 46°45'W.
154	18	4	Not until the 22nd that bergs, newly arriving once again crossed the 45th parallel.
155	18	6	Icebergs persisted across the western slope of the Banks through 25 May ...
156	18	7	At that time (25 May) the northern slope was rather well populated from Cape Pine eastward and bergs extended southward along the eastern slope as far as latitude 43°N.
157	18	11	Two bergs were sighted near St. Pierre on 25 May by SS Cleopatra (Ger.)
158	18	13	Hordes of icebergs now arriving at the Newfoundland coast, 200 bergs were sighted within a 10-mile radius of Cape Bonavista.
159	18	15	More bergs were sighted in Trinity and Conception Bays than at any time in the recollection of many local residents.
160	18	17	The month's end found the southernmost berg at 42°50'N. 48°40'W.
161	18	20	Several bergs remained grounded in the area near 45°45'N. 54°W.
162	18	21	Most (bergs) lay east of longitude 54°30'W. and north of lat. 46°N.
163	18	23	During May a total of about 180 bergs drifted south of latitude 48°N. and of these 22 crossed the 43d parallel.
164	18	25	The first week in June marked the end of the field ice south of latitude 50°N. and in Newfoundland coastal waters.
165	18	26	A small field of rotting brash ice, sighted 3 June between Cape Bonavista and Cape Freels was gone by the 5th.

Index No.	Page No.	Line No.	STATEMENT
166	18	28	As previously stated, however, a large belt of pack ice extended southward from off Labrador to about latitude $51^{\circ}30'N$. These fields of 4-7 tenths ice cover were well offshore.
167	18	32	This ice actually advanced through the 13th of the month when, at its southernmost extent, it resembled a southward pointing spike averaging 75 miles in width and the extremity at $50^{\circ}15'N$. $50^{\circ}W$.
168	18	35	The inshore edge lay about 30 miles east of Bell Isle.
169	18	38	On 20 June sea ice was no longer a factor for consideration by transatlantic shipping.
170	18	40	Icebergs during June drifting southward along the eastern slope of the Grand Banks achieved a near steady state pattern of conditions and would invariably recurve to the northeast between latitudes $46^{\circ}N$. and $43^{\circ}N$.
171	18	43	The southernmost occurrence was on 15 June in position $42^{\circ}05'N$. $48^{\circ}25'W$.



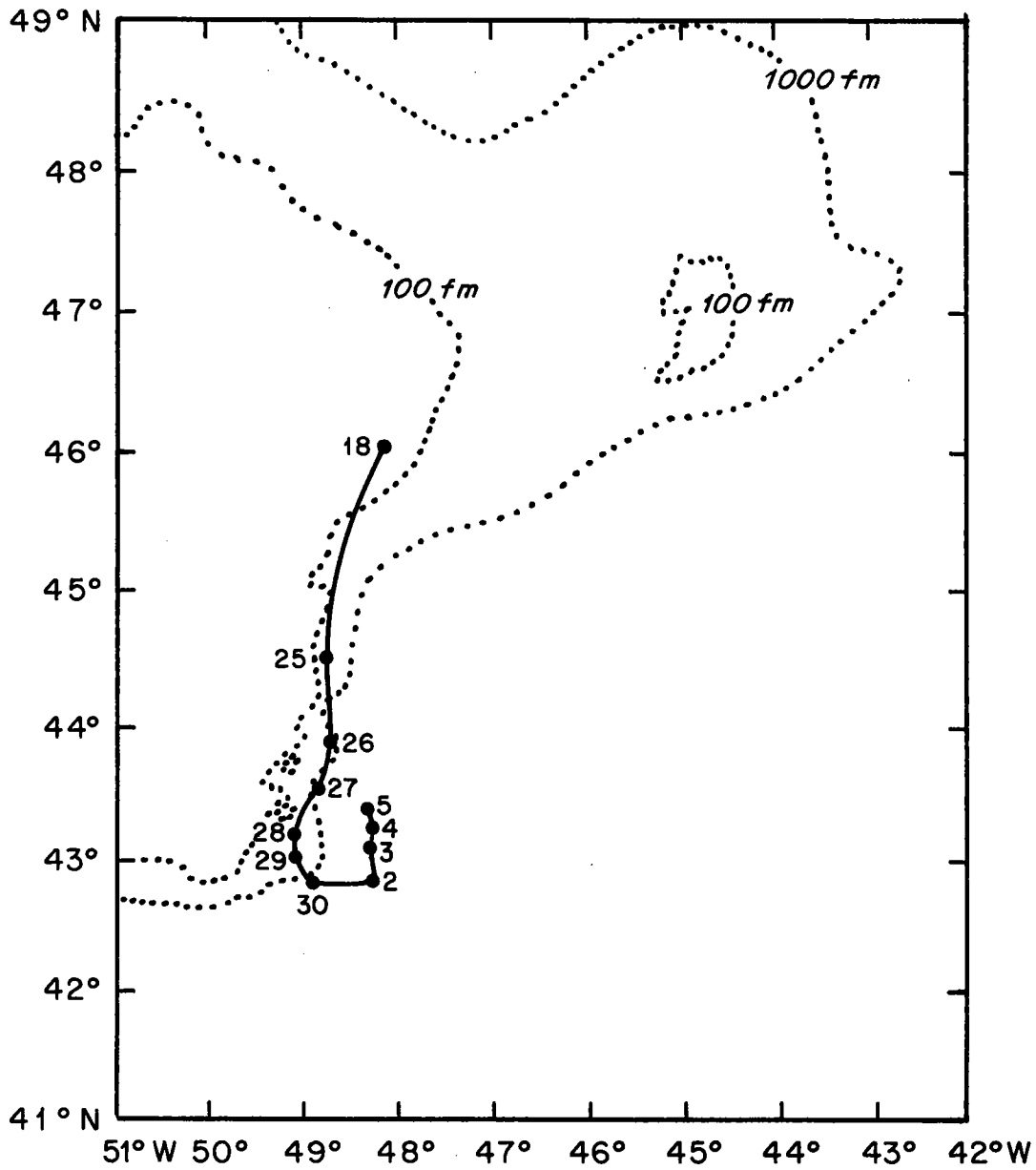
ICEBERG TRACKS
MARCH 24 - APRIL 2, 1959

Figure III.1a



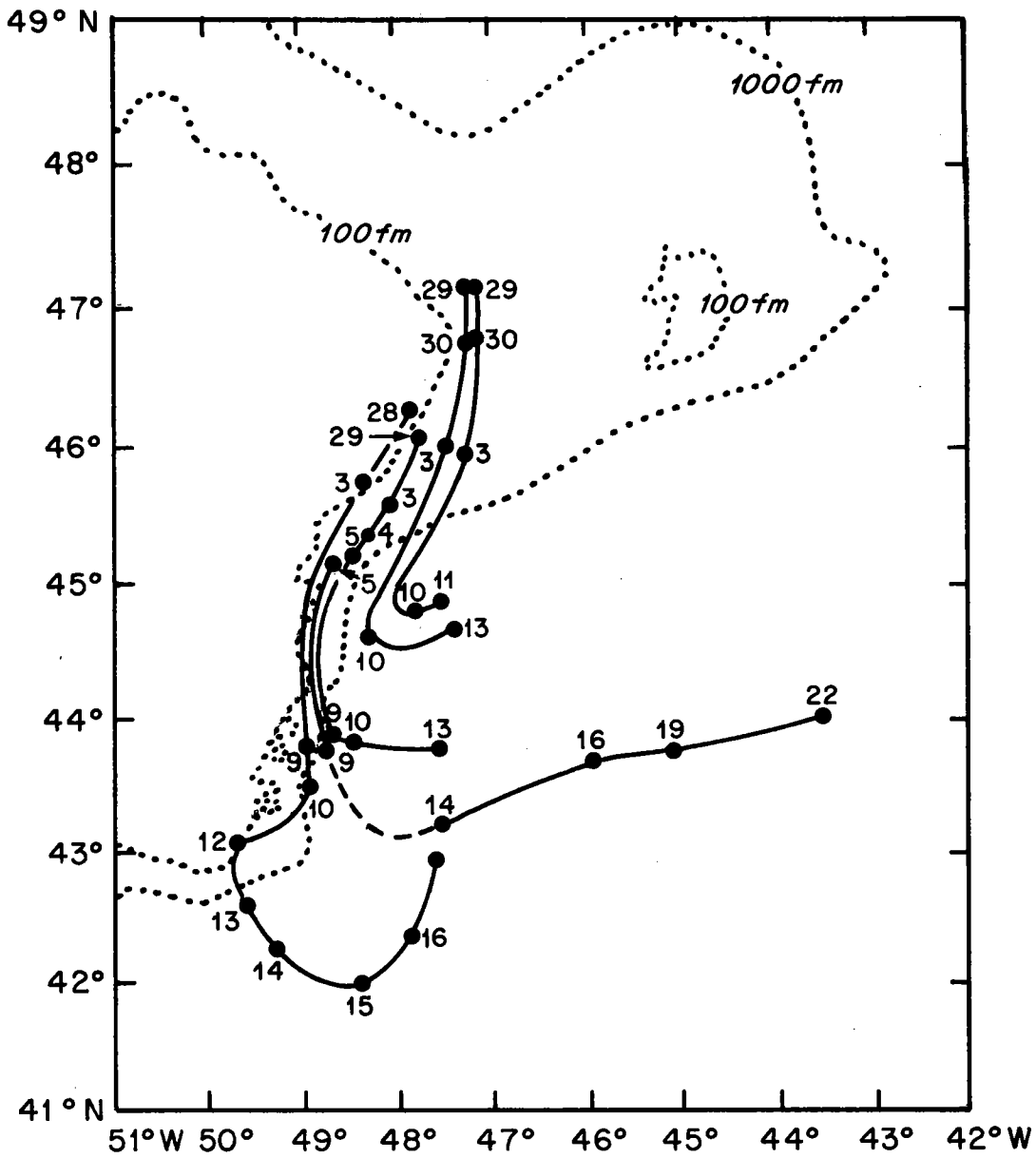
ICEBERG TRACKS
APRIL 8 - APRIL 15, 1959

Figure III.1b



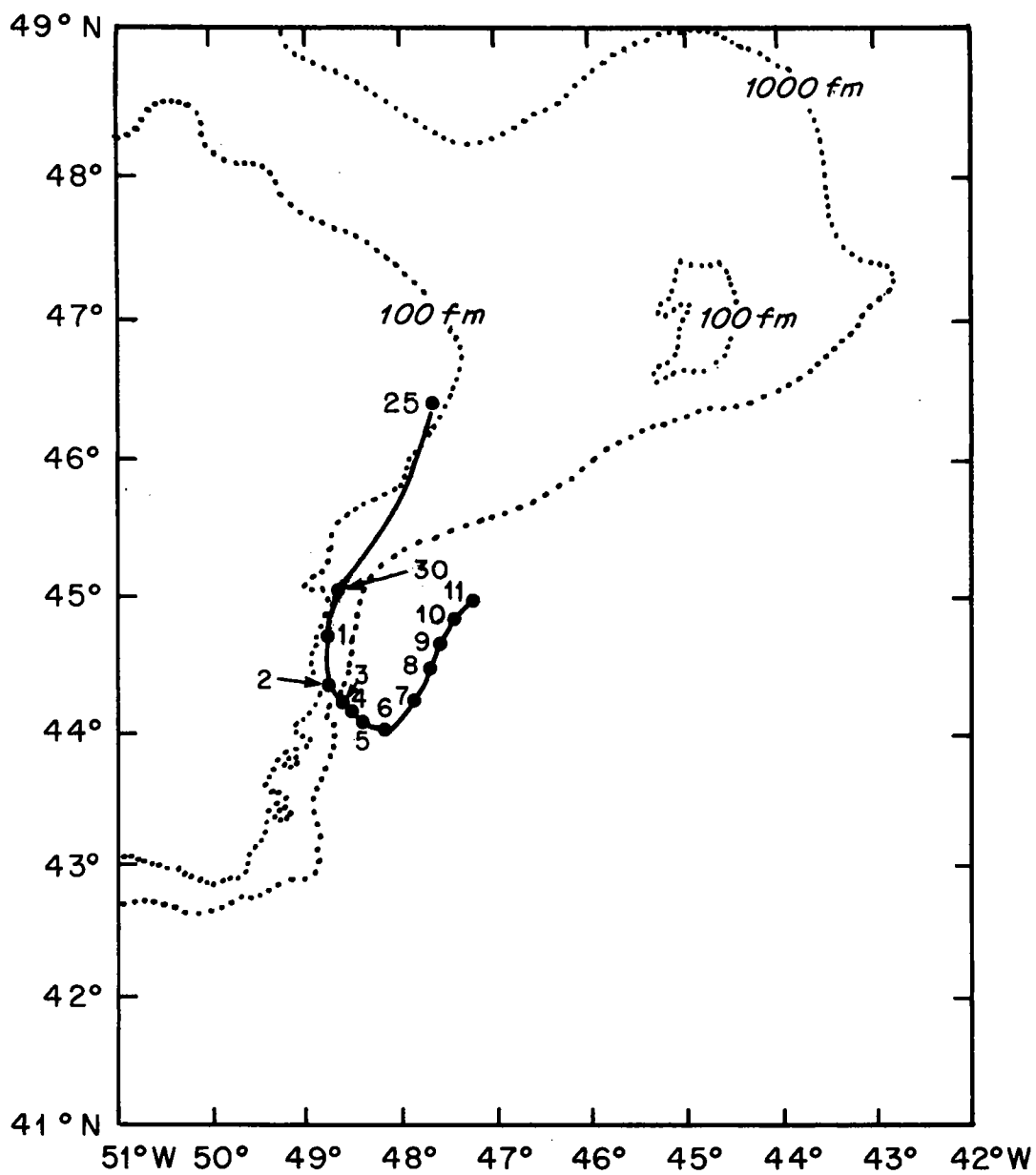
ICEBERG TRACKS
MAY 18—JUNE 5, 1959

Figure III.1c



ICEBERG TRACKS
MAY 29 - JUNE 16, 1959

Figure III.1d



ICEBERG TRACKS
JUNE 25 - JULY 11, 1959

Figure III.1e

ICEBERG MOTION ACCORDING TO TEXT
 COMPARED TO
 CALCULATED MOTIONS

<u>Index No.</u>	<u>Date from</u>	<u>to</u>	<u>Location by Section</u>	<u>Ice Type</u>	<u>Motion Direction</u>	<u>Verifi- cation Result</u>
11,12	2/26	3/01	14	Berg	North	TRUE
53	2/(22)	2/28	15	Pack	South	TRUE
78	3/09	3/31	15	Berg	South Net	TRUE
80	3/24	3/31	14/15	Berg	Out Net	TRUE
85	4/01	4/10	15	Pack	North Net	TRUE
103	4/01	4/15	14/15	Berg	Out Net	TRUE
107,100	4/(01)	4/09	15	Berg	North Net	TRUE
109,107	4/(09)	4/20	15,16	Berg	South Net	TRUE
113,112	4/(25)	4/30	15/16	Berg	Out Net	TRUE
135	5/(01)	5/(07)	17	Berg	South Net	TRUE
	7/(01)	7/(15)	15/16	Berg	Out Net	FALSE
	7/(19)	7/22	15	Berg	South	FALSE

TABLE III.1

ICEBERG MOTIONS ACCORDING TO DRIFT CHART
 COMPARED TO
 CALCULATED MOTIONS

Number of Iceberg Tracks	Date from	to	Location by Section	Type of Motion	Verifi- cation Result
	<u>Mar. 24 Apr. 2</u>				
2	3/24	3/30	15	South Out	TRUE
	3/30	4/02	14/15		TRUE
	<u>Apr. 8 Apr. 15</u>				
4	4/09	4/15	15	South Net Out Net	TRUE
	4/09	4/15	14/15		TRUE
	<u>May 18 June 5</u>				
1	5/18	5/25	16	South Net	(FALSE)
	5/25	5/29	17	South Net	TRUE
	5/18	5/26	16/17	Not Out Net	TRUE
	<u>May 29 June 16</u>				
5	5/29	6/01	16	South Net	FALSE
	6/06	6/12	17	South Net	FALSE
	6/09	6/(12)	16/17	Out Net	TRUE
	5/30	6/09	16/17	In Net	TRUE
	<u>June 25 July 11</u>				
1	6/25	6/30	16	South Net	TRUE
	6/30	7/02	17	South Net	TRUE
	7/02	7/03	16/17	Out Net	FALSE

TABLE III.2

- Aagaard, K., 1970, Wind Driven Transports in the Greenland and Norwegian Seas. Deep-Sea Res., 17, 281-291.
- Amos, D. E., and L. H. Koopmans, 1963, Tables of the distribution of the Coefficient of Coherence for Stationary Bivariate Gaussian Processes. Sandia Corporation Monograph SCR-483.
- Bendant, J. S., and A. G. Piersol, 1966, Measurement and Analysis of Random Data. John Wiley and Sons, Inc., N.Y.
- Ekman, V. W., 1905, On the Influence of the Earth's Rotation on Ocean Currents. Arkiv Matematik, Astronomi, Fysik, Band 2, No. 11, Royal Swedish Academy of Science.
- Ekman, V. W., 1922, Über Horizontalzirkulation bei winderzeugten Meeresströmungen. Arkiv für Matematik, Astronomi och Fysik. 17, (26), pp 1-74. Translated by Doug Moore (personal communication).
- Fofonoff, N. P., 1962, Machine computations of Mass Transport in the North Pacific Ocean. Jour. of the Fish. Res. Bd. of Canada, 19, (6), pp. 1121-1141.
- Fofonoff, N. P., and F. W. Dobson, 1963a, Transport Computations for the North Atlantic Ocean 1950-1959. Manuscript Report Series of the Fisheries Research Board of Canada (162).
- Fofonoff, N. P., and F. W. Dobson, 1963b, Transport Computations for the North Pacific Ocean 1950-1959. Manuscript Report Series of the Fisheries Research Board of Canada (166).
- Froese, C., 1963, Computation of Mass Transport in the Ocean from Atmospheric Pressure Data. Manuscript Report Series of the Fisheries Research Board of Canada (163).
- Groves, G. W., 1955, Numerical Filters for Discrimination against Tidal Periodicities. Trans. of the Amer. Geophysical Union, 36, (6), 1073-1084.
- Groves, G. W., and E. J. Hannan, 1968, Time Series Regression of Sea Level on Weather. Rev. of Geophys., 6, (2), 129-174.
- Hellerman, S., 1965, Computations of Wind Stress Fields over the Atlantic Ocean. Monthly Weather Rev., 93 (4), 239-244.

- Hellerman, S., 1967, An Updated Estimate of the Wind Stress on the World Ocean. Monthly Weather Rev., 95, (9), 607-626. Sept. 1967, pp. 607-626, Note correction in MWR January 1968.
- Hidaka, K., 1958, Computation of the Wind-Stresses over the oceans. Records of the Oceanographic Works in Japan, 4, (2), 77-123.
- Knauss, John A., 1969, A note on the Transport of the Gulf Stream. Deep-Sea Res., Supp. to Vol. 16, 117-123.
- Montgomery, R. B., 1936a, Transport of Surface Water due to the Wind System over the North Atlantic. Papers in Physical Oceanography and Meteorology of M.I.T. and W.H.O.I.
- Montgomery, R. B., 1936b, Computation of the Transport of Surface Water due to the Wind System over the North Atlantic. Nat. Res. Council Trans. of the A.G.U., 17th Annual Meeting.
- Munk, W. H., 1950, On the Wind Driven Ocean Circulation. Jour. of Met., 7, (2), 79-93.
- Reid, R. O., 1948, The Equatorial Currents of the Eastern Pacific as maintained by the Stress of the Wind. J. Mar. Res., 7, 74-99.
- Roll, H. U., 1965, Physics of the Marine Atmosphere. Academic Press, 426 pp.
- Rosby, C.-G. and R. B. Montgomery, 1935, The Layer of Frictional Influence in Wind and Ocean Currents. Papers in Physical Oceanography and Meteorology published by M.I.T. and W.H.O.I., April, 1935.
- Scripps Institute of Oceanography, 1948, The Field of Mean Wind Stress over the North Pacific Ocean. Oceanographic Report No. 14, 1-12.
- Stommel, H., 1948, The Westward Intensification of Wind Driven Ocean Currents. Trans. of the A.G.U., 50, (2), 202-206
- Sverdrup, H. U., 1947, Wind Driven Currents in a Baroclinic Ocean with Application to the Equatorial Currents of the Eastern Pacific. Proc. of the Nat. Acad. of Sci., 33, (11), 318-326.

Bibliography (cont.)

- Sverdrup, H. U., M. W. Johnson, and R. H. Fleming, 1942, The Oceans. Prentice Hall, New York, 1087 pp.
- Tolkien, J. R. R., 1937, The Hobbit, Ballantine Books, New York, p. 207.
- United States Coast Guard, 1959, International Ice Observations and Ice Patrol Service in the North Atlantic Ocean - Season of 1959. Bulletin No. 45.
- U. S. Dept. of Commerce, N.O.A.A., 1971, Technical Procedures Bulletin #65, New Initialization Procedure for the 6-layer (PE) Numerical Prediction Model.
- U. S. Navy, Chief of Naval Operations, 1955, 1958, Marine Climatic Atlas of the World Vol. 1, 1955, Vol. IV, 1958.
- United States Weather Bureau, 1938, Predominant Direction, Constancy, and Force, Surface Winds. Atlas of Climatic Charts of the Oceans, W. B. No. 1247. Chart 3 (January) and Chart 9 (July).
- Veronis, G., 1970, Effect of Fluctuating Winds on Ocean Circulation. Deep-Sea Res., 17, 421-434.
- Wickett, W. Percy, 1969, Transport Calculations for the North Pacific Ocean 1968. Fish. Res. Board of Canada Technical Report 126.
- Worthington, L. V., 1970, The Norwegian Sea as a Mediterranean Basin. Deep-Sea Res., 17, 77-84.
- Worthington, L. V., and H. Kawai, 1972, Comparisons between Deep Sections across the Kuroshio and the Florida Current and the Gulf Stream. A Treatise on the Kuroshio, Chapter 13, H. Stommel and K. Yoshida, Ed. (in press).
- Wunsch, C. I., 1972, Bermuda Sea Level in Relation to Tides, Weather and Baroclinic Fluctuations. Rev. of Geophysics and Space Physics, February, 1972, (in press).

BIOGRAPHICAL SKETCH

The author was born in Hartford, Connecticut in 1942 and was immediately moved to West Hartford, Connecticut, where he grew up without incident for eighteen years. He attended Wesleyan University in Middletown, Connecticut from September 1960 until November 1962, when he withdrew.

For the next two years, he lived in Sunnyvale, California. There he met Betty Hand and attended Leland Stanford Jr. University, from which he graduated in 1966 with a B.S. in physics.

Betty consented to marry him and he moved to Cambridge to attend M.I.T. She followed and the couple were married on February 1, 1967 whereupon they were promptly engulfed in a snowstorm of monstrous proportions. It is not known when or how they escaped from Cambridge, but the author and Betty are reported to be living in Gloucester Point, Virginia, where the author is working for the Virginia Institute of Marine Science (VIMS).

MANDATORY DISTRIBUTION LIST
FOR UNCLASSIFIED TECHNICAL REPORTS, REPRINTS, & FINAL REPORTS
PUBLISHED BY OCEANOGRAPHIC CONTRACTORS
OF THE OCEAN SCIENCE AND TECHNOLOGY DIVISION
OF THE OFFICE OF NAVAL RESEARCH
(REVISED OCTOBER 1971)

DEPARTMENT OF DEFENSE

1 Office of the Secretary of Defense
Washington, D. C. 20301
ATTN: Office, Assistant Director
(E & LS)

NAVY

Office of Naval Research
Department of the Navy
Washington, D. C. 20360

2 Attn: Ocean Science & Technology
Div (Code 480)
1 Attn: Naval Applications & Analysis
Div (Code 460)
1 Attn: Earth Sciences Div (Code 410)

1 Office of Naval Research
Branch Office
495 Summer Street
Boston, Massachusetts 02210

1 LCDR T. L. Miller, (USN)
ONR Representative
Woods Hole Oceanographic Institution
Woods Hole, Massachusetts 02543

Director
Naval Research Laboratory
Washington, D. C. 20390
6 Attn: Library, Code 2029 (ONRL)
6 Attn: Library, Code 2000

Commander
Naval Oceanographic Office
Washington, D. C. 20390
1 Attn: Code 1640 (Library)
1 Attn: Code 70

OTHER GOVERNMENT AGENCIES

12 Defense Documentation Center
Cameron Station
Alexandria, Virginia 22314

1 Director
National Oceanographic Data Center
Bldg. 160
Navy Yard
Washington, D. C. 20390

DOCUMENT CONTROL DATA - R&D

(Security classification of title, body of abstract and indexing annotation must be entered when the overall report is classified)

1. ORIGINATING ACTIVITY (Corporate author) Woods Hole Oceanographic Institution Woods Hole, Massachusetts		2a. REPORT SECURITY CLASSIFICATION Unclassified	
		2b. GROUP	
3. REPORT TITLE ON THE CALCULATION OF WIND STRESS CURL OVER THE OPEN OCEAN AREAS FROM SYNOPTIC METEOROLOGICAL DATA WITH APPLICATION TO TIME DEPENDENT OCEAN CIRCULATION			
4. DESCRIPTIVE NOTES (Type of report and inclusive dates) Technical Report			
5. AUTHOR(S) (Last name, first name, initial) Welch, Christopher S.			
6. REPORT DATE February 1972	7a. TOTAL NO. OF PAGES 189	7b. NO. OF REFS 37	
8a. CONTRACT OR GRANT NO. N00014-66-C0241; NR 083-004 and the U.S. Coast Guard DOT-CG-10618-A	9a. ORIGINATOR'S REPORT NUMBER(S) REFERENCE NO. 72-6		
c.	9b. OTHER REPORT NO(S) (Any other numbers that may be assigned this report)		
d.			
10. AVAILABILITY/LIMITATION NOTICES			
11. SUPPLEMENTARY NOTES		12. SPONSORING MILITARY ACTIVITY Office of Naval Research Ocean Science & Technology Division Arlington, Virginia 22217	
13. ABSTRACT The method used by N. P. Fofonoff for estimating wind stress curl from surface atmospheric pressure maps is developed for use with the National Meteorological Center analysis grid. A formula is developed relating the wind stress curl directly to geometrically apparent features of the surface pressure analyses. The sensitivity of the formula to small deviations in the basic pressure field is estimated. Some statistical properties of the resulting formula as applied to actual pressure analyses are investigated. In particular, the geostrophic wind estimated for two finite difference grids is compared to observed winds from an independent anemometer located at W.H.O.I. site "D". The statistical distribution of wind stress curl estimates is found to be non-Gaussian. The difficulty in estimating a mean value from such distributions is discussed. The root mean square values of wind stress curl are found to be approximately 10 times the mean values. Means are estimated and found to be inadequate to drive the mean transports in the Gulf Stream and Kuroshio. The formula is applied at Bermuda and the results compared to the record from the tide gauge located there. A significant relation between wind stress curl and sea level is found after tidal and inverted barometer effects are suppressed. The formula is applied to time dependent motions of the Labrador Current as evidenced by iceberg drifts for the 1959 ice season. Agreement is found between calculated and observed iceberg motions on the eastern slope of the Grand Banks using Sverdrup dynamics.			

14. KEY WORDS	LINK A		LINK B		LINK C	
	ROLE	WT	ROLE	WT	ROLE	WT
1. Wind stress curl						
2. Sea-level pressure field						
3. Iceberg drift						

INSTRUCTIONS

1. **ORIGINATING ACTIVITY:** Enter the name and address of the contractor, subcontractor, grantee, Department of Defense activity or other organization (*corporate author*) issuing the report.

2a. **REPORT SECURITY CLASSIFICATION:** Enter the overall security classification of the report. Indicate whether "Restricted Data" is included. Marking is to be in accordance with appropriate security regulations.

2b. **GROUP:** Automatic downgrading is specified in DoD Directive 5200.10 and Armed Forces Industrial Manual. Enter the group number. Also, when applicable, show that optional markings have been used for Group 3 and Group 4 as authorized.

3. **REPORT TITLE:** Enter the complete report title in all capital letters. Titles in all cases should be unclassified. If a meaningful title cannot be selected without classification, show title classification in all capitals in parenthesis immediately following the title.

4. **DESCRIPTIVE NOTES:** If appropriate, enter the type of report, e.g., interim, progress, summary, annual, or final. Give the inclusive dates when a specific reporting period is covered.

5. **AUTHOR(S):** Enter the name(s) of author(s) as shown on or in the report. Enter last name, first name, middle initial. If military, show rank and branch of service. The name of the principal author is an absolute minimum requirement.

6. **REPORT DATE:** Enter the date of the report as day, month, year; or month, year. If more than one date appears on the report, use date of publication.

7a. **TOTAL NUMBER OF PAGES:** The total page count should follow normal pagination procedures, i.e., enter the number of pages containing information.

7b. **NUMBER OF REFERENCES:** Enter the total number of references cited in the report.

8a. **CONTRACT OR GRANT NUMBER:** If appropriate, enter the applicable number of the contract or grant under which the report was written.

8b, 8c, & 8d. **PROJECT NUMBER:** Enter the appropriate military department identification, such as project number, subproject number, system numbers, task number, etc.

9a. **ORIGINATOR'S REPORT NUMBER(S):** Enter the official report number by which the document will be identified and controlled by the originating activity. This number must be unique to this report.

9b. **OTHER REPORT NUMBER(S):** If the report has been assigned any other report numbers (*either by the originator or by the sponsor*), also enter this number(s).

10. **AVAILABILITY/LIMITATION NOTICES:** Enter any limitations on further dissemination of the report, other than those

imposed by security classification, using standard statements such as:

- (1) "Qualified requesters may obtain copies of this report from DDC."
- (2) "Foreign announcement and dissemination of this report by DDC is not authorized."
- (3) "U. S. Government agencies may obtain copies of this report directly from DDC. Other qualified DDC users shall request through _____."
- (4) "U. S. military agencies may obtain copies of this report directly from DDC. Other qualified users shall request through _____."
- (5) "All distribution of this report is controlled. Qualified DDC users shall request through _____."

If the report has been furnished to the Office of Technical Services, Department of Commerce, for sale to the public, indicate this fact and enter the price, if known.

11. **SUPPLEMENTARY NOTES:** Use for additional explanatory notes.
12. **SPONSORING MILITARY ACTIVITY:** Enter the name of the departmental project office or laboratory sponsoring (*paying for*) the research and development. Include address.
13. **ABSTRACT:** Enter an abstract giving a brief and factual summary of the document indicative of the report, even though it may also appear elsewhere in the body of the technical report. If additional space is required, a continuation sheet shall be attached.
- It is highly desirable that the abstract of classified reports be unclassified. Each paragraph of the abstract shall end with an indication of the military security classification of the information in the paragraph, represented as (TS), (S), (C), or (U).
- There is no limitation on the length of the abstract. However, the suggested length is from 150 to 225 words.
14. **KEY WORDS:** Key words are technically meaningful terms or short phrases that characterize a report and may be used as index entries for cataloging the report. Key words must be selected so that no security classification is required. Identifiers, such as equipment model designation, trade name, military project code name, geographic location, may be used as key words but will be followed by an indication of technical context. The assignment of links, roles, and weights is optional.